UNIVERSIDADE FEDERAL DE SANTA CATARINA
CENTRO DE CIÊNCIAS FÍSICAS E MATEMÁTICAS
PROGRAMA DE PÓS-GRADUAÇÃO EM QUÍMICA

Eloah Latocheski

Influence of the oxidation state of palladium nanoparticles on carbon coupling and bioorthogonal uncaging reactions

Florianópolis
2021

Eloah Latocheski

Influence of the oxidation state of palladium nanoparticles on carbon coupling and bioorthogonal uncaging reactions

Dissertação/Tese submetida ao Programa de Pós-Graduação em Química da Universidade Federal de Santa Catarina para a obtenção do título de Doutora em Química.
Orientador: Prof. Josiel Barbosa Domingos, Dr.
Coorientador: Prof. Gonçalo Bernardes, Dr.

Florianópolis
2021

Ficha de identificação da obra elaborada pelo autor,
através do Programa de Geração Automática da Biblioteca Universitária da UFSC.

Latocheski, Eloah
Influence of the oxidation state of palladium nanoparticles on carbon coupling and bioorthogonal uncaging reactions / Eloah Latocheski ; orientador, Josiel Barbosa Domingos, coorientador, Gonçalo Bernardes, 2021.
114 p.

Tese (doutorado) - Universidade Federal de Santa Catarina, Centro de Ciências Físicas e Matemáticas, Programa de Pós-Graduação em Química, Florianópolis, 2021.

Inclui referências.

1. Química. 2. Nanopartículas de paládio. 3. Reação de acoplamento. 4. Clivagem bio-ortogonal. 5. Ativação de pró fármaco. I. Domingos, Josiel Barbosa. II. Bernardes, Gonçalo. III. Universidade Federal de Santa Catarina. Programa de Pós-Graduação em Química. IV. Título.

Eloah Latocheski

Influence of the oxidation state of palladium nanoparticles on carbon coupling and bioorthogonal uncaging reactions

O presente trabalho em nível de doutorado foi avaliado e aprovado por banca examinadora composta pelos seguintes membros:

Prof. Dr. Brenno Amaro da Silveira Neto
Relator
Universidade de Brasília

Prof. Dr. Adolfo Horn Junior
Universidade Federal de Santa Catarina

Prof. Dr. Bruno Silveira de Souza
Universidade Federal de Santa Catarina

Certificamos que esta é a **versão original e final** do trabalho de conclusão que foi julgado adequado para obtenção do título de Doutora em Química.

Documento assinado digitalmente
Giovanni Finoto Caramori
Data: 16/12/2021 22:08:10-0300
CPF: 280.927.338-30
Verifique as assinaturas em https://v.ufsc.br

Coordenação do Programa de Pós-Graduação

Documento assinado digitalmente
Josiel Barbosa Domingos
Data: 16/12/2021 18:09:14-0300
CPF: 709.404.520-49
Verifique as assinaturas em https://v.ufsc.br

Prof. Dr. Josiel Barbosa Domingos
Orientador

Florianópolis, 2021.

Este trabalho é dedicado ao meu pai.

ACKNOWLEDGMENTS / AGRADECIMENTOS

Ao meu pai, por tudo, por tanto.

À minha família, pelo constante apoio. Que sorte a minha!

Ao meu orientador Professor Josiel, que apesar de todas as adversidades para se fazer pesquisa no Brasil, ainda consegue manter o brilho nos olhos ao falar de ciência. Ao Josiel também agradeço por todos os esforços que possibilitaram o doutorado sanduíche realizado por mim, e por diversos colegas, por meio do CAPES-PrInt.

Ao meu coorientador Professor Gonçalo Bernardes que não só me recebeu de braços abertos ao seu grupo na Universidade de Cambridge, mas também me ofereceu todo o suporte necessário para que eu permanecesse lá para concluir o trabalho durante a Pandemia.

À Aline por ser uma constante na minha vida inteira, e ter me brindado com um pedacinho de casa/família na Inglaterra.

À Letícia, pelo apoio, cuidado e por me apresentar novos caminhos toda vez que acho que estou perdida.

Ao Gean, por estar sempre disposto a discutir ideias e resultados.

Aos colegas de LaCBio, passado e presente. Afinal, ao longo de 10 anos, tive o prazer de conviver com muita gente incrível nesse lugar.

To my lab mates from the Team GB, with whom I spent a chaotic year, but they were great and made it a lot better. Special thanks to Juri for all the Palladium discussions and help with the synthesis and cells. And to Lavinia, also for helping me with the cells and contributions on our side projects.

To my lads from Cambs, I can only imagine how tedious lockdown would have been without you. You were lovely house mates.

Ao relator desta tese e aos professores que compõem a banca de avaliação, por contribuírem enormemente na correção e discussão deste trabalho.

Ao Laboratório Central de Microscopia Eletrônica da UFSC, Central de Análises do departamento de química e ao LNLS pelo respaldo nas análises. À Dra. Daniela C. de Oliveira, pelas análises de XPS e pelo apoio técnico e científico durante as análises realizadas no LNLS-Campinas.

Aos professores e funcionários do Departamento de Química da UFSC, especialmente à Andrezza e ao Henrique.

Ao CNPq, CAPES, UFSC, University of Cambridge e Instituto de Medicina Molecular de Lisboa.

RESUMO EXPANDIDO

Introdução

Nanopartículas (NPs), materiais isoláveis com tamanho compreendido na nanoescala, exibem propriedades diferentes dos materiais da mesma composição, mas com um tamanho maior. As propriedades relacionadas ao tamanho reduzido, como aumento da área superficial por volume e aumento das superfícies energéticas, em além da morfologia ajustável, a hidrofobia e a biocompatibilidade tornam as nanopartículas vantajosas para a catálise. Nanopartículas compostas por metais de transição (M-NPs), mais especificamente, têm mostrado grande sucesso em várias reações orgânicas porque combinam as funcionalidades dos metais de transição, há muito conhecidos como catalisadores versáteis para reações orgânicas, com os benefícios que surgem na nanoescala. Mais recentemente, vários estudos têm mostrado que a catálise por M-NPs ocorre por meio de mecanismos mais complexos do que a catálise tradicional heterogênea ou homogênea, uma vez que o meio reacional pode conter uma profusão de espécies ativas. Portanto, para que os catalisadores de M-NPs sejam racionalmente projetados, o conhecimento sobre a dinâmica dos catalisadores nas reações é de suma importância, bem como a aplicação de procedimentos e técnicas que possibilitem este estudo. Nanopartículas de paládio (Pd-NPs) se destacam como catalisadores em reações de acoplamento carbono-carbono (C-C), que é extremamente relevante em química orgânica, pois produz moléculas de grande valor e difícil obtenção. Um exemplo é a alquenilação de arila que leva à formação de alquenos substituídos. Isso pode ser alcançado, por exemplo, pela reação entre um sal de diazônio e uma olefina, que pode ocorrer por meio de mecanismos distintos: um mecanismo radicalar por meio de uma transferência de um único elétron (SET) ou de um mecanismo envolvendo a adição oxidativa do precursor de paládio. Ambas as reações têm etapas de catálise por metal e, devido às semelhanças nos reagentes e produtos, a diferenciação de uma reação para a outra pode ser muito sutil. Outro campo em que o uso de metais de transição se tornou proeminente é na mediação de reações bio-ortogonais. Mais especificamente, a clivagem bio-ortogonal, que compreende a desproteção de pró-fármacos por meio de reações de clivagem de ligação. E, para tanto, o paládio também está entre os ativadores mais interessantes, sendo capaz de promover a clivagem das ligações C-N e C-O resultando na ativação de fármacos e fluoróforos para imageamento de tumores, por exemplo. Embora o crescimento na aplicação de reações de desproteção bio-ortogonal seja evidente, não há tantos estudos na literatura que tragam percepções mecanísticas sobre essas reações, e aqueles que existem estão relacionados apenas a compostos metálicos mais simples, como sais ou pequenos complexos e nenhum por Pd -NPs. Portanto, é fundamental para o desenvolvimento racional do campo estudar sistematicamente a cinética da reação, bem como o modo de ação dos mediadores. Além disso, as reações de clivagem bio-ortogonal são projetadas para aplicações em meio biológico. Isso adiciona outra camada de complexidade à compreensão desejada, uma vez que os frascos de reação são extremamente simples em comparação com o ambiente celular. Com base nisso, é imperativo estudar a reação em ambas as condições para compreender os padrões de comportamento e como eles se traduzem em sistemas biológicos.

Objetivos

O objetivo deste projeto foi contribuir para a compreensão do modo de ação das nanopartículas de paládio na catálise de reações de alquenilação de arila e na clivagem de ligações C-O. Por meio de estudos sistemáticos cinéticos e mecanísticos, o projeto teve como objetivo auxiliar na racionalização do papel do paládio, de diferentes valências atômicas, nas reações de formação e quebra de ligações químicas. O projeto visou, inicialmente, a síntese e caracterização de nanopartículas de paládio, (Pd-NPs) com composição, tamanho e morfologia semelhantes,

diferindo apenas nos estados de oxidação do Pd como 0 e +2, sendo Pd(0)-NPs e PdI_2-NPs, respectivamente. Posteriormente, objetivou-se o estudo das Pd-NPs aplicadas na reação de alquenilação de arila e a avaliação do efeito da valência do metal no ciclo catalítico. A última etapa visou o estudo das Pd-NPs na reação de clivagem de ligações reunindo informações acerca da influência da valência do metal na cinética e elucidar o destino das nanopartículas ao longo da reação. E, por fim, objetivou a aplicação das nanopartículas para mediar, por meio de clivagem de ligação, a ativação de um pró-fármaco em células cancerosas e elucidar o efeito do ambiente extra e intracelular nas partículas.

Metodologia

Sintetizaram-se nanopartículas de paládio (II) e paládio (0) com composição, tamanho e dispersidade equivalentes. Estas partículas foram caracterizadas por técnicas de microscopia eletrônica de transmissão (TEM), espectroscopia de fotoelétrons excitados por raios X (XPS), espalhamento de raios X a baixos ângulos (SAXS) e espectroscopia de absorção de raios X (XAS). Os catalisadores foram aplicados na reação de alquenilação de arila entre um sal de bromoarenodiazônio e estireno, realizada em temperatura ambiente, na ausência de atmosfera inerte e de base. As nanopartículas também foram aplicadas na clivagem da ligação C-O de cumarinas protegidas na forma de carbamatos propargílico. As reações foram conduzidas em condições fisiologicamente relevantes e sob monitoramento cinético pela técnica de espectroscopia de fluorescência. Para elucidar as espécies ativas na reação mediada por nanopartículas, utilizaram-se métodos indiretos baseados em comparações com padrões comerciais e na inibição, por envenenamento, das diferentes espécies potencialmente catalíticas. Os catalisadores também foram testados em células vivas de câncer de mama da linhagem SKBR3 e de colo do útero da linhagem HeLa, para ativar localmente um fármaco antineoplásico Doxorubicina. Na última etapa empregou-se o fluoróforo rodamina 110, também protegido na forma de carbamato propargílico e alílico, para a visualização da reação de ativação do fluoróforo em ambiente intracelular pela técnica de microscopia de epifluorescência.

Resultados e Discussão

A etapa experimental consistiu na síntese e caracterização de Pd-NPs. As nanopartículas de Pd (II) foram preparadas na forma de iodeto de paládio, PdI_2-NPs, por uma reação de troca de ligante do íon acetato, proveniente do $Pd(OAc)_2$ por iodeto, na presença de um polímero como estabilizante (PVP). Da mesma forma, Pd(0)-NPs foram sintetizadas reduzindo-se $Pd(OAc)_2$ por $NaBH_4$ na presença de PVP. Para confirmar a formação de nanopartículas, a suspensão foi caracterizada por TEM e SAXS. As partículas resultantes eram esféricas, com baixa dispersão e, em geral, sem aglomerados. A contagem de partículas indicou um diâmetro médio de 2,1 nm ± 1,1 nm. As caracterizações realizadas para ambas as nanopartículas sintetizadas mostram que os sistemas possuem muitas equivalências: mesmo tamanho, forma e estabilizador, dispersidade e estabilidade. Eles diferem, no entanto, no estado de oxidação do átomo de metal. Este fato é importante por permitir o isolamento de demais parâmetros, possibilitando a avaliação do efeito do estado de oxidação do paládio nas reações. As PdI_2-NPs foram aplicadas na reação de acoplamento entre o sal de bromoarenodizônio e estireno e parâmetros como quantidade de catalisador e solvente foram avaliados. Observou-se que a reação levava aos melhores rendimentos em água e com 1 mol% de paládio. As nanopartículas de paládio divalente foram comparadas com Pd(0)-NPs e com outros padrões comerciais, sendo os melhores resultados obtidos com PdI_2-NPs. Para elucidar o principal mecanismo operante na reação, foram realizados alguns testes. A adição de um *trap* radical mostrou que no meio reacional ocorria a formação de um intermediário radical e assim, foi possível propor o mecanismo para a reação mediada pelas PdI_2-NPs. Para a segunda parte, o estudo das reações

de clivagem, utilizou-se como substrato o propargilcarbamato de cumarina, uma vez que sua desproteção resultava na formação de produto fluorescente e permitia o acompanhamento cinético pela técnica de fluorimetria. Os testes preliminares da reação em meio aquoso tamponado, 37 ºC forneceram indicativos de que as nanopartículas estavam sofrendo alterações no meio reacional não sendo possível atingir conversão total. Então, por meio de testes de envenenamento das prováveis espécies ativas de paládio, foi possível confirmar que as Pd-NPs estão de forma dinâmica se alterando no meio reacional e que essas diferentes espécies podem também levar à formação de produto. Mas, de modo geral, a reação de despropargilação foi favorecida, em termos de conversão e velocidade de reação, pela presença de espécies divalentes de paládio. De posse dessas informações, passou-se a estudar as reações de clivagem mediadas pelas Pd-NPs em células vivas, por meio da ativação de um fármaco antineoplástico. Como substratos utilizaram-se carbamatos alílicos e propargílico de doxorubicina. Observou-se uma maior eficiência de desalilação com paládio (0) e despropargilação com paládio (II) e, assim como no frasco reacional, observou-se que as Pd-NPs sofriam alterações em meio celular. Todavia, ajustando-se a administração das doses de nanopartículas para reduzir sua desativação, foi possível alcançar, nas células, os bons resultados observados nos experimentos cinéticos. Além disso, as condições otimizadas puderam ser reproduzidas com sucesso em células de uma linhagem distinta com meio de cultura diferente, mostrando a robustez do método. Por fim, os experimentos de microscopia de epifluorescência mostrou a liberação do fluoróforo encontra-se no espaço intracelular.

Considerações Finais

Nanopartículas de paládio foram sintetizadas com procedimento, tamanho e dispersidade semelhante e variando apenas no estado de oxidação do átomo metálico, sendo composto por paládio (II) ou (0). Essas partículas foram caracterizadas por técnicas relevantes como TEM e SAXS para elucidar suas propriedades morfológicas e XAS e XPS quanto à sua composição. Os Pd-NPs foram inicialmente aplicados em uma reação de acoplamento carbono-carbono do tipo alquenilação de arila. Neste estudo, os catalisadores de paládio foram reagidos com sal arenediazônio e estireno em meio aquoso, à temperatura ambiente e na ausência de base e atmosfera inerte. A formação do produto foi observada, segundo uma reação tradicional de Heck-Matsuda. No entanto, esforços na investigação do mecanismo de reação na presença de nanopartículas de paládio (II) revelaram um caminho diferente. Ao adicionar um *trap* radicalar ao meio reacional, observou-se a formação de um intermediário radicalar, que implica em u mecanismo de transferência de um único elétron, possibilitada pelas PdI_2-NPs. Posteriormente, as nanopartículas foram aplicadas na reação de clivagem da ligação C-O de substratos protegidos na forma de carbamatos de propargila. Estudos cinéticos e de envenenamento das Pd-NPs mostraram que essa reação é favorecida pelo paládio divalente. No entanto, como eles consistem em aglomerados nanopartículas do metal, processos dinâmicos como lixiviação e reestruturação de superfície podem estar ocorrendo ao longo da reação e diferentes espécies de paládio podem contribuir para a formação do produto. As nanopartículas também foram aplicadas em células cancerosas de duas linhagens distintas, câncer de mama e câncer do colo do útero, onde suas biocompatibilidades foram confirmadas e a ativação local de pró-fármacos se mostrou possível. A racionalização dos resultados na transferência da reação do frasco para o meio celular mostrou que o conhecimento adquirido em condições simples pode ser extremamente útil para encontrar a melhor forma de administrar o pró-fármaco às células. Ao compreender o comportamento das reações, especificamente neste caso, a maior atividade na liberação de substratos protegidos por propargiloxicarbonil com Pd (II) e protegidos por aliloxicarbonil com Pd (0), e como o meio biológico afetaria essas espécies, tornou-se possível atingir não apenas uma grande eficiência, mas também manter a seletividade dos pares

compostos por pró-fármaco e metal ativador. Assim, este trabalho constitui um amplo estudo sobre a preparação, compreensão e aplicação de nanocatalisadores de paládio em importantes reações orgânicas, tanto na formação quanto na quebra de ligações. Portanto, as contribuições quanto ao modo de ação das partículas em condições de bancada, bem como em ambiente celular, constituem uma etapa importante na elucidação do mecanismo de clivagem bio-ortogonal que fornece mais dados para a racionalização de sistemas catalíticos que possam ser usados em ambientes biológicos mais complexos e até in vivo.

Palavras-chave: Nanopartículas de paládio. Catálise. Reação de acoplamento. Mecanismo radicalar. Clivagem bio-ortogonal. Despropargilação. Reações intracelulares. Ativação de pró-fármacos.

RESUMO

O presente trabalho visou a compreensão do modo de ação de nanopartículas de paládio na mediação de reações de acoplamento carbono-carbono do tipo alquenilação de arila e em reações de clivagem bio-ortogonal visando o desenvolvimento de catalisadores racionais e biocompatíveis. Este estudo compreende a investigação cinética de nanocatalisadores de paládio em diferentes valências atômicas e sintetizados de forma análoga buscando-se restringir a comparação ao estado de oxidação do átomo metálico. Para tanto, sintetizaram-se nanopartículas de paládio (II) e paládio (0) com composição, tamanho e dispersidade equivalentes. Estas partículas foram caracterizadas por técnicas de microscopia eletrônica de transmissão, espectroscopia de fotoelétrons excitados por raios X e espalhamento de raios X a baixos ângulos. Os catalisadores foram aplicados na reação de alquenilação de arila entre um sal de bromoarenodiazônio e estireno, realizada em temperatura ambiente, na ausência de atmosfera inerte e de base. As nanopartículas também foram aplicadas na clivagem da ligação C-O de cumarinas protegidas na forma de carbamatos propargílico. As reações foram conduzidas em condições fisiologicamente relevantes e sob monitoramento cinético pela técnica de espectroscopia de fluorescência. Para elucidar as espécies ativas na reação mediada por nanopartículas, utilizaram-se métodos indiretos baseados em comparações com padrões comerciais e na inibição, por envenenamento, das diferentes espécies potencialmente catalíticas. Os resultados mostraram que a reação de alquenilação de arila é favorecida por nanopartículas de paládio (II), e que, nesse caso, a reação ocorre via mecanismo radicalar. Para a reação de despropargilação, observou-se que em termos de velocidade e conversão, a reação também é favorecida na presença de paládio (II), mas as diferentes espécies de paládio estão presentes no meio reacional e contribuem para o progresso da reação. Os catalisadores também foram testados em células vivas de câncer de mama e de colo do útero, para ativar localmente um fármaco antineoplásico. Os resultados mostraram que, se ministrados da forma adequada, a atividade observada nos ensaios de bancada pode ser reproduzida também in vitro. Esses resultados propiciaram uma maior compreensão da atividade de nanopartículas de paládio para que o desenvolvimento de novas espécies possa ser pensado a partir do seu modo de ação e visando sua aplicação em sistemas biológicos complexos.

Palavras-chave: Nanopartículas de paládio. Catálise. Reação de acoplamento. Mecanismo radicalar. Clivagem bio-ortogonal. Despropargilação. Reações intracelulares. Ativação de pró-fármacos.

ABSTRACT

The present work aimed to understand the mode of action of palladium nanoparticles in mediating carbon-carbon coupling reactions of the aryl alkenylation type and in bioorthogonal cleavage reactions aiming at the development of rational and biocompatible catalysts. This study comprises the kinetic investigation of palladium nanocatalysts in different atomic valences and synthesized in an analogous manner, seeking to restrict the comparison to the oxidation state of the metallic atom. For this purpose, palladium (II) and palladium (0) nanoparticles with equivalent composition, size and dispersity were synthesized. These particles were characterized by techniques such as transmission electron microscopy, X-ray photoelectron spectroscopy and small angle X-ray scattering. The catalysts were applied in the aryl alkenylation reaction between a bromoarene diazonium salt and styrene, carried out at room temperature, in the absence of an inert atmosphere and base. The nanoparticles were also applied to cleave the C-O bond of protected coumarins in the form of propargyl carbamates. The reactions were carried out under physiologically relevant conditions and under kinetic monitoring using the fluorescence spectroscopy technique. To elucidate the active species in the reaction mediated by nanoparticles, indirect methods based on comparisons with commercial standards and on the inhibition, by poisoning, of different potentially catalytic species were used. The results showed that the aryl alkenylation reaction is favoured by palladium (II) nanoparticles, and that, in this case, the reaction occurs via a radical mechanism. For the depropargylation reaction, it was observed that in terms of rate and conversion, the reaction is also favoured in the presence of palladium (II), but different palladium species are present in the reaction medium and contribute to the reaction progress. The catalysts have also been tested in living cells of breast and cervical cancer to locally activate an anticancer drug. The results showed that, if administered properly, the activity observed in reaction flasks can also be reproduced in vitro. These results provided a greater understanding of the activity of palladium nanoparticles so that the development of new species can be thought of based on their mode of action and aiming at their application in complex biological systems.

Keywords: Palladium nanoparticles. Catalysis. Coupling reaction. Radical mechanism. Bioorthogonal cleavage. Depropargylation. Intracellular reactions. Activation of prodrugs.

LIST OF FIGURES

LIST OF SCHEMES

LIST OF TABLES

LIST OF ABBREVIATIONS

5-FU – 5-fluorouracil

ADC – Antibody drug conjugate

^{13}C NMR – Carbon-13 nuclear magnetic resonance

^{1}H NMR – Proton nuclear magnetic resonance

Alloc – Allyloxycarbonyl as a protecting group

Au(0)-NPs – Zerovalent gold nanoparticles

CH_3CN – Acetonitrile

CTAC – Cetyltrimethylammonium chloride

dba – Dibenzylideneacetone

DCM - Dichloromethane

DFT – Discrete Fourier Transform

DMEM – Dulbecco's Modified Eagle Medium

DMF – Dimethylformamide

DMSO – Dimethyl sulfoxide

DNPPE – 2,4-dinitrophenyl propargyl ether

DOX – Doxorubicin

DS – Diazonium salt

DS-Br – 4-bromobenzenediazonium salt

EDTA – Ethylenediamine tetraacetic acid

Eq. – Equivalent

ESI-MS – Electrospray ionisation mass spectrometry

EtOAc – Ethyl acetate

FAAS – Flame Atomic Absorption Spectrometry

Gly – Glycine

Gn – Guanidine

GSH – Glutathione

HPA – 3-hydroxypropanal

HRTEM – High Resolution Transmission Electron Microscopy

IC_{50} – Half maximal inhibitory concentration

IEDDA – Inverse Electron Demand Diels–Alder

LC-MS – Liquid Chromatography–Mass Spectrometry

m/z – Mass-to-charge ratio

MeOH – Methanol

MMAE – Monomethyl auristatin E

M-NPs – Metal nanoparticles

NaAsc – Sodium ascorbate

Neu – Neuramic acid

Neu5Proc – N-(propargyloxycarbonyl)neuramic acid

NPs – Nanoparticles

PBS – Phosphate Buffered Saline

Pd(0)-NPs – Zerovalent palladium nanoparticles

$Pd(OAc)_2$ – Palladium acetate

PdI_2-NPs – Palladium iodide nanoparticles

Pd-NPs – Palladium nanoparticles

Pro – Propargyl as a protecting group

Proc – Propargyloxycarbonyl as a protecting group

PVP – Polyvinylpyrrolidone

Rho – Rhodamine 110

RPKA – Reaction Progress Kinetic Analysis

RPM – Revolution per minute

RPMI – Roswell Park Memorial Institute

SAXS – Small Angle X-ray Scattering

SET – Single Electron Transfer

STB – Stilbene

TEM – Transmission Electron Microscopy

TEMPO – 2,2,6,6-Tetramethylpiperidine 1-oxyl

TFP – Tri-2-furylphosphine

TLS – Turnover limiting step

TON – Turnover number

TPPTS – 3,3′,3″-Phosphanetriyltris(benzenesulfonic acid) trisodium salt

UV-vis – Ultraviolet-visible spectrometry

XANES – X-ray absorption near edge structure

XAS – X-ray absorption spectroscopy

λ_{max} – Maximum wavelength

TABLE OF CONTENTS

1 INTRODUCTION

Nanoparticles (NPs), isolable materials with size comprehended in the nanoscale, exhibit different properties than materials of the same composition but with a larger size.[1] The properties related to reduced size, such as increased surface area per volume and increased energetic surfaces, in addition to tuneable morphology, hydrophobicity and biocompatibility make nanoparticles advantageous to catalysis.[2–4]

Nanoparticles comprised of transition metals (M-NPs), more specifically, have shown great success in various organic reactions because they combine the functionalities of transition metals, long known as versatile catalysts for organic reactions with the benefits that arise in the nanoscale.[5]

More recently, several studies have shown that catalysis by M-NPs occurs through more complex mechanisms than traditional heterogeneous or homogeneous catalysis, since the reaction medium might contain a profusion of active species.[6,7] Therefore, for M-NPs catalysts to be rationally designed, knowledge about the dynamics of catalysts in reactions is of paramount importance, as well as the application of procedures and techniques that allow this study.[8,9]

Palladium nanoparticles (Pd-NPs) excel as catalysts in carbon-carbon (C-C) coupling reactions. C-C coupling is extremely relevant in organic chemistry, because it yields molecules of great value and difficult obtention.[10] One example is the aryl alkenylation that leads to the formation of substituted alkenes. This can be achieved, for instance, by the reaction between a diazonium salt and an olefin, which can occur via distinct mechanisms: a radical pathway by means of a single electron transfer (SET) or from a mechanism involving oxidative addition of a oxidised palladium precursor.[11,12] Both reactions have metal catalysis steps, and due to the similarities in reagents and products, the differentiation from one reaction to the other is very subtle.

Another field in which the use of transition metals, as nanoparticle or bulk, has become prominent is in the mediation of bioorthogonal reactions.[13–16]More specifically, bioorthogonal uncaging which comprises of the deprotection of prodrugs by means of bond cleavage reactions.[16,17] And for this purpose, palladium is also amongst the most interesting triggers, being able to promote the cleavage of C-N and C-O bonds resulting in the activation of drugs and fluorophores for tumour imaging, for instance.[18–20]

Although the growth in the application of uncaging reactions is evident, there are not as many studies in the literature that bring mechanistic insights into these reactions, and those that do exist are only related to simpler triggers such as salts or small complexes and none by Pd-NPs. Therefore, it is crucial to the rational development of the field to systematically study the kinetics of the reaction, as well as the mode of action of the mediators.

Besides that, bioorthogonal uncaging reactions are designed for applications in biological medium. This adds another layer of complexity to the desired comprehension once reaction flasks are incredibly simple in comparison to cellular environment. On this basis, it is imperative to study the reaction in both conditions to understand the behavioural patterns and how they translate to biological systems.

In this context, this work aims to contribute to the elucidation of the mode of action of palladium nanoparticles in the catalysis of cross-coupling reactions between arenediazonium salts and olefins and in the activation of caged molecules in flask and biological medium.

1.1 AIMS OF THE PROJECT

The aim of this project was to contribute to the understanding of the mode of action of palladium nanoparticles in the catalysis of aryl alkenylation reactions and in the cleavage of C-O bonds. By means of systematic kinetic and mechanistic studies, the project was designed to aid in the rationalization of the role of palladium, bearing different atomic valences, in the reactions of making and breaking chemical bonds.

For such, the project initially aimed for the palladium nanoparticles synthesis and characterization, presented below as common ground for both applications. And afterwards, specific aims were established to study each reaction in its singularity.

1) Synthesize palladium nanoparticles (Pd-NPs) with similar composition, size, and morphology, differing, however, in the oxidation states of Pd as 0 and +2, Pd(0)-NPs and PdI_2-NPs, respectively.

2) Characterise the Pd-NPs by transmission electron microscopy (TEM), small angle X-ray scattering (SAXS), X-ray absorption near edge structure spectroscopy (XANES), X-ray photoelectron spectroscopy (XPS), and flame atomic absorption spectrometry (FAAS).

1.1.1 Aims in the aryl alkenylation study

1) Apply the Pd-NPs in aryl alkenylation reactions.

2) Evaluate the effect of metal valence on the catalytic cycle, by means of comparison with different Palladium precursors.

3) Collect evidence of the mode of action of the Pd-NPs in the catalytic cycle of the alkenylation reaction.

1.1.2 Aims in the bond cleavage study

1) Gather kinetic insights into the bond cleavage reactions of carbamate- and carbonate-coumarins mediated by the palladium nanoparticles with different metal valence states.

2) Employ poisoning experiments to, indirectly, probe the fate of the nanoparticles and the influence of the metal oxidation state throughout the course of the reaction.

3) Apply the nanoparticles to mediate, through bond cleavage, the uncaging of prodrug in cancer cells and elucidate the effect of the extra- and intracellular environment in the particles.

4) Visualise the intracellular uncaging of a fluorophore mediated by the nanoparticles through epifluorescence microscopy.

2 LITERATURE REVIEW

2.1 METAL NANOPARTICLES

Nanoparticles (NPs) are defined as three-dimensional structures that have at least one of their domains in the range from 1 to 100 nm and, therefore, exhibit distinct properties of materials of larger size with the same composition.[1] In this scale, matter has unique optical, magnetic and catalytic properties, which have fascinated scientists for centuries.[21] However, it was only recently that the rational development of these materials, especially metal nanoparticles (M-NPs), gained prominence in research and industry.[22] This advance was only possible due to the evolution of optical technologies and synchrotron radiation that are used in the characterisation of structures in this size range.[9,23]

In a general manner, the synthesis of M-NPs is based on physical (top down) or chemical (bottom up) methods. The physical method consists of mechanically subdividing the extended metal, for example, by ball milling, until it becomes fine enough to be comprehended in the nanometric scale.[24] Chemical methods of M-NPs synthesis are mainly based on the reduction of metal ions in the presence of the stabiliser or in the decomposition of organometallic precursors to generate nanoparticles made of zerovalent atoms.[3]

Nanoparticles have maximised surface area per volume, and, for this reason, they become unstable in solution.[25] To avoid their aggregation, nanoparticles are synthesised in the presence of stabilizing agents which consist of polymers, surfactants, binders, cyclodextrins, among others.[2] In addition to providing protection against agglomeration, stabilisers can also act in the tunning of the properties of the nanoparticles and, thus, control size, shape, dispersibility and compatibility with the medium of interest.[2]

Nonetheless, the nanoparticles present the advantage of possessing a high surface area per volume: since it is inversely proportional to the radius, small spherical particles present a higher percentage of their atoms on the surface. This attribute provides a high energy surface that results in materials with excellent properties for catalysis.[3]

2.2 METAL NANOPARTICLES AS CATALYSTS

In recent years, catalysis of organic reactions by transition metals is one of the most prolific areas of chemistry in terms of synthetic and industrial applications.[5] Naturally, with the

development of nanotechnology and their promising results in catalysis, metal in bulk form has been replaced by metal in its nanometric form.[26] Under NPs catalysis, better results can be achieved with smaller amounts of the, usually quite expensive, transition metals. And, in addition to the potentially greater activity when compared to traditional catalysts, nanoparticles are usually favoured in terms of reproducibility, solubility, reuse and selectivity.[5]

Metal nanoparticles (M-NPs) have already been successfully applied in a wide range of reactions. Under M-NPs catalysis, it became possible to perform C-C coupling reactions in ambient conditions,[27] "click" reactions in a cellular medium,[28] hydrogenations with modular selectivity,[29] in addition to hydrogen evolution reactions.[30]

The study of M-NPs mode of action in catalysis began to be explored by the last decade of the 20th century. At first, it was attributed to nanoparticles only the ability to provide a larger surface area per volume for adsorption of substrates that would lead to the formation of products, analogous to a traditional heterogeneous catalysis, as illustrated in Scheme 1 a).

By that time, it was known that the PdNPs-catalysed Heck coupling, for instance, was sensitive to surface structure and to the atoms in different sites of the particle (defects and terraces), being those atoms with lower metal-metal coordination number responsible for higher activity.[31] Then, however, lacked evidences and, in some cases, means to gather information regarding leaching and other insights for a possible homogeneous pathways.

In the first decade of this century, another aspect of M-NP catalysis was identified.[7] Investigations about the leaching of metal atoms in the reaction medium showed that, in certain cases, the active species was the metal atom dissociated from the surface of the nanoparticle and the reaction took place in solution.

In 2006, Vries very categorically classified PdNPs as reservoir of palladium that leached from the surface in his perspective manuscript entitled "A unifying mechanism for all high-temperature Heck reactions. The role of palladium colloids and anionic species".[32] According to his views, M-NPs provided metal atoms to the reaction medium that were inserted in the catalytic cycle similar to that of reactions with traditional metal complexes or salts.[6] This mode of action is illustrated in Scheme 1 b).

Scheme 1. Schematic representation of the mode of action of metallic nanoparticles in the catalysis of organic reactions. In a) heterogeneous and in b) homogeneous pathway.

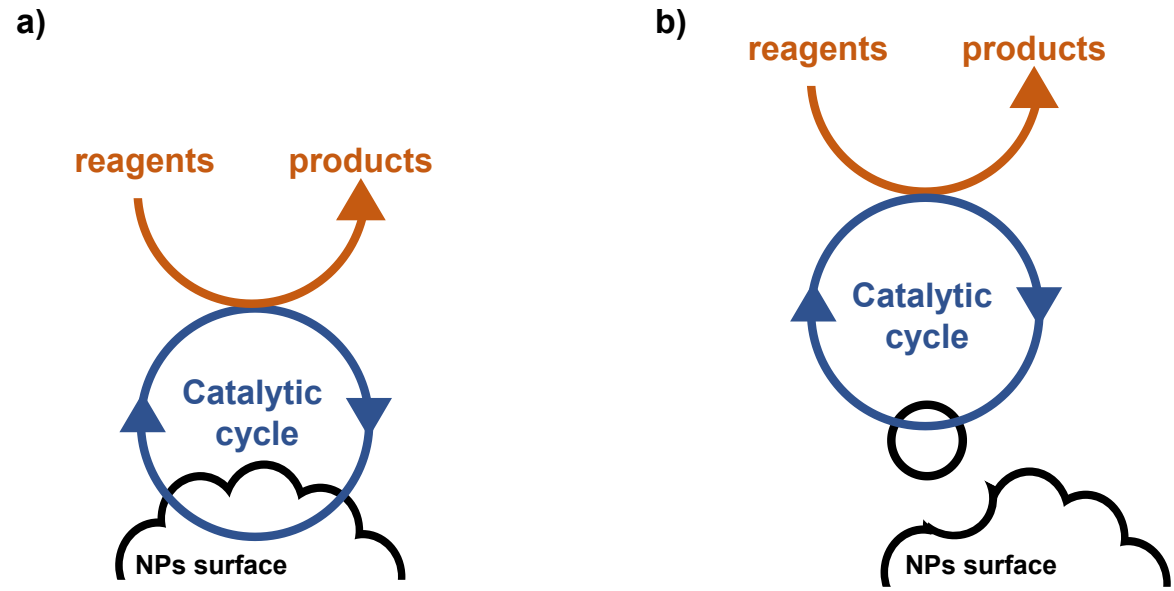

Source: the author, 2021.

It is extremely complex to probe features such as structure and oxidation state in a reaction medium and, for this reason, indirect strategies, and non-standard techniques as synchrotron radiation-based spectroscopy and high-resolution microscopy are able to shed a light in all these processes taking place in a reaction flask and in many cases, only with the combination of these strategies.[33–35]

For example, Huang and co-authors studied the removal of Pd by resin- and silica bound thiol scavengers to elucidate the true catalytic species in Heck coupling of bromobenzene and styrene.[8] They made use of catalyst poisoning by the scavengers, filtration testing, and TEM studies, to show that Pd clusters were inactive in this Heck reaction with Pd(0)/SiO_2, whilst dissolved Pd(0) was the only active species.

Currently, there is a much more dynamic view of how transition metals are capable of mediate chemical reactions.[7] While there are many examples that show that nanoparticles are formed *in situ* during the reaction that initially contained complexes or metal salts, there are also examples that show the opposite: nanoparticles are converted to metal atoms soluble in the reaction medium (leaching). The idea that the added metallic precursor is always the only catalyst in the reaction is no longer accepted, just as the idea that there can only be one catalytically active species is bygone. The current understanding is that different types of metallic species undergo interconversion, and that these different catalysts may contribute differently to the product formation. Thus, the reaction medium is composed of a “cocktail” of

catalytic species that act in different ways and dependent on factors such as temperature, solvent, substrates, in addition to other experimental parameters.[6] Scheme 2 exemplifies the possible forms that can be found for palladium in the reaction medium.

Scheme 2. Representative scheme of the definition of catalyst cocktail. Possible forms of interconversion of different palladium species in the reaction medium.

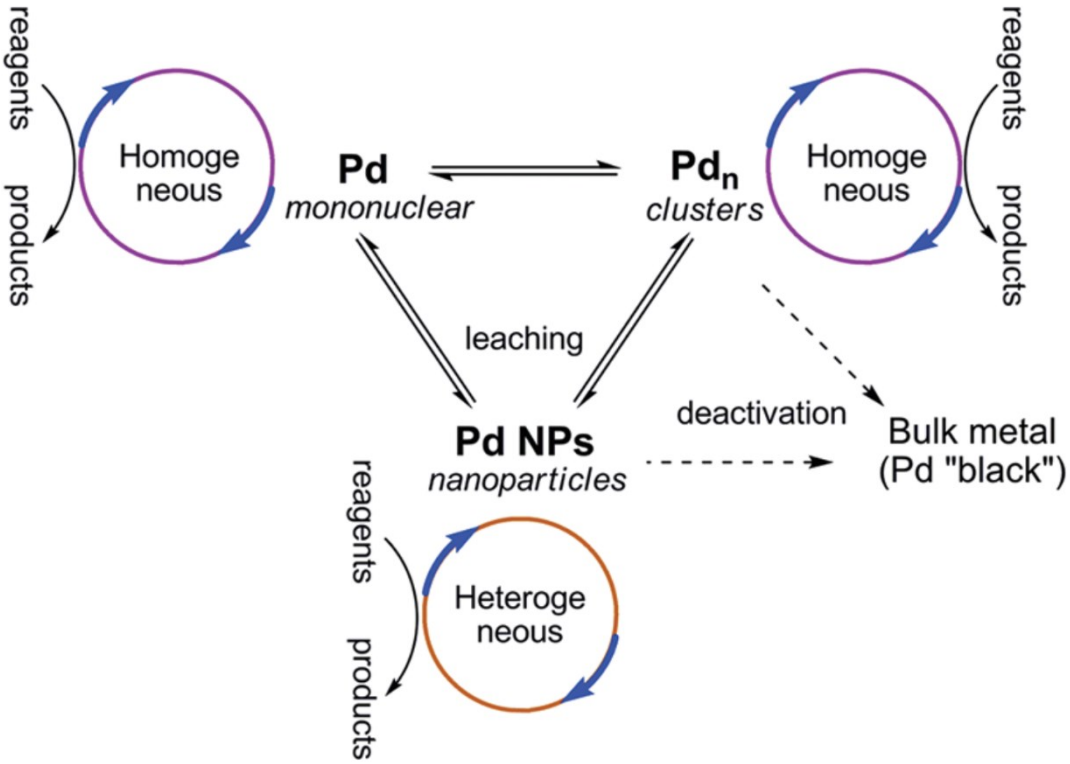

Source: Reprinted with permission from Organometallics Toward the Ideal Catalyst: From Atomic Centers to a "Cocktail" of Catalysts, Valentine P. Ananikov, Irina P. Beletskaya. Copyright (2012) American Chemical Society.

Even though it may seem beneficial to have reactions catalysed by species generated regardless the source of the metal, when it comes to more sophisticated applications as the ones in biological environment, for instance, the comprehension of the nature of the catalytic species becomes imperative in order to avoid issues such as contamination, deactivation and also to improve the possibilities towards a rational design.[6]

The current approach to catalysis by metal nanoparticles was only achieved due to kinetic and mechanistic studies of their reactions and, above all, thoroughly characterising the catalyst, in solution, prior and throughout the progress of the reaction.[7]

Therefore, kinetic studies of the dynamics of catalysts in solution can lead to a better understanding of the factors that influence and favour certain reaction pathways. This

knowledge is essential for the rational development of catalysts and to the design of "tailor-made" catalyst that can achieve optimal catalytic efficiency.

2.3 CARBON-CARBON COUPLING

Carbon coupling reactions catalysed by palladium have created a great impact in synthetic organic chemistry culminating with their recognition with the 2010 Nobel Prize.[36] C-C coupling reactions are amongst the most versatile tools for synthetic organic chemistry in both academic and industrial contexts.[10] This class of reactions allows the formation of complex molecules of great value and difficult obtention, such as substituted alkynes or alkenes, in addition to the formation of C-C bonds between substrates of varied structures with few limitations.[37]

Figure 1 shows the most common coupling reactions catalysed by palladium, all of them starts with an aryl halide (or false halides such as triflates) and were named after their discoverers: Sonogashira, in which an alkyne is reacted to yield substituted alkynes;[38] Suzuki, starts with a boronic acid;[39] Stille with an organotin compound;[40] and Negishi with an organozinc lead to the formation of substituted olefins,[41] styrenes, and substituted biphenyls; and Heck, starting with an alkene to yield substituted olefins.[42]

Figure 1. Example of the main carbon coupling reactions catalysed by palladium.

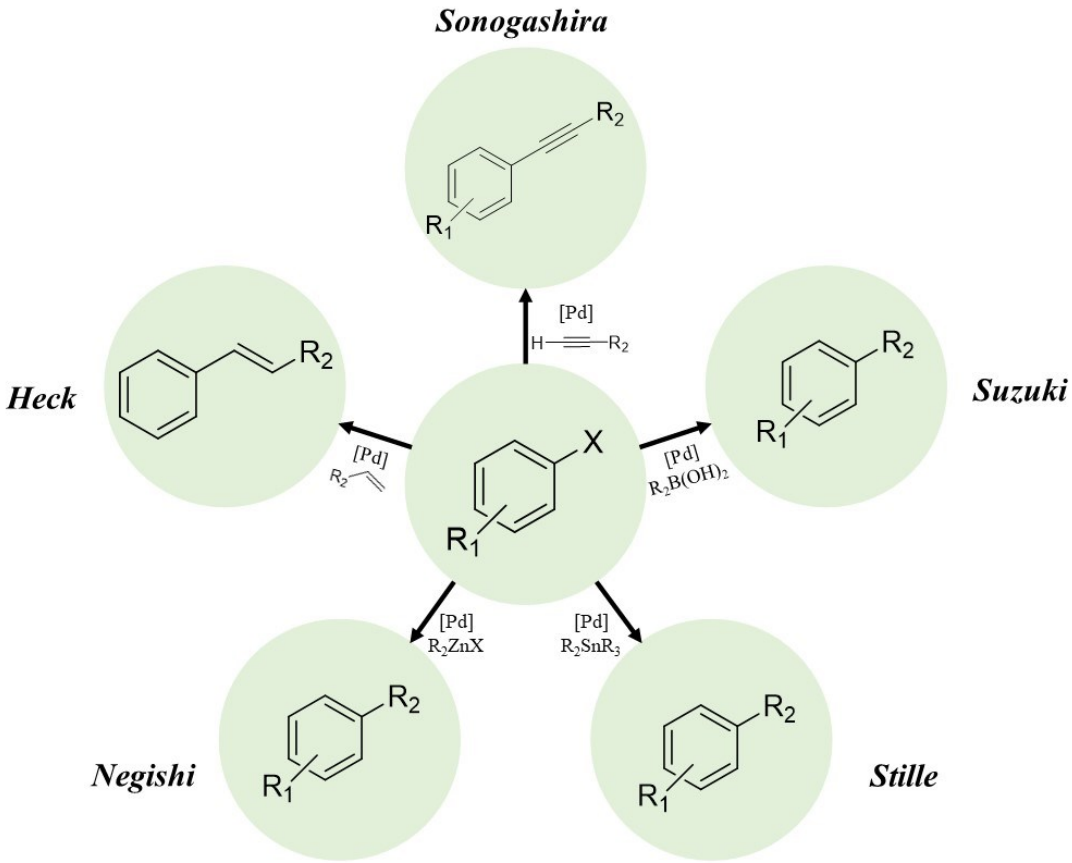

Source: the author, 2021.

The importance of palladium in these reactions is based on its ability to alternate between oxidation states 0 and +2. In this way, palladium can be inserted in R-X species (usually aryl halides or "false halides") making them more electron deficient and more reactive for the subsequent nucleophile attack.[43]

One modification to C-C coupling reactions that is often executed is the replacement of the aryl halide with a diazonium salt. The use of this electrophile has some benefits such as straightforward methods for obtaining the substrate, higher coupling conversions and the possibility to be performed under milder conditions on account to the high reactivity of the salts.[12]

When reacting a diazonium salt with an olefin, the reaction can proceed through at least two different mechanisms. The first one is analogous to the mechanism represented in Scheme 3. In this case, under catalysis by Pd (0) and oxidative addition induced by the diazonium salt, assigned with the name of Heck-Matsuda reaction.[12]

Scheme 3. Generic catalytic cycle of the transition metal catalysed carbon coupling reaction

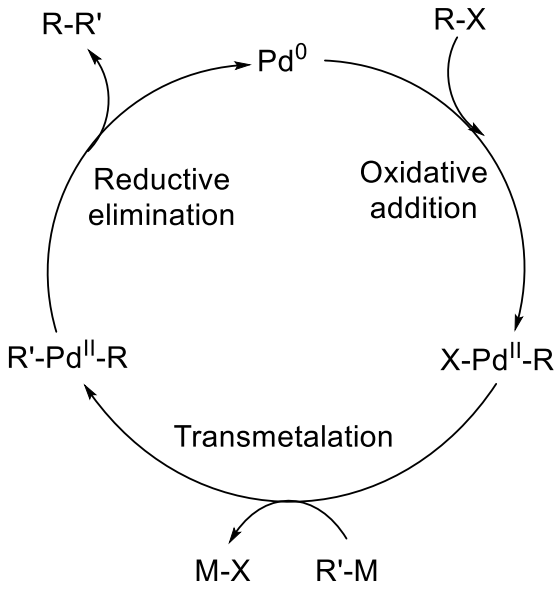

Source: the author, 2021.

The Heck-Matsuda mechanism, with little variation, has been proposed since the begin when Matsuda first published his set of seminal papers on the matter.[44–46] The catalytic cycle is strongly inspired in Heck's mechanism and consists in four steps: oxidative addition, migratory insertion, *syn* β-elimination, and reductive elimination as shown in Scheme 4.

Scheme 4. General catalytic cycle proposed for the Heck-Matsuda reaction.

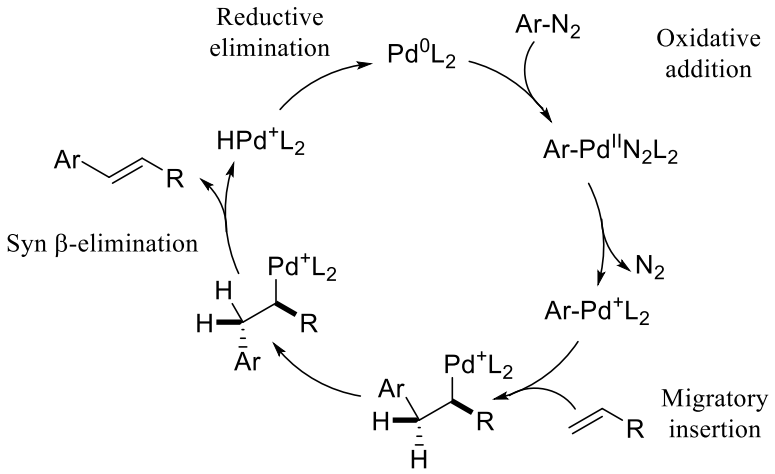

Source: the author, 2021.

More recently, Correia and co-authors have provided evidence that support the cycle proposed above. They investigated the reaction between 2,3-dihydrofuran and 4-methoxybenzenediazonium tetrafluoroborate and applied $Pd_2(dba)_3$ as catalyst.[47] Using electrospray ionization mass spectrometry (ESI-MS) they were able to detect key intermediates to the proposed catalytic cycle and even show the complicated equilibrium in which the palladium complex is involved.

It is important to note that the majority of the previous studies of the Heck-Matsuda reaction were conducted with $Pd_2(dba)_3$ or $Pd(PPh_3)_4$ as catalyst, which is reasonable considering the initial step is an oxidative addition of the palladium.[12] However, there are also plenty examples that show the reaction taking place with Pd^{II} precursors, specially $Pd(OAc)_2$. In these cases, it was required the addition of a reducing agent such as CO,[48] or in some cases, it was said that the metal reduction is induced by the solvent and a base, which is mandatory under traditional conditions.[49]

In another interesting contribution of Correa and co-authors, they showed, again through ESI-MS, that the zerovalent palladium active in the Heck-Matsuda reaction is formed by a Wacker olefin oxidation process.[50] In this fashion, they observed the formation of the oxidation product of 2,3-dihydrofuran while palladium (II) is reduced to palladium (0) and capable of initiating the Heck-Matsuda catalytic cycle.

Another plausible pathway to aryl alkenylation is via a radical mechanism, as in the case of the Meerwein arylation.[51] Traditionally under copper catalysis, the diazonium salt gives rise to an aryl radical which is then added to olefin and under oxidative conditions result in the coupling product, as shown in Scheme 5.[11,52]

Scheme 5. Generic scheme representing the Meerwein arylation reaction under transition metal catalysis.

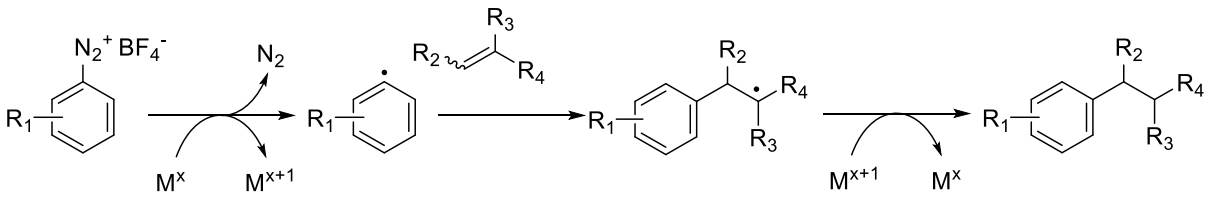

Source: the author, 2021.

Initially, Meerwein suggested a cationic mechanism formed after the loss of molecular nitrogen by the diazonium salt.[53] Even though this mechanism explained the preference for

electron-withdrawing groups (which, by the way, is reversed in the case of Heck-Matsuda reaction), it failed to explain the direction of addition to asymmetric olefin, for instance.[54]

Almost two decades later, Kochi proposed a free-radical mechanism after studying the fate of the precursor copper (II) throughout the course of the reaction.[55] The identification of the active catalytic species as copper (I), led to the assumption the reaction occurs by means of a single electron transfer (SET) process. More evidence were gather through the years but this proposal remains as the most accepted with little variations when it comes to the steps following the radical generation.[51,56]

The Heck-Matsuda and Meerwein reactions have many similarities in relation to the initial reactive species and both provide aryl alkenylation product, consisting of C-C coupling reactions. However, their reaction mechanisms are quite different even though the conditions that influence the preferential reaction path may be very subtle. For this reason, and because many studies of this class of reactions focus exclusively on the synthetic scope, several radical reaction systems have been misinterpreted as Heck-type reactions.[11] The slight mechanistic differences represent a challenge to distinguish these reactions, however, their understanding is fundamental to the mastery of reaction conditions and rationalization of their catalytic systems.

2.4 BIOORTHOGONAL CHEMISTRY

Bioorthogonal chemistry is a concept first introduced to scientific literature by Carolyn Bertozzi, in 2003, to refer to chemical reactions that take place in biological environments with little or without interaction with endogenous moeities.[57,58] Figure 2 exemplifies a complex system composed of several functionalities, however, the reaction occurs exclusively between the bioorthogonal substrates (green and red components attached in the first cell) and the trigger (the blue sphere), leaving the other molecules and biological components unchanged.

Figure 2. A general bioorthogonal chemical reaction scheme. Two bioorthogonal elements the prodrug (represented by green and red components attached) react selectively with the catalyst (represented by the blue sphere) in the presence of other biological components.

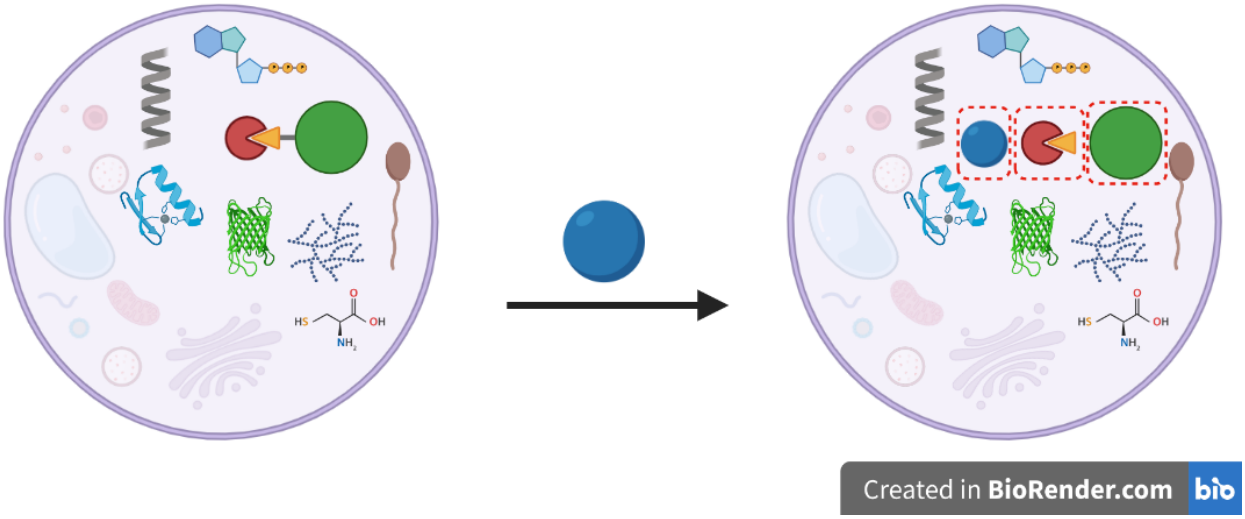

Source: the author, 2021.

By definition, bioorthogonal reactions must occur through a highly specific mechanism, in order to reduce the interaction with the other functional groups present in the reaction site. In addition, these reactions must occur in an aqueous medium, at restrict pH, temperature and physiological pressure, with a favourable reaction rate to take place rapidly under lower concentrations. Moreover, these reactions are in general designed to occur in vivo, hence cannot display highly reactive or toxic intermediates and products, unless such properties are desired.[58,59]

Obeying the criteria imposed by bioorthogonal chemistry, several systems were developed with emphasis on ligation strategies. The click reaction is an interesting example, since one of its variations occurs between an azide and an alkyne which have excellent

biocompatibility and consists of a kinetically favoured orthogonal reaction.[60] Reactions such as [4 + 2] cycloaddition were also applied due to their high reaction rates and the biological inertness of its substrates and products.[61]

Although all the reactions mentioned above focus on the formation of bonds, the cleavage of bonds (dissociative reactions) in a cellular environment has also attracted interest from researchers. This interest lies in the possibility of activating a protected drug at its site of action, thus reducing interactions with other features of neighbouring systems.

2.4.1 Bioorthogonal cleavage reactions

The protection of functional groups is common practice since the beginning of synthetic chemistry, especially when it is necessary to protect specific moieties of complex molecules. The purpose of protecting functional groups is to selectively carry out a reaction in a specific site of a multifunctional compound and ensure that the other sites will be temporarily blocked, preventing unwanted parts of the molecule from undergoing side reactions.[62] The recovery of the functionality is then obtained after deprotection by chemoselective means (triggering).

However, the application of these concepts to biological substrates are fairly recent. Only in the last 40 years, with the work of Merrifield, the protection of functional groups have been employed to provide orthogonality to biological molecules.[63]

Crossing paths with bioorthogonal chemistry, the deprotection of biologically inactive substrates has recently emerged under a nomenclature of bioorthogonal cleavage reactions, in some references as bioorthogonal dissociative reactions, uncaging reactions or even clip chemistry.[17,64,65] In these approach, the breaking of a bond of a "caged" substrate, usually triggered by a exogenous component, leads to the final product consisting of a molecule with restored biological activity (uncaged substrate).[17]

As for exogenous trigger, that ones that stand out are based on transition metals because they exhibit great catalytic versatility by acting in a large variety of reactions and biorthogonal properties that can be tuned according to the environment and conditions. In fact, chemical reactions catalysed by transition metals that are not present or with low incidence in biological systems also constitute an increasing class in the development of bio-orthogonal chemistry. Scheme 6 shows examples of bioorthogonal cleavage reactions (uncaging reactions) that stand out amongst this class. Scheme 6 i) shows the C-O cleavage in carbamates mediated

by light when protected with *o*-nitrobenzyl, by ruthenium when protected with an allyl (Scheme 6 ii), by palladium with propargyl (Scheme 6 iii), by copper with tertiary propargyl (Scheme 6, iv) and by 1,2,4,5-tetrazine in the case of a reaction induced by inverse electron-demand Diels–Alder (IEDDA) "click and release" reaction.

Scheme 6. Examples of bond cleavage reactions in bioorthogonal chemistry.

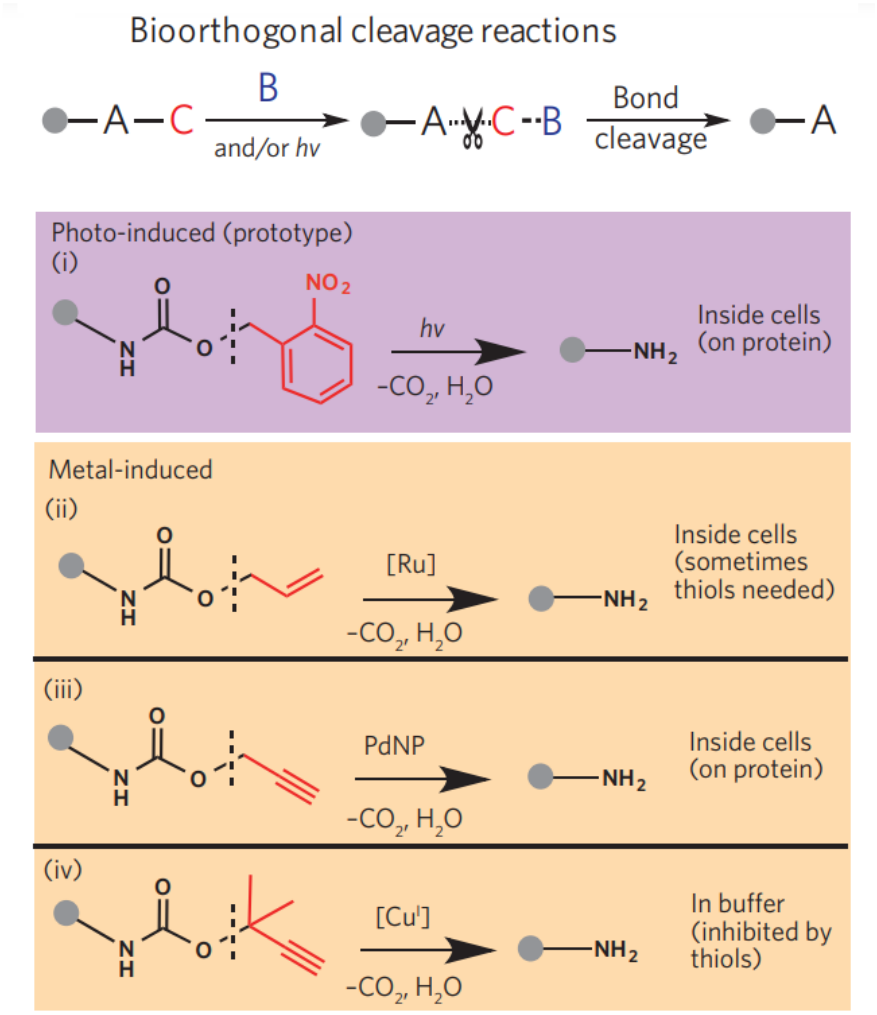

Source: Adapted by permission from Springer Nature Customer Service Centre GmbH: Springer Nature NATURE CHEMISTRY BIOLOGY Development and application of bond cleavage reactions in bioorthogonal chemistry, Jie Li *et al*, Copyright (2016).

2.4.1.1 Bioorthogonal uncaging reactions mediated by transition metals

The first metal-mediated bioorthogonal cleavage reaction was introduced by Streu and Meggers, in 2006.[66] They reported the use of a ruthenium(II) half sandwich complex, for the cleavage of allylcarbamates yielding free primary amines under biologically-relevant conditions (37 °C, in the presence of water, air and thiols). In addition, by making use of bis-allyloxycarbonyl-caged rhodamine 110 (Alloc-Rho), they were able to perform the uncaging inside living HeLa cells and, by confocal imaging, it became visible the increase in fluorescence inside the cytoplasm in respect to the uncaged rhodamine 110.

Thereafter, in 2011, Mark Bradley and co-authors explored, for the first time, palladium to promote deallylation.[67] They applied Pd(0) nanoparticles supported in polystyrene microspheres which were able to penetrate the cell membrane and mediate the uncaging of Alloc-Rho in HeLa cells.

By 2014, Unciti-Broceta and co-authors expanded the scope of supported Pd(0) to mediate, for the first time in the bioorthogonal context, depropargylation reactions.[18] In this work, heterogeneous Pd(0)-functionalised polyethylene glycol–polystyrene resins triggered the activation of the prodrug 5-fluoro-1-propargyl-uracil (Pro-5FU). They went further and evaluated the efficiency of the reaction *in vivo* by performing the depropargylation of propargyloxycarbonyl-caged rhodamine 110 (Proc-Rho) in zebrafish yolk. They observed an increase in fluorescence near the Pd0-resin in the yolk sac, ensuring the device is catalytically active *in vivo*.

A few years later, Unciti-Broceta's research group brought another addition to the toolbox of bioorthogonal depropargylation strategies. In 2017, they reported for the first time the *in vivo* gold-catalysed uncaging of propargylic prodrugs and fluorophore.[68] Again using resin as support for nanoparticles, this time Au(0)-NPs, they locally activated drugs in cancer cell and a fluorescent dye in the brain of a zebrafish. Interestingly, even though gold has high affinity with thiols, this work showed that the solid support prevented the metal inactivation and satisfactory yields were achieved even amongst a large variety of proteins.

Copper was also incorporated in this group of triggers for depropargylation. However, differently from the other metals, copper works better when the protecting group is a disubstituted propargyl. In 2013, Finn and co-workers showed the deprotection of Proc-Rho in the presence of a Cu(I)–tris(3-hydroxypropyltriazolylmethyl)amine) complex under physiologic-like conditions (37 °C, in water).[69]

More recently, Chen and co-authors screened 24 different transition-metals species, to uncage amino- and hydroxy-protected coumarins.[70] They found that when it comes to the uncaging of dual-substituted propargylic groups the best results were found for coordination complexes of copper (I). *In vivo* assays showed the successful uncaging of doxorubicin from a disubstituted propargyl linked to an antibody conjugate targeting anti-HER2 positive cells.

Protecting groups that allow substitutions without jeopardising the uncaging efficiency are of great interest because they can potentially be built into an antibody-drugconjugate (ADC). ADCs consists of an emergent class of therapeutic agents that links small cytotoxic molecules (drugs) to monoclonal antibodies to treat cancer in a targeted therapy manner.[71] Bearing this in mind, Stenton *et al.* reported a bifunctional thioether substituted alkyne linker for prodrugs activation by palladium.[72] This linker, containing in one handle Doxorubicin, was incorporated into the cysteine site of proteins and allowed them to design an ADC that targeted and killed HER2+ cells in the presence of Pd.

Conceivably, the most recent additions to the toolbox of cages and triggers are Oliveira and co-authors' study on platinum uncaging. They showed for the first time that deprotecting secondary amines (masked as amides) releases a fluorescent probe triggered by platinum (K_2PtCl_4 or Cisplatin (CisPt)).[73] In HeLa cells, the same strategy was applied to uncage the prodrug MMAE-am, the antineoplastic drug monomethylauristatin E (MMAE) protected as a pentynoyl amide. They also showed that platinum could trigger the uncaging of an ADC with a pentynoyl linker containing an amide protected MMAE to extracellularly release the drug to cancer cells. Moreover, they showed the reduction in the size of the tumour by using CisPt, one of the most traditional chemotherapeutic agents, to uncage a derivative of 5-FU in a colorectal zebrafish xenograft model.

Scheme 7. Transition metal-mediated uncaging strategies developed in the context of bioorthogonal chemistry.

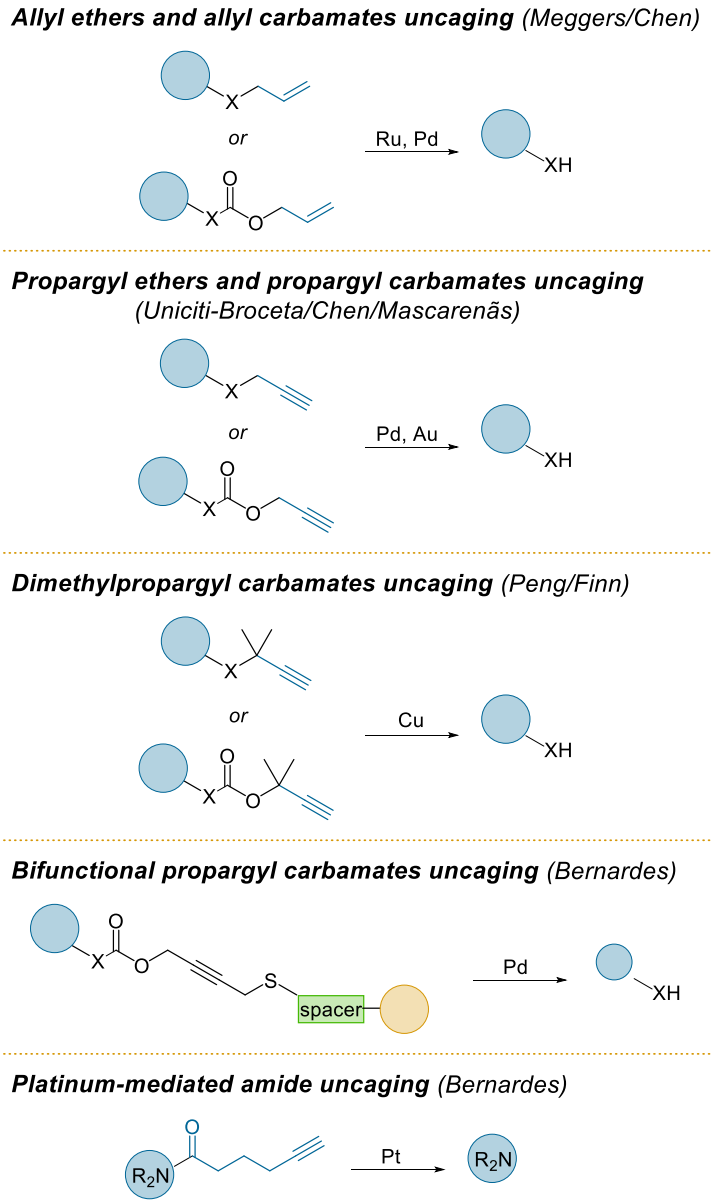

Source: the author, 2021.

All these different strategies for bond cleavage have been applied in the context of bioorthogonal chemistry with several different outcomes: protein modification, cell engineering, fluorophore, and prodrug activation.

In 2014, Li and co-authors reported for the first time the activation of a target protein by palladium-mediated cleavage reaction in living cells.[74] The strategy consisted in protecting

a lysine residue with a propargyl carbamate group that in the presence of a palladium complex released the protein analogue in its free form that, in turn, could be incorporated into a protein in a spatio-temporally controlled fashion. This work led the way to manipulate the activity of proteins of interest selectively and intracellularly by means of bond-cleavage reactions.

A great example of bioorthogonal cleavage being used in cell engineering is the work of Wang *et al.* published in 2015.[75] They design a procedure to generate neuramic acid (Neu), a type of sialic acid, within living cells by means of a palladium-triggered cleavage reaction. They used palladium nanoparticles in the depropargylation of *N*-(propargyloxycarbonyl)neuramic acid (Neu5Proc) that led to the direct conversion into Neu on cell-surface glycans. The strategy was also applied to modulate cell-surface charge which becomes neutral and clusters by the removal of the protecting group of Neu5Proc. It is important to highlight that Neu5Ac consists of a receptor for influenza viruses, and it is directly involved in the initial process of infection by this sort of viruses. Therefore, being able to manipulate it locally in biological environment provides wide range of future applications from cells to tissue engineering for regenerative medicine.

In 2019, Wang and co-authors managed to achieve reversible masking and reactivation of amines and alcohols on cancer drugs, protein side chains, and unmodified cell surface. Copper (I) complexes were employed to mediate the depropargylation of substituted propargylcarbamates in living cells, which provide them with a temporal and reversible conjugation strategy.

Li *et el*, developed a system in which a fluorescent marker, for cellular imaging, and an anti-cancer drug are released simultaneously.[20] This was achieved by protecting a coumarin as a propargyl ether and functionalising it with the anticancer drug nitrogen mustard. In the presence of palladium, by breaking the carbamate C-O bond, a chain reaction is initiated and results in the release of the highly interesting products. This system was tested in rats and was found to be efficient in inhibiting tumour growth.

It is not a coincidence that the main trigger in the examples is palladium. After 2011, when Yusop and co-authors published a seminal paper in which palladium was used for the first time as mediator for biorthogonal cleavage reactions intracellularly,[67] this soon expanded to become the most studied method for prodrug activation.[76,73]

2.4.1.1.1 Mechanism of palladium-mediated cleavage reactions

Mechanistic aspects of the deallylation reaction

Originally thought as an allylic substitution reaction, the removal of allyl protecting groups by means of C-O bond cleavage catalysed by palladium is present in the literature since the late 70s and currently it is known as Tsuji-Trost reaction.[77,78]

Aiming at biological applications, Koide and co-authors were the first to explore it in aqueous medium.[79] They developed a fluorescent sensor for palladium detection in pharmaceutical and mining industries. The probe consisted of allyl ether fluorescein caged derivatives, which fluorescent product is released in the presence of Pd and PPh_3. It is important to note that palladium can be detected in any oxidation state and that is due to the PPh_3 acting as both the reducing agent and ligand, no reaction takes place in its absence. Based on their results, they proposed the reaction occurs via an allylic oxidative insertion of Pd(0), forming a π-allylpalladium intermediate, that suffers a nucleophilic attack leading to the formation of an allyl-nucleophile product and the uncaged fluorophore, just accordingly to the mechanism of a traditional Tsuji–Trost reaction (Scheme 8).[80,81]

Scheme 8. Catalytic cycle of the palladium-catalysed deallylation of ethers carbamates (analogous to a Tsuji–Trost reaction).

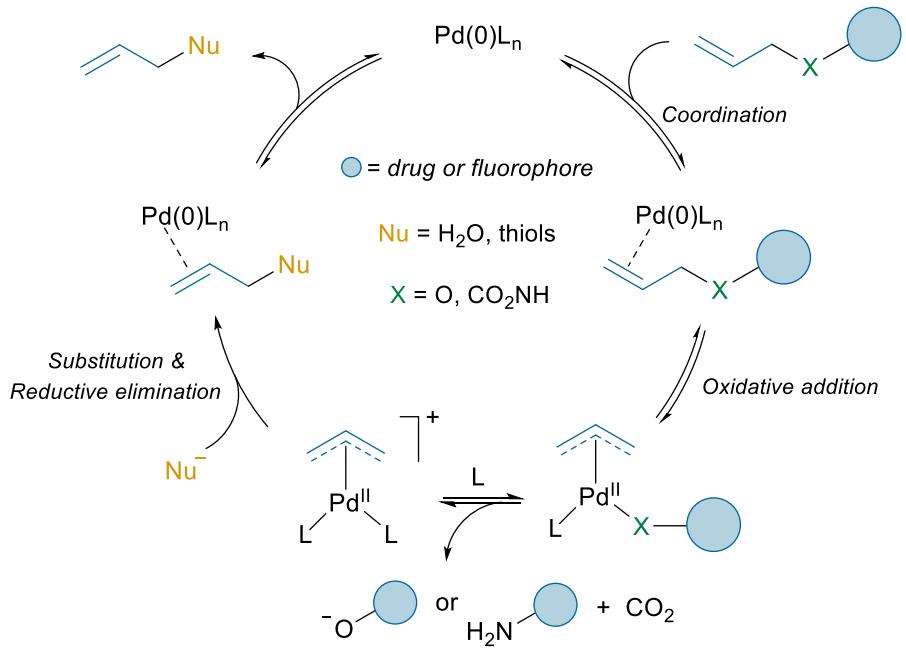

Source: the author, 2021.

Koide's group deepened the knowledge about the catalytic system and, in 2009, published a follow-up study. It was hypothesised that the electron-rich triphenylphosphine complex would convert palladium to a coordination saturated species and therefore, inactivate it. This would justify their low TON, because the $Pd(0)(PPh_3)_4$ complex would exchange any ligand by the substrate and the π-allylpalladium intermediate would not be formed.[82] Besides, the reaction was completely inhibited in the presence of sulphides due to the strong affinity between sulphur and palladium that deactivates the catalyst. Alternatively, they proposed the use of $NaBH_4$ that in solution generates hydrides that can compete with sulphides and rapidly reduce Pd(II) to Pd(0). Then, different ligands were tested being the best results achieved with tri-2-furylphosphine (TFP). The explanation presented was that TFP, an electron-poor ligand, favours the turnover of the π-allylpalladium species by making the complex more labile, leaving the d-orbitals available for the oxidative insertion.

As mentioned previously, a paper published in 2011 by Mark Bradley and co-authors explored for the first time the deallylation mediated by palladium nanoparticles in a biological setup.[67] In biological-like conditions, they reached turnover numbers up to 30, however extremely low conversion in all different media (PBS, RPMI, DMF and cell extract). Nevertheless, no mechanistic aspects for the use of nanoparticles were brought to attention.

In a previously mentioned paper by Li *et al,* it was reported a palladium-mediated rescue strategy to activate a protein within living cells by means of an uncaging reaction.[74] Prior to their investigation in living cells, they screened six palladium complexes to identify an efficient catalyst for Alloc-Rho and Proc-Rho deprotection. Using 1 equivalent of Pd in aqueous conditions (5% DMSO), the Alloc-Rho deprotection was less efficient than the reaction with Proc-Rho for all catalysts tested but, in both cases, the highest conversions were obtained with $Pd(dba)_2$ and $Allyl_2Pd_2Cl_2$. Besides, an interesting result was that adding a phosphine ligand (TPPTS) to $Pd(NO_3)_2$ affected positively the conversion for deallylation but not for depropargylation. In regard to mechanistic aspects, the authors evoke the π-allylpalladium pathway, which is coherent with observation of the phosphine effect considering it might be working to reduce the metal precursor as well as stabilise zerovalent palladium species.

Unciti-Broceta and co-workers reported novel prodrugs consisting of protected gemcitabine, a known antineoplastic agent, and its release mediated by Pd(0)-nanoparticles trapped in amino-functionalised polystyrene resin-microspheres.[19] The drug was masked in a carbonate fashion, in the sugar 5′-OH position, and also in a carbamate fashion, in the 4-NH_2 position, however the carbamate was not stable enough in cell media for biorthogonal purposes.

When deallylation was tested in different cell lines, BxPC-3 and Mia PaCa-2, with similar sensitivity to the drug, a higher decrease in cell viability was detected for the BxPC-3 cells, indicating the drug was released more efficiently in this linage. Once the results are closely connected to the cell type, it is only logical to consider the media must have played a role in the uncaging activity. BxPC-3 the cells were grown in RPMI medium, while Mia PaCa-2 cells were grown in DMEM. It was noted one relevant difference in these media composition when it comes to palladium mediated reactions: RPMI contains glutathione (GSH),[16] which is known for potentially increasing the efficiency of deallylation.[67] Even though this work had little to add in terms of mechanistic discussions, it is relevant for showing how delicate it is to shift from lab benches conditions to cell environment and how subtleties may cause a great impact in the reaction progress.

When investigating uncaging reactions mediated by discrete palladium (II) phosphine complexes, Mascareñas' group demonstrated the enhancing effect of sodium ascorbate or GSH addition to the deallylation efficiency in water at 37 °C.[83] In the presence of these additives, the yield for 24 h of reaction was 50% and 94% respectively. In their absence, it was up to only 10%. These evidence strongly support the hypothesis that the deallylation occurs by Pd(0) that is formed by the reduction of the Pd(II) complexes when combined with reducing agents sodium ascorbate (NaAsc) and GSH.

In 2019, Koide *et al.* made a meticulous study of kinetic parameters associated with DFT calculations of the Tsuji–Trost allylic cleavage in aqueous milieu.[84] It was explored effect of the concentration of substrate, phosphine (tris(2-furyl)phosphine) (TFP), phosphate ion (buffer), $NaBH_4$, palladium and DMSO on the deprotection of the allylated fluorophore Pittsburgh Green. The experiments revealed the turnover limiting step (TLS) for this reaction alters according to the conditions resulting in three different kinetic regimes: Regime 1, when $\Delta H^{\ddagger} > 0$, the TLS corresponds to the oxidative addition; Regime 2, when $\Delta H^{\ddagger} \approx 0$, TLS is the nucleophilic attack; and Regime 3, $\Delta H^{\ddagger} < 0$, TLS is the association step. The regime is dependent on different temperatures or even substrate concentrations, meaning that in the course of the reaction the regime might shift due to substrate consumption. Another significant addition presented in this paper was the identification of the nucleophile. Under the evaluated conditions, there are three species that can potentially act as nucleophiles: phosphate, water, and the phosphine. The LC-MS data showed (and it was also supported by DFT calculations) an allylated-tris(2-furyl)phosphine specie at the end of the reaction, revealing that the phosphine acts not only as a palladium ligand but also as a nucleophile. When it comes to cellular and

biological applications, extremely low concentrations are common practice. Therefore, it is noteworthy that with computational studies they showed that at micromolar or nanomolar concentrations of the substrate the TLS may be the association step. Before these findings, the literature never referred to the association step as a possible TLS.

Scheme 9. Catalytic cycle of a Tsuji–Trost reaction with different Turnover Limiting Steps as proposed by Koide and co-authors.

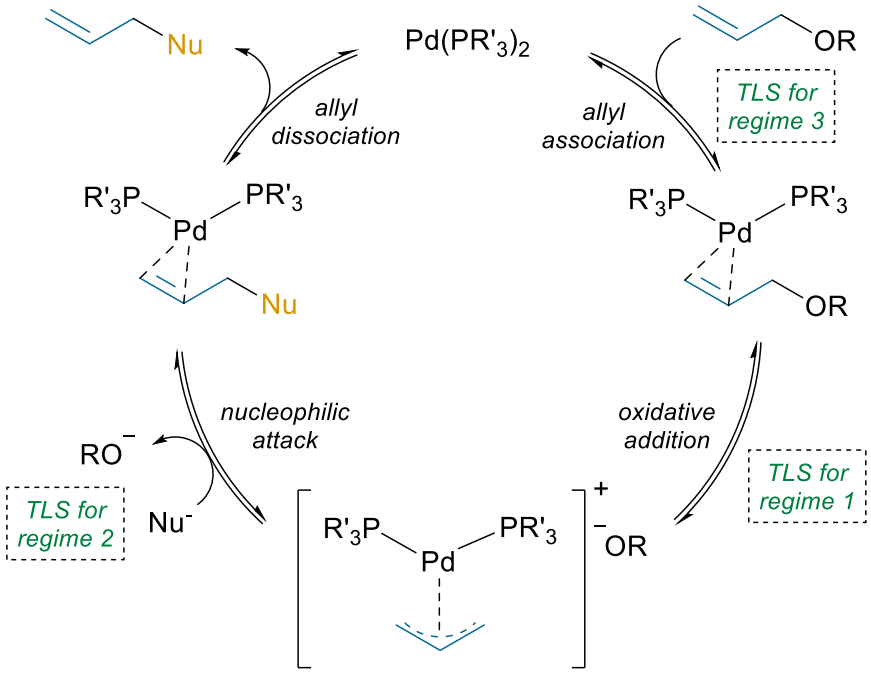

Source: the author, 2021.

Perhaps one of the latest additions in the topic of palladium catalysed deallylation was brought by Zhize Ou *et al.* in 2021.[85] Even though it was not in the context of bioorthogonal chemistry, yet, once again interested in fluorescent probes for palladium determination, it was reported the successful allylic C-N bond cleavage triggered by palladium. The deallylation of a quaternary ammonium modified phenanthroimidazole derivative occurred in ethanol or aqueous media (with addition of CTAC) at room temperature and exhibited selectivity for Pd(0). However, by adding the ligand TFP or PPh_3, that also act as reducing agent, the reaction could also be mediated by Pd(II) precursors. In terms of mechanism, it is stated, just as the previous studies, that Pd(0) in the presence of *N*-allylpyridinium leads to the formation of the π-allyl complex, that undergoes dissociation to yield the deallylated product (Scheme 10. Proposed mechanism for the deallylation of AL-PPI catalysed by Pd(0), proposed by Ou and

co-authors.Scheme 10). Interestingly, there are no mentions to possible ways the dissociation might occur.

Scheme 10. Proposed mechanism for the deallylation of AL-PPI catalysed by Pd(0), proposed by Ou and co-authors.

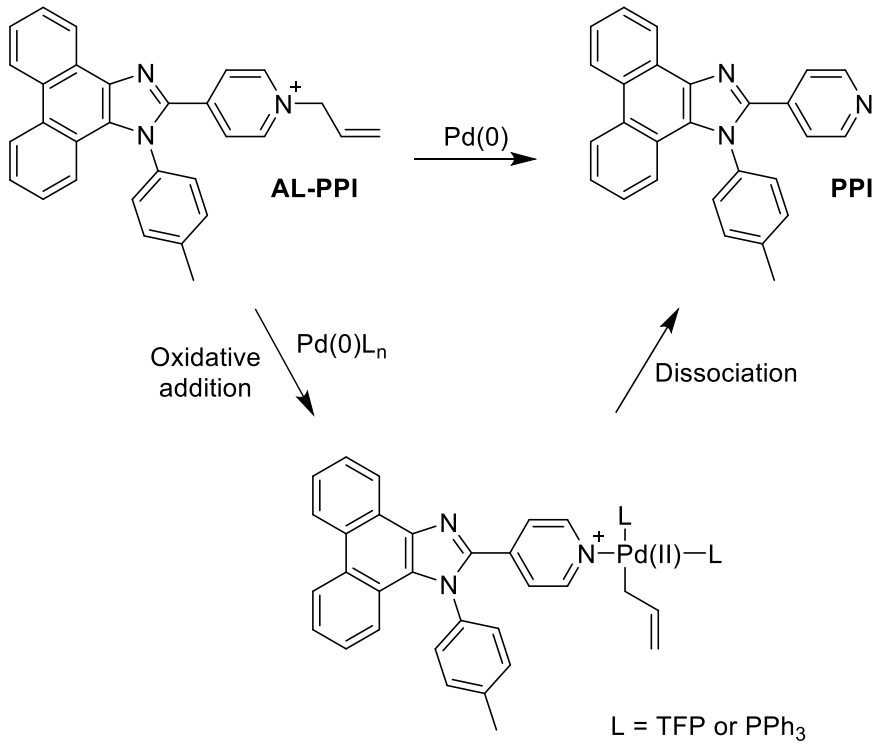

Source: the author, 2021.

Regarding the deallylation reaction in water, great advance was made in terms of mechanistic insights. Nevertheless, when it comes to transposing this strategy to complex milieu such as the biological one, many aspects are not fully understood, and the transition is somewhat erratic. Obviously, the selection of studies presented provide a direction such as the preference for Pd(0) and the enhancing effect of nucleophiles such as GSH. However, the above reports also show how delicate it is to tune parameters to find proper catalyst-substrate affinities. Besides, these systems are dynamic and in biological medium they may undergo uncountable transformations, making it even harder to rationalise.

Mechanistic aspects of the depropargylation reaction

Palladium-mediated depropargylation reaction in aqueous medium debuted in the literature in 2003, in a publication by Manojit Pal and co-authors.[86] Their focus was from a synthetic point of view, however it suited perfectly to protect amines and hydroxylic substrates for bioorthogonal applications. The deprotection of aryl propargyl ethers and amines was performed in DMF/water (2:1) at 80 °C, with triethylamine as a base. For mechanistic proposal it was considered to occur through an allenylpalladium charged intermediate, formed by the oxidative addition of the substrate to the zerovalent palladium (Scheme 11). Of note, the majority of metallic precursors employed contained Pd(II) and they were reduced *in situ* to generate the catalytically active species Pd(0). The evidence that the reduction takes place lies in the fact that base (Et_3N or $NaHCO_3$) and heat were mandatory for the product obtention.

Scheme 11. Proposed mechanism for the depropargylation promoted by Pd(0) formed *in situ* and followed by an oxidative addition. Initially proposed by Manojit Pal.

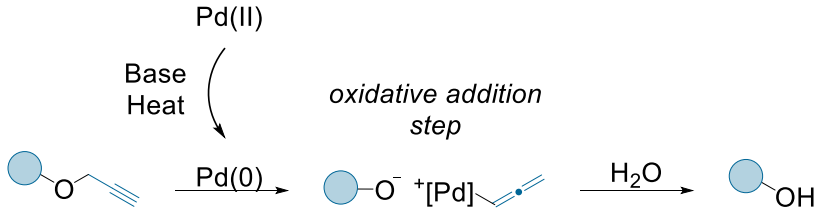

Source: the author, 2021.

Working in the uncaging of a propargyl ether fluorescein with Pd(0), Pd(II) and Pd(IV) complexes, Santra *et al.* found results there were not in agreement with the mechanism that was until then proposed.[87] The reaction was conducted in aqueous medium (10% CH_3CN), room temperature and without additives that could act as nucleophile or reducing agent for the metallic precursors. Those conditions did not favour the formation of Pd(0) and, therefore, another mechanism, based on Pd(IV) or Pd(II) species, should be operating. The proposal consisted of the coordination with Pd(II/IV) species followed by the hydration of the propargyl ether, leading to a terminal carbonyl compound, that can undergo β-elimination (Scheme 12). An internal alkyne was also employed, resulting in the complete inhibition of the reaction with Pd(0) and in a decreased yield with Pd(II) and Pd(IV). This result is extremely interesting because in the case of an internal alkyne, the oxidative addition step is not possible, which justifies the Pd(0) inactivity. Under these circumstances, the authors suggest that via Pd(0), the

mechanism in action is the one proposed by Manojit Pal (Scheme 11) and with Pd(II/IV), the hydration pathway is favoured (Scheme 12).

Scheme 12. Mechanism proposed by Ahn for the Pd(II/IV) mediated depropargylation, the hydration pathway.

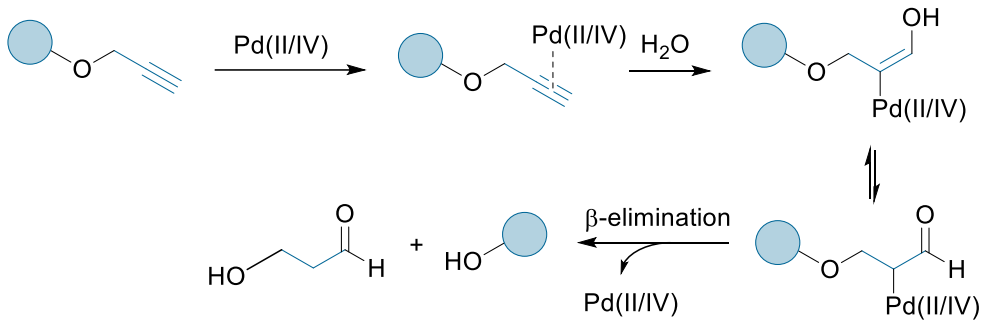

Source: the author, 2021.

In 2013, Rambabu and co-authors studied the depropargylation of aryl ethers and amines in water promoted by palladium supported on carbon.[88] The reaction was conducted under nitrogen, 80 °C, for 5-6 h in the presence of 2-ethanolamine. It was attributed to ethanolamine two essential roles, since in its absence no reaction took place: of aiding in the solubilisation of substrates also yielding catalytic active species soluble in water. The addition of Hg(0) also inhibited the reaction, probably due to its strong dπ–dπ interaction with palladium leading to the catalyst inactivation. They also invoked the Pd(0) oxidative addition mechanism, but cited the formation of 1-hydroxyacetone as product, without providing experimental data, though.

As mentioned before, the first time that the depropargylation reaction, promoted by palladium, was used in the context of bioorthogonal uncaging was in 2014 by Unciti-Broceta *et al.*[89] Besides what was before mentioned, and even though it was not suggested a new pathway suggested, this work is relevant in terms of mechanism because for the first (and only) time, the formation of acetol ([M + Na]+, m/z = 96.8) was identified, by ESI-MS. This data supports the oxidative addition mechanism previously proposed by Manojit Pal.[88]

In their studies to modulate the activity of proteins, Li *et al.* showed that the palladium-triggered uncaging of Proc-Rho and Proc-lysine were more efficient than the Alloc-Rho and Alloc-lysine.[74] The choice of metal complexes was $Allyl_2Pd_2Cl_2$ and $Pd(dba)_2$ for the sake of comparison between palladium oxidation states Pd(II) and Pd(0), respectively. They suggested that $Allyl_2Pd_2Cl_2$ would generate Pd(0) and react similarly to $Pd(dba)_2$ and since they showed higher efficiency than Na_2PdCl_4, they assumed that it was due to Pd(0) being more active than

Pd(II/IV) to mediate this reaction. Bearing this in mind, they showed that the addition of NaAsc to the different Pd precursors increased the reaction rate and yield, including for Na_2PdCl_4, but no effect was observed when the additive was combined with $Allyl_2Pd_2Cl_2$ and $Pd(dba)_2$. They justified this by saying that since both of these complexes generated Pd(0) in solution after an *in situ* reduction by means of a nucleophilic attack and a reductive elimination, NaAsc was ineffective. Even though there are examples of the Pd(II) reduction with the assistance of hard nucleophiles, such as hydroxide, alkoxide, fluoride and even water, it is only known to occur in the presence of phosphine ligands.[90] However, there is no systematic evidence that the same reaction could take place in phosphine-free systems, under milder conditions like in PBS buffer at 37 °C.

In 2019, Coelho *et al.* thoroughly studied the kinetics of the depropargylation of the 2,4-dinitrophenyl propargyl ether (DNPPE) mediated by Na_2PdCl_4 in aqueous medium (phosphate buffer, pH 7.4) without bases or ligands.[91] A wide range of experimental techniques such as ESI-MS, X-ray absorption spectroscopy (XAS), high-resolution transmission electron microscopy (HRTEM), and computational analysis provided data showing the reaction obeys a biphasic kinetics, being composed of a fast and a slow reaction. In the faster phase (Rx1), the displacement of two chloride ions from the precursor Na_2PdCl_4 occurs due to substrate coordination and ends after two turnovers, because the metal is inhibited by the propargyl hydrolytic product, forming the Pd(3-hydroxypropanal)$_2Cl_2$ complex ($Pd(HPA)_2Cl_2$, Scheme 13). The catalytically active species in the first phase of the reaction were determined through poisoning experiments (Hg, CS_2 and EDTA). Only the addition of EDTA resulted in the reaction inhibition. The rate determining step for Rx1 was attributed to the β-O elimination from a Pd(II) complex intermediate to release the product at each turnover (Scheme 13). Computational analysis also showed that the replacement of a third chlorine atom, or of the hydrolytic product attached to Pd ($Pd(HPA)_2Cl_2$, Scheme 13), by the substrate is disfavoured due to a high energetic barrier. After the two turnovers, the slow phase (Rx2) takes place through a different path. Rx2 was proposed to be the hydrolysis of the substrate by Pd(0) nanoparticles. The Pd(0)-NPs are allegedly formed by decomposition of $Pd(HPA)_2Cl_2$ and they were identified by dynamic light scattering, HRTEM and had their state of oxidation confirmed by XAS. It was showed that the chlorides of the $Pd(HPA)_2Cl_2$ are less labile because of the coordination with the product formed in the Rx1, as assessed by DFT studies. This reduced lability prevents the coordination of new molecules of substrate and, in turn, limits the number of turnovers.

Scheme 13. Mechanism proposed for the fast phase (Rx1) of the depropargylation of DNPPE by Na_2PdCl_4.

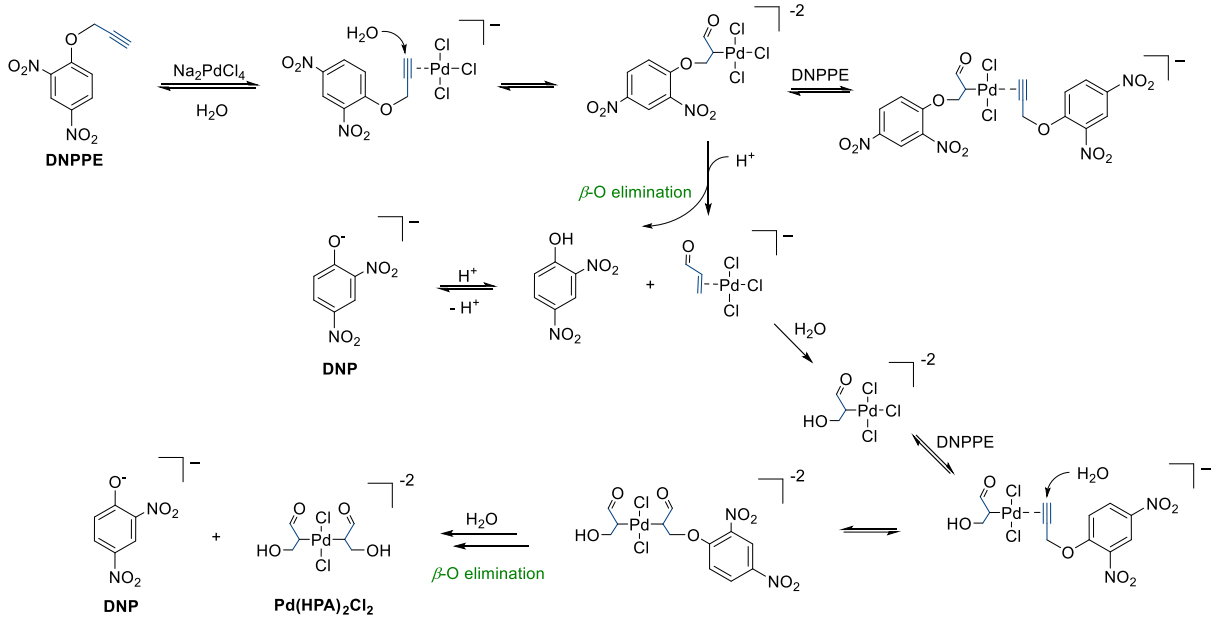

Recently, when Brik's research group was investigating gold-mediated uncaging for protein synthesis and manipulation, a novel method for propargylamide uncaging by palladium on model peptide was developed.[92] Amongst a set of catalysts containing both Pd(II) and Pd(0), the best depropargylation results were achieved with $PdCl_2$ and $Pd_2(dba)_3$, 90% and 30%, respectively, in biological-like conditions (Gn·HCl/Na_2HPO_4 buffer, pH 6–7, 42 °C, 3 h). Motivated by the better yields exhibited by Pd(II), another set of eight Pd(II) complexes was screened with results varying from 0-90% of yield for the peptide depropargylation, only $Pd(NO_3)_2$ was able to match the reactivity of $PdCl_2$. Foreseeable, when the uncaging of allylated-peptides was tested under the same conditions and even for longer times, no reaction was detected. To evaluate scope, the model peptide reaction was expanded to a library consisting of 10 synthetic peptides based on different amino acids combined with Gly. The outcome was disappointing since conversions varied from 5-20%, even after modifying the conditions such as increasing the temperature up to 60 °C.

Another recent contribution came from the field of ratiometric sensing systems. Ahn and co-authors investigated the detection of palladium by fluorescent probes, based on a benzocoumarin dye, by comparing three propargyl aryl ethers bearing electronically-different

self-immolative linkers.[93] The evaluation was conducted in aqueous medium (10% CH_3CN) with Pd(0) and Pd(II) and showed that the more electron-deficient linker, with a *o*-dichlorophenyl moiety, reacted faster than the mono-chloro- and non-chloro analogues. Remarkably, it was mentioned the data suggested the depropargylation reaction was slower with Pd(II) when compared to Pd(0), even though previous examples reported otherwise.[91,92] They went further and tested the system in A549 cells to show that the system is able to detect Pd in both oxidation states in biological systems.

The collection of articles aforementioned shows that there is not a consensus about mechanistic pathways or even the effectiveness of one palladium species in regard to the other. This accentuates the complexity of the depropargylation reaction considering that it can be triggered by both Pd(II) and Pd(0) and in some reports, even the rare Pd(IV) makes an appearance. Nonetheless, some trends are visible: in most cases, Pd(0) mediates deallylation while Pd(II) is more reactive towards depropargylation. Also, electronic and steric effects should always be accounted when modulating the reactivity of the pair catalyst-substrate.

Moreover, when it comes to biological milieu, factors such as pH, presence of nucleophiles and reducing agents will have a strong implication on the catalyst integrity and in the reaction progress. Notwithstanding, considering there are some controversies concerning these processes in a reaction flask, it is reasonable that in living systems, with a profusion of parameters to tune, it is even harder to make predictions and rationalisations. In this way, a higher understanding of the uncaging for bioorthogonal purposes will only be achieved by intensifying studies in a systematic manner taking into considerations what is known up to this point.

Of note, the mechanistic proposals were developed for traditional catalysts, salts, and complexes of palladium. There is not a single mechanism proposed in the literature for the reaction catalysed by palladium nanoparticles.

3 EXPERIMENTAL PROCEDURES

This section describes the materials, methods, and techniques employed in this work which was developed as a collaboration between the Laboratory of Biomimetic Catalysis (LaCBio, Federal University of Santa Catarina - Brazil) and GBernardesLab (University of Cambridge – United Kingdom).

3.1 REACTANTS AND SOLVENTS

Palladium acetate (Sigma-Aldrich, 98%), potassium iodide (Nuclear, ACS) sodium borohydride (Sigma-Aldrich, 98%), L-(+)-ascorbic acid sodium salt (Alfa Aesar, 99%), sodium azide (Alfa Cesar, 99%),

Ultrapure water (resistivity of 18.2 mΩ cm) was used in all experiments. All glassware was washed with concentrated nitric acid and rinsed copiously with deionised water prior use.

3.2 PALLADIUM NANOPARTICLES SYNTHESIS

The palladium (II) nanoparticles were prepared according to the procedure developed priorly.[94] The formation of PdI_2-NPs occurs through a ligand exchange in which the acetate coordinated to the metal is replaced by the iodide provided by KI. To prevent the growth and further precipitation of PdI_2, this reaction is conducted in the presence of a polymer which acts as stabilising agent.

In a typical procedure, 12 mL of deionised water were poured to a centrifuge tube, followed by the addition of 3.6 mL of 0.1 mol L^{-1} aqueous solution of the polymer (PVP) and 1.8 mL of a 0.1 mol L^{-1} solution of $Pd(OAc)_2$ in acetonitrile. After mixing it, the tube was left to rest for 10 minutes. After that, 0.54 mL of a 0.5 mol L^{-1} aqueous solution of KI was added. After homogenising it, the tube rested for 2 hours giving time for the particles to grow.

After this period, the PdI_2-NPs were isolated by an addition of acetone as co-solvent and followed by centrifugation. The total volume of the suspension of nanoparticles was split in two tubes, and 36 mL of acetone was added to each tube, and they are centrifuged at 6000 RPM for 20 minutes. Then, the supernatant was removed, and the tubes were left in the oven to dry at 60 °C.

The synthesis of the palladium (0) nanoparticles was conducted in similar manner, however instead of a ligand exchange reaction a metal reduction takes place. For such, the synthesis followed the same procedure, but the KI solution was replaced by a 0.5 mol L^{-1} solution of $NaBH_4$. The isolation steps were also identical. All solutions used in these syntheses were fresh.

3.3 CHARACTERISATION OF THE NANOPARTICLES

3.3.1 Transmission Electron Microscopy

For the TEM analysis, the Pd-NPs were dispersed in water (or DMSO when stated) and ten drops of 4 μL were applied onto a 200-mesh copper grid coated with formvar® and left to dry at ambient temperature. The experiments were conducted in the *Laboratório Central de Microscopia Eletrônica* (LCME - UFSC), on a JEOL JEM-1011 microscope operating at 100 kV. At least 150 particles were manually measured with the software *ImageJ*®. The average particle size was determined by a Gaussian fit of the size distribution.

3.3.2 Small angle X-ray scattering

SAXS experiments were performed on the SAXS1 beamline of the Brazilian Synchrotron Light Laboratory (LNLS, Brazil). The Pd-NPs suspensions were loaded into a temperature-controlled vacuum flow-through cell composed of two mica windows separated by 1 mm, normal to the beam. The collimated beam (k = 1.55 Å) crossed the sample through an evacuated flight tube and was scattered to a Pilatus 300 K 2D detector (Dectris) and a 2D CCDmarCCD 165 detector, respectively. The incident beam was detected at 500 mm distance on the SAXS1 beamline to achieve the scattering vector range q, from 0.1 to 5 nm^{-1}. The sample-to-detector distance was calibrated using silver behenate as a standard. The resulting scattering curves were normalised and fitted with *SASfit*® software, applying the Sphere and Beaucage Power Law models.[95]

3.3.3 X-ray absorption near edge structure

XANES experiments were performed on the XDS beamline of the Brazilian Synchrotron Light Laboratory (LNLS, Brazil). Spectra were acquired at room temperature in transmission mode with three ionization chambers using a Si (311) double-crystal monochromator and a toroidal focusing mirror. As standard, Pd foil was used to perform energy calibration in all scans. Five to ten spectra were collected to improve the signal-to-noise ratio. Spectra were acquired in the range of 24150−25400 eV with 2-6 s/point around the Palladium k-edge energy at 24.35 keV. Data were processed using the *Ifeffit* and *Demeter* packages and fitted using *FEFF* and *Artemis in Demeter* package in R-space applying the k^2-weight functions in a first-shell approach.

3.3.4 X-ray photoelectron spectroscopy

XPS data of samples were obtained with an SPECSLAB II (Phoibos-Hsa 3500 150, 9 channeltrons) SPECS spectrometer using an X-ray source Al Kα which provide photons with 1486.6 eV on Brazilian Synchrotron Light Laboratory (LNLS, Brazil). The acquisition parameters were Epass = 40 eV, 0.1 eV energy step and acquisition time of 1 s/point. The samples were placed on stainless steel sample-holders and were transferred under inert atmosphere to the XPS analysis chamber where the residual pressure inside was about 1×10^{-8} Torr. The binding energies (BE) of Pd 3d and C 1s were referenced to the C 1s peak at 284.5 eV, providing accuracy within ±0.2 eV.

3.3.5 Flame atomic absorption spectrometry

The FAAS analyses were carried out with a Hitachi Z-8230 Polarized Zeeman spectrometer available at the *Central de Análises do Departamento de Química* (UFSC, Brazil). In triplicates, 1 mL of freshly prepared aqua regia was added to 1 mg of Pd-NPs and left for 12 hours for the sample digestion. After that, the solutions were diluted to 10 mL and submitted to analysis.

3.4 ARYL ALKENYLATION REACTION

3.4.1 Synthesis of the diazonium salts

The diazonium salt (DS) was synthesized according to the methodology previously described and represented in Scheme 14.[96] Regardless of the substituent, the DS was synthesized in a similar way to tetrafluoroborate of 4-bromobenzenodiazonium (DS-Br), whose description follows. In an Erlenmeyer, 4-bromoaniline (10 mmol) was suspended in 2.5 mL of deionized water and followed by the addition of 2.5 mL of HCl. This suspension was kept under stirring for 20 minutes and then it was cooled to -10 ºC. When the temperature was reached, 1.8 mL of a 7.2 mol L^{-1} aqueous solution of $NaNO_2$ was added dropwise, keeping the temperature always below -5 ºC through the whole step. After 10 minutes, 3 mL of a 4.7 mol L^{-1} $NaBF_4$ solution was added and resulted in the formation of a precipitate. Then, ethyl ether was added, and the precipitate was filtered using a Buchner funnel. The solid was dissolved in acetone and filtered again. Finally, ethyl ether was added to the filtrate and, after cooling it in an ice bath, the precipitate was vacuum dried.

Scheme 14. Synthesis of the diazonium salt DS-Br.

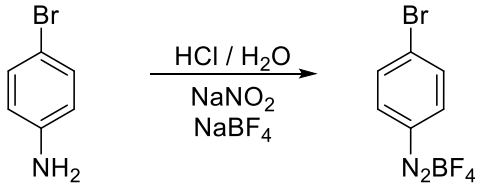

Source: the author, 2021.

3.4.2 Aryl alkenylation catalysed by Pd-NPs

The typical procedure (Scheme 15) consisted of the addition of the diazonium salt (0.39 mmol) to a round bottom flask with the palladium catalyst (0.039 mmol) and 2 mL of deionized water. The mixture was sonicated until complete dissolution. Then styrene (0.26 mmol) was added, and the solution was kept under stirring, at 25 ºC. After 24 hours, dichloromethane (2.5 mL) was added and organic fraction separate was washed with saturated NaCl aqueous solution, dried over anhydrous sodium sulfate, and evaporated under reduced pressure. The crude material was purified by silica gel chromatography with hexane to afford the corresponding pure coupling product.

Scheme 15. Aryl alkenylation reaction between a substituted arenediazonium salt and styrene in water, catalysed by palladium nanoparticles and all possible products.

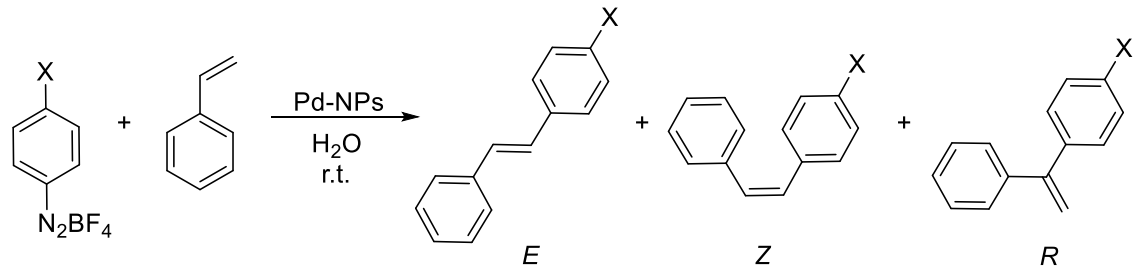

X = Br, Cl, Me, Et, OMe

Source: the author, 2021.

3.5 PALLADIUM MEDIATED UNCAGING REACTIONS

3.5.1 Synthesis of the propargyloxycarbonyl-coumarins

The insertion of the propargyloxycarbonyl protecting group in the coumarins was performed as shown in Scheme 16, in a similar fashion to the procedure described in the literature.[75]

50 mg of 7-amino-4-methylcoumarin was suspended in 750 µL of CH_2Cl_2 and transferred to a 10 ml flask. The system remained under stirring and in an ice bath for a few minutes until the temperature stabilised at -5 ºC. After that, 33.4 µL of propargyl chloroformate solubilised in 750 µL of CH_2Cl_2 was added dropwise. About 10 minutes after the end of the addition, 0.0287 g of $NaHCO_3$ was added. The ice bath was then removed, and the system was kept under stirring for 24 hours. After that period, 40 ml of 0.5 mol L^{-1} HCl was added to the reaction mixture. The resulting suspension was filtered through a Buchner funnel and the solid was washed with ethyl ether to yield a white powder consisting of the pure product.

Scheme 16. Synthetic scheme for the protection of substituted coumarins with propargyl chloroformate, yielding X-proc-coumarins.

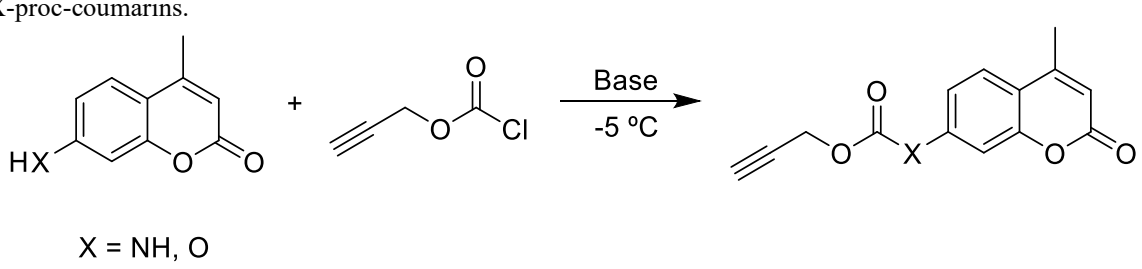

X = NH, O

Source: the author, 2021.

The reaction with 7-hydroxy-4-methylcoumarin was carried out similarly. However, due to the higher coumarin pK_a, a stronger base was required. In this case, the reaction and work-up followed the same procedure, but $NaHCO_3$ was replaced by Cs_2CO_3 instead.

3.5.2 Synthesis of the propargyloxycarbonyl-doxorubicin

This synthesis was carried out by Dr. Juraj Konc as follows. To a suspension of doxorubicin·HCl (116 mg) in 5 mL of anhydrous DMF, 140 µL of DIPEA was added dropwise under N_2 atmosphere. The reaction mixture was stirred at room temperature for 15 min. Then, it was cooled to -10 °C and 22 µL of propargyl chloroformate in 0.5 mL of anhydrous DMF was added dropwise. The mixture was kept under ice bath for 10 more minutes and then the bath was removed, and it was kept at room temperature for 30 minutes. Deionized water was used to quench the reaction (100 µL). The solvents were removed under reduced pressure (co-evaporation with toluene, 5 times). The resulting red solid was washed three portions of 5 mL of EtOAc. The remaining starting material was filtered off while the filtrate was concentrated under reduced pressure and purified by flash chromatography (3% MeOH in DCM) to yield the propargyl carbamate doxorubicin (45%) as a red solid.

Scheme 17. Synthetic scheme for the protection of Doxorubicin with propargyl chloroformate, yielding Proc-Dox.

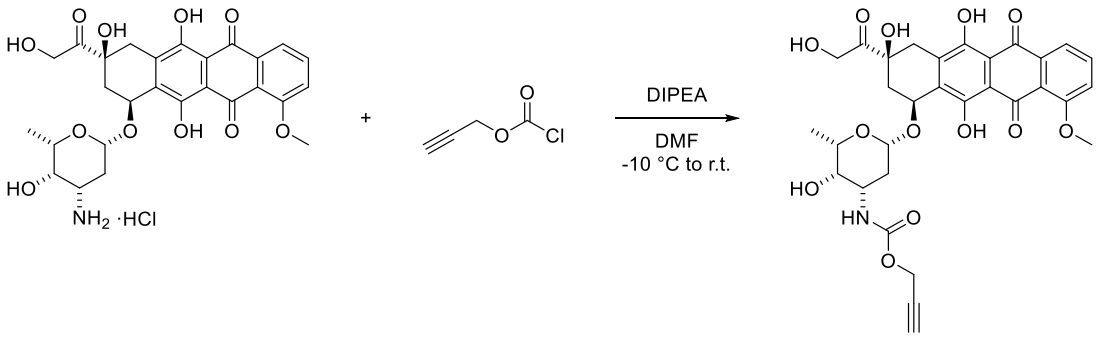

Source: the author, 2021.

3.5.3 Synthesis of the allyloxycarbonyl-doxorubicin

This synthesis was carried out by Dr. Juraj Konc as follows. To a suspension of doxorubicin·HCl (116 mg) in 5 mL of anhydrous DMF, 140 µL of DIPEA was added dropwise under N_2 atmosphere. The reaction mixture was stirred at room temperature for 15 min. Then, it was cooled to -10 °C and 22 µL of allyl chloroformate in 0.5 mL of anhydrous DMF was added dropwise. The mixture was kept under ice bath for 10 more minutes and then the bath was removed, and it was kept at room temperature for 30 minutes. Deionized water was used to quench the reaction (100 µL). The solvents were removed under reduced pressure (co-evaporation with toluene, 5 times). The resulting red solid was washed three portions of 5 mL of EtOAc. The remaining starting material was filtered off while the filtrate was concentrated under reduced pressure and purified by flash chromatography (2% MeOH in DCM) to yield the propargyl carbamate doxorubicin (36%) as a red solid.

Scheme 18. Synthetic scheme for the protection of Doxorubicin with allyl chloroformate, yielding Alloc-Dox.

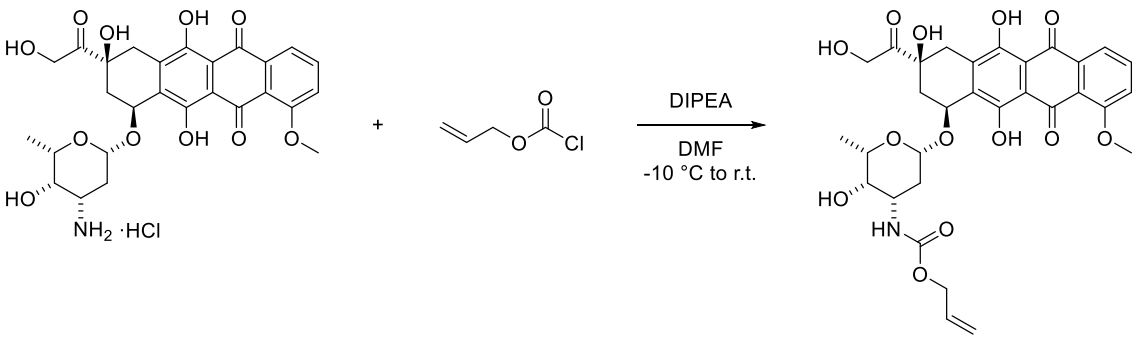

Source: the author, 2021.

3.5.4 Synthesis of the allyloxycarbonyl-rhodamine

The procedure to synthesize the Alloc-Rho was based on a previous description of the literature.[66] To a suspension of Rhodamine 110·HCl (50 mg) in anhydrous DMF (0.8 mL) cooled with ice bath and under N_2 atmosphere, anhydrous pyridine (35 µL, in 0.2 mL of anhydrous DMF) and allyl chloroformate (30 µL) were added dropwise. The reaction mixture was left to warm up to room temperature overnight under stirring. Then the reaction mixture was diluted with EtOAc (10 mL), washed with HCl solution (5%, 2×10 mL), then the aqueous phase was extracted with EtOAc (2×10 mL). The joined organic phases were washed with 15 mL of a saturated $NaHCO_3$ solution, dried with anhydrous $MgSO_4$ and solvents were removed under reduced pressure. The crude product was purified by flash chromatography (1% MeOH in DCM) to afford the Alloc Rhodamine 110 (64%) as a colourless solid.

Scheme 19. Synthetic scheme for the protection of rhodamine 110 with allyl chloroformate, yielding Alloc-Rho.

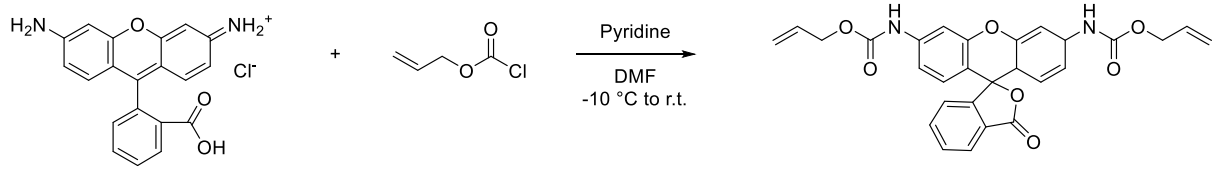

Source: the author, 2021.

3.5.5 Synthesis of the propargyloxycarbonyl-rhodamine

Rhodamine 110·HCl (50 mg) was dissolved in dry 800 µL of dry DMF under N2 atmosphere and cooled in an ice bath. Then, 30 µL of propargyl chloroformate and 35 µL of pyridine were added dropwise. This reaction mixture was left stirring under room temperature overnight. Then, EtOAc (10 mL) was added to the solution which was washed twice with 5% HCl (2 x10 mL each). The aqueous phase was extracted with EtOAc (2x10 mL), then the organic phase was washed with 15 mL of NaHCO3 saturated solution and dried with anhydrous $MgSO_4$. After the solvent removal under low pressure, the crude product was purified by column chromatography with hexane/ethyl acetate (2:1). The resulting product was isolated as a white solid (18%).

Scheme 20. Synthetic scheme for the protection of rhodamine 110 with propargyl chloroformate, yielding Proc-Rho.

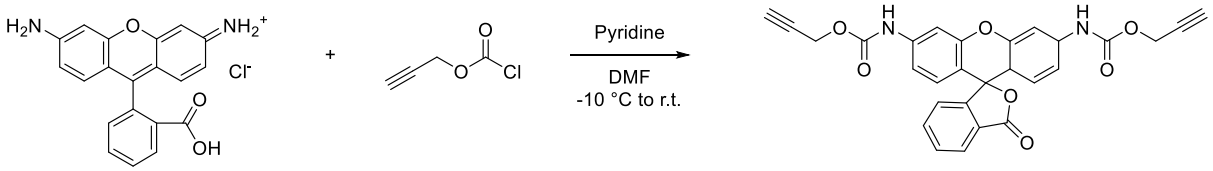

Source: the author, 2021.

3.5.6 General procedure for the UV-vis kinetic studies

The kinetic study of the uncaging of the *O*-Proc-coumarin was performed by means of UV-vis spectroscopy in a spectrophotometer UV-vis Varian Cary 50 BIO connected to a thermostatic bath with capacity of up to 18 cuvettes. The reactions were conducted in quartz cuvettes, in aqueous medium (5% DMSO), controlled pH, temperatures of 37 °C (Scheme 21). The progress was followed by the appearance of the product in λ_{max} = 364 nm, according to the calibration curve. The addition of the reagents to the cuvette always respected the same order: buffer, DMSO, palladium catalyst followed at last the substrate solution, which started the reaction. All kinetics experiments were performed at least twice, in duplicates.

Scheme 21. General scheme for the coumarin uncaging mediated by palladium nanoparticles.

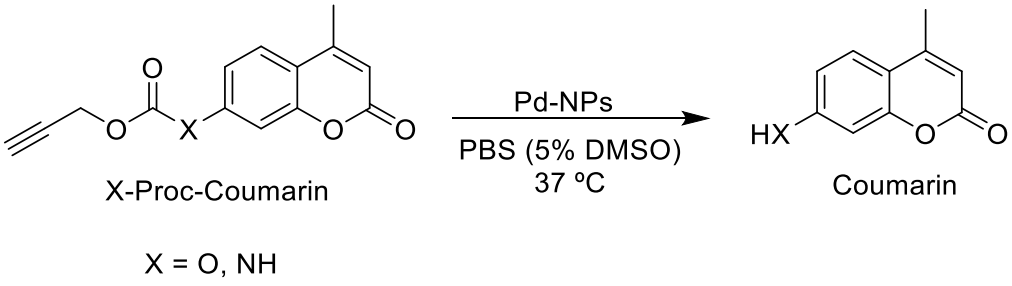

Source: the author, 2021.

3.5.7 General procedure for the fluorescence kinetic assays

The uncaging of both *N*-Proc- and *N*-Alloc-coumarin were assessed via fluorometric assays. The experiments were performed on a TECAN Infinite M200 microplate reader and a SpectraMax i3x Microplate Reader. Most of the experiments were performed on Greiner 96-

well, flat bottom, black microplates. The microplates were sealed with optically clear heat seals or peelable adhesive seals. The poisoning kinetic experiments were performed on 4 mL quartz cuvettes. The kinetics followed the increase in the fluorescence intensity which resulted from the uncaging of the coumarin, $\lambda_{excitation}$ = 380 nm and $\lambda_{emission}$ = 500 nm. The linear correlation between fluorescence intensity and coumarin concentration is shown in the results. All experiments were performed at least in duplicates.

3.5.8 Mechanistic investigation: Poisoning experiments

3.5.8.1 Mercury poisoning

To investigate the possibility of superficial, heterogenous catalysis, mercury was added to the reaction medium. It is known that Hg reacts with Pd(0) species by amalgamating the surface which leads to catalyst inhibition.[97] In this case, the standard procedure for the kinetics experiments was repeated but prior to the addition of the substrate, a drop of mercury was added to the cuvette. Then, the kinetic data were acquired as previously described.

3.5.8.2 CS_2 poisoning

Insights about the nature of the Pd(0) contribution to the catalysis, being of heterogeneous or homogeneous type, can be assessed through quantitative CS_2 poisoning experiments. Carbon disulphide is known to bind strongly to zero valent metal centres, which make them unavailable to interact with the substrate. [97,98]

The addition of different amounts of CS_2 in relation to the total number of metal atoms provides evidence that the reaction is taking place on the surface or with leached atoms of Pd(0). If the reaction is inhibited with less than 1 equivalent of CS_2, it is indicative that not all atoms are active and accessible by the substrate implying that only the surface is involved. If more than 1 equivalent of CS_2 is required to inhibit the reaction, all atoms must be contributing to the reaction and therefore, the catalyst homogenous behaviour is assumed. [98]

In these poisoning experiments, 0 – 1.0 equivalent of CS_2 was added from a stock solution (200 μmol L^{-1}) freshly prepared in DMSO, prior to the addition of the substrate.

3.5.8.3 EDTA poisoning

Palladium (II) and ethylenedinitrilotetracetic acid (EDTA) have an extremely strong affinity, with log K greater than 25, at room temperature and ionic strength 0.1.[99] For this reason, the addition of EDTA to the reaction medium will result in the unavailability of Pd(II), which is strongly bound to the chelating ligand, and will, therefore, inhibit the catalysed reaction. For such, 10 μL of 400 μmol L^{-1} a solution of EDTA in PBS was added to the cuvette after the addition of the palladium solution and before adding the substrate. After that, the kinetic was followed as the standard setup.

3.6 UNCAGING STUDIES IN LIVING CELLS

3.6.1 Cell viability assays

SKBR3 cells were grown in a humidified incubator at 37 °C under 5% CO_2 with 90% humidity and split at approximately 70% confluence using Trypsin-EDTA solution 0.25%. The cells were grown in McCoy's 5A (modified), GlutaMAX™ medium supplemented with 10% heat inactivated FBS. Cells were grown to 70% confluency before seeding in 200 μL at 5000 cells/well into a Corning Costar 96-well clear, flat bottom plate. CellTiter-Blue® assays were employed to determine toxicity and they were performed after replacing the medium with 100 μL of fresh medium followed by the addition of 20 μL of cell CellTiter-Blue® solution to each well and incubating for 6 h. After this period, the fluorometric determination of cell viability was conducted according to the supplier's guidelines. The fluorescence intensity was measured at λ_{ex} = 555 nm and λ_{em} = 585 nm. The residual fluorescence of CellTiter-Blue® in the cell medium was treated as background and therefore it was subtracted from each well. To the cell viability calculation, it was considered the resulting fluorescence intensity in the wells as a percentage of the control, which contained 0.25% of DMSO and was set as 100% viable. All experiments were performed in triplicate.

The experiments conducted with HeLa cells were performed in analogous fashion with the exception of DMEM glucose GlutaMax™ being used instead of McCoy's cell medium.

3.6.2 Epifluorescence microscopy

In an ibidi μ-slide 8 well chamber slide, 300 μL of cell medium containing $1x10^5$ cells/cm^3 were added to each chamber and incubated at 37 ºC for 24 h. Then, after changing the medium, 1 μL of Pd-NPs in DMSO suspension (Pd final concentration = 12.5 μmol L^{-1}) was added and incubated for 24 h. After this period, the medium was changed again, and the protected-rhodamine solution was added (1 μmol L^{-1} of a 20 mmol L^{-1} DMSO stock). After 1.5 h if incubation, cell culture medium was then removed, cells were briefly washed with PBS and cell nuclei were stained with Hoechst 33342 (5 μg mL^{-1}). Cells were washed again with PBS and fixed with 4% paraformaldehyde in PBS for 10 min. At last, after washing the cells with PBS (3x), cells were imaged on an EVOS M5000 microscope. DAPI EVOS and GFP EVOS light cubes were used to image nuclei stained by Hoechst 33342 and Rhodamine 110, respectively. The acquired images were processed using *ImageJ*® software.

4 RESULTS AND DISCUSSION

4.1 SYNTHESIS AND CHARACTERISATION OF THE NANOPARTICLES

The initial step of this work consisted of the synthesis and characterisation of Pd-NPs. The Pd(II) nanoparticles were prepared in the form of palladium iodide, PdI_2-NPs, by a ligand exchange reaction of the acetate ion from $Pd(OAc)_2$ by iodide, in the presence of a polymer as stabiliser (PVP), as described in the experimental section.

The ligand exchange reaction was evidenced by the change in the colour of the initially yellow solution that instantly became a dark brown suspension. To confirm the formation of nanoparticles, the suspension was characterised by TEM and SAXS.

Figure 3 a) shows the micrograph and histogram with the size distribution of the synthesized PdI_2-NPs. The resulting particles were spherical, with low dispersion and, in general, without agglomerates. The particle count indicated an average diameter of 2.1 nm ± 1.1 nm.

The scattering curve obtained in SAXS measurements is shown in Figure 3 b. The experimental data, in black, was fitted by the sphere and Beaucage models according to the procedure described in the experimental section. The fitted curve, in red, indicated a diameter of 2.26 nm and dispersion of 23%.

Figure 3. Micrograph of PdI_2-NPs with respective histogram (a) and curve of SAXS scattering (b).

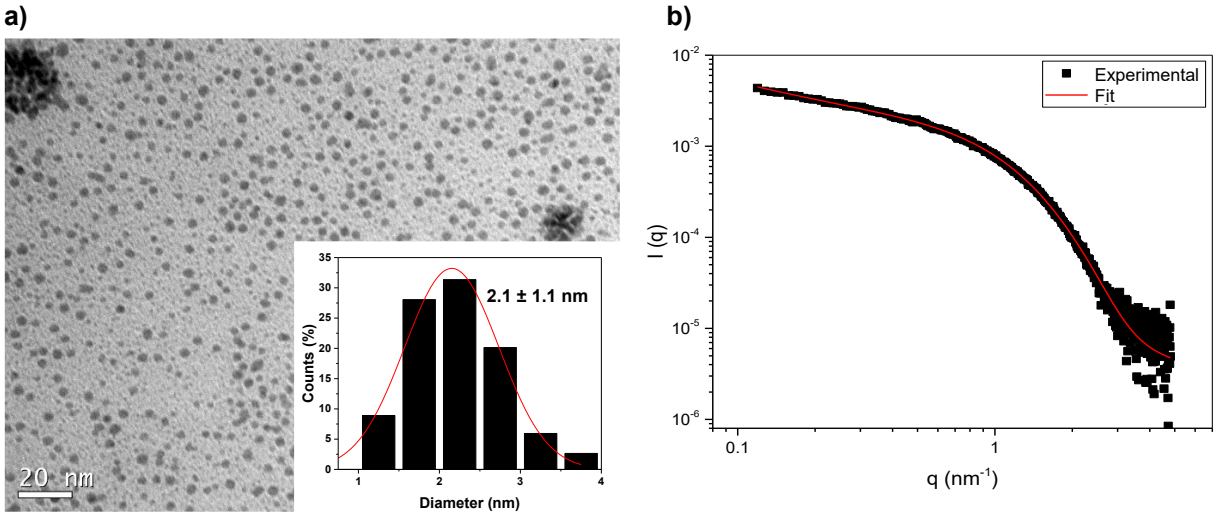

Source: the author, 2021.

Similarly, Pd(0)-NPs were synthesized by reducing $Pd(OAc)_2$ by $NaBH_4$ in the presence of PVP. The reaction was also evidenced by the change in solution's colour that became black and by the release of gases resulting from the decomposition of sodium borohydride. This system was also characterised by TEM and SAXS.

The micrograph and the size distribution chart shown in Figure 4 a) indicate the formation of nanoparticles that are also spherical, little agglomerated and with low dispersion. The average diameter, shown in the histogram, is 2.2 ± 1.0 nm. The SAXS scattering curve, shown in Figure 4 b), the curve fitting resulted in a diameter of 2.18 nm with 23% dispersion.

Figure 4. Micrograph of Pd(0)-NPs with respective histogram (a) and curve of SAXS scattering (b).

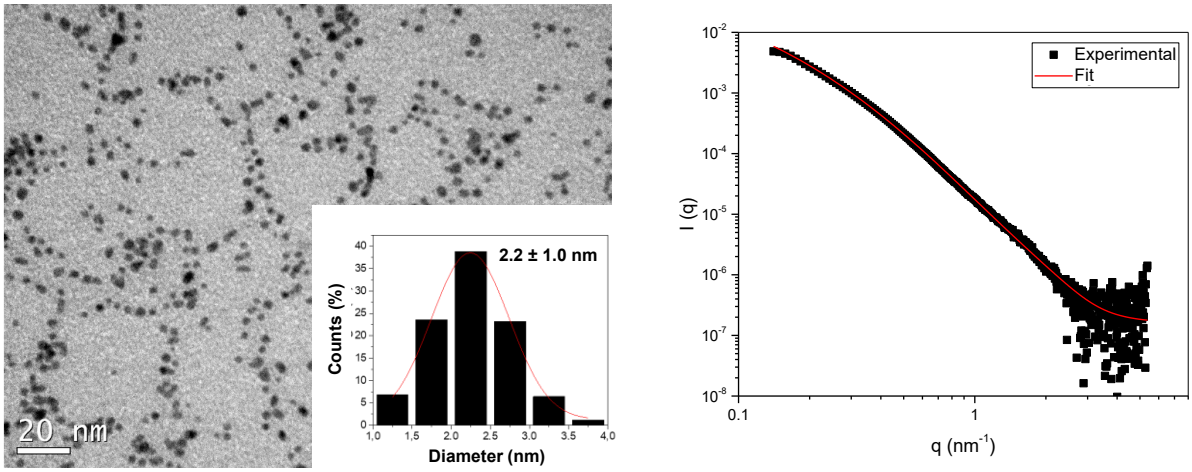

Source: the author, 2021.

To evaluate the composition of the nanoparticles, the colloidal suspensions were subjected to X-ray absorption spectroscopy analysis. Figure 5 shows the XANES spectra obtained for the Pd-NPs along with the standard for the oxidation states of the palladium +2, palladium iodide (bulk), and 0, palladium foil.

The XANES spectra showed similarities between the nanoparticles prepared with potassium iodide and PdI_2 bulk that present the same profile, the peak points at the same energy, as well as the energy of the absorption edge. The same occurs when comparing the spectra of the palladium foil and the nanoparticles prepared by the reduction with $NaBH_4$. The spectrum and energy profiles of the peaks and valleys are fairly similar, indicating the equivalence in chemical composition. Besides, it is observed that, at the energy edge, the Pd(0)-NPs and the Pd(0) foil start the jump in energy slightly lower than the PdI_2-NPs and bulk PdI_2. This fact is

indicative of the different oxidation states of the samples, since the higher the valence, the more energy is needed to excite an electron from its core.[100]

Figure 5. Comparative XANES spectra of the synthesized palladium nanoparticles, PdI_2-NPs and Pd(0)-NPs, along with the respective standards, palladium iodide and palladium foil.

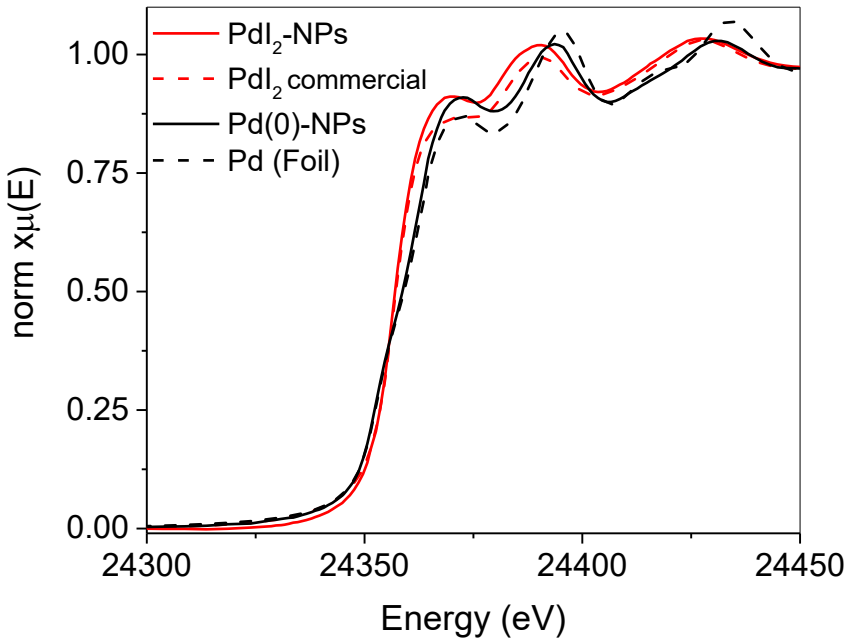

Source: the author, 2021.

To assess whether the oxidation status of Pd-NPs remains unaltered after the isolation step, an analysis of X-ray spectroscopy excited by photoelectrons (XPS) was performed. For both materials, the high resolution XPS spectra in the energy region of palladium were obtained, shown in Figure 6.

Figure 6. XPS spectra and respective deconvolutions for the palladium region of a) PdI_2-NPs and b) Pd(0)-NPs.

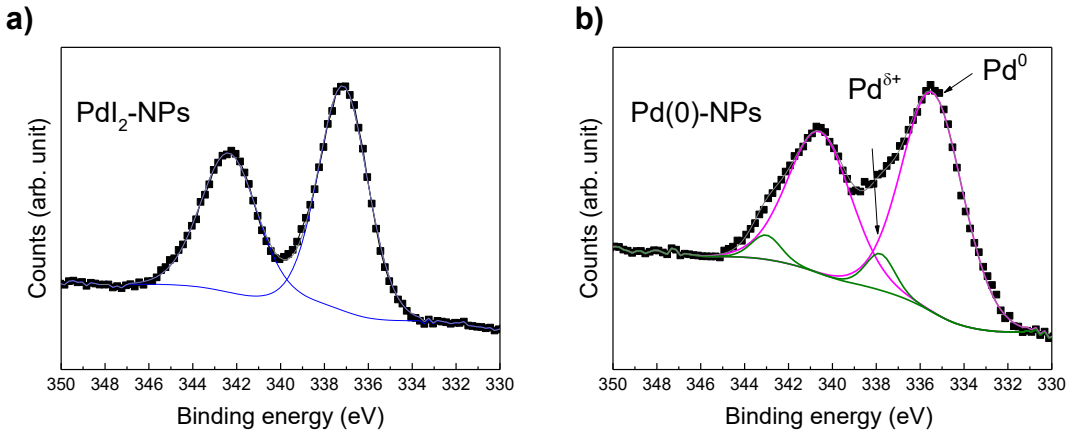

Source: the author, 2021.

For the PdI_2-NPs, the deconvolution of the experimental data resulted in only two peaks referring to the Pd in the oxidation state +2. As for Pd(0)-NPs, in addition to the large peaks related to Pd(0), there is also a small contribution from the peaks related to Pd(II). The binding energies for each oxidation state, as well as the quantification of each species in the samples are contained in Table 1.

Table 1. Binding energy and relative atomic concentration to Pd(0) and Pd(II) species in Pd-NPs.

Sample	**Binding energy (eV)**	**Relative atomic concentration (%)**	
	Pd $3d_{5/2}$	**Pd^0**	**$Pd^{\delta+}$**
PdI_2-NPs	337.1	-	100
Pd(0)-NPs	337.8	-	7
	335.4	93	-

The data in Table 1 suggests that even after isolation and removal of excessive stabiliser and other synthesis residues, the materials remain stable to their electronic nature. In particular, the Pd(0)-NPs stand out since they have a large exposed surface area that can be oxidised and yet remain in the form of Pd(0) with a minimum amount of oxide formed (7%). This is probably due to the presence of PVP and hydride on the surface of the particle that acts as protection against oxidation.[101]

To determine the palladium loading in the isolated materials, a flame atomic absorption spectrometry (FAAS) analysis was performed. For this test, the samples were digested with aqua regia for about 12 hours, as described in the experimental section. The results obtained are shown in Table 2.

Table 2. Mass percentage of palladium in isolated Pd-NPs, obtained by flame atomic absorption analysis.

Sample	**%Pd**
PdI_2-NPs	20.6 ± 8.4
Pd(0)-NPs	41.7 ± 9.3

Source: the author, 2021.

The percentage by mass of palladium in the nanoparticles shows that in Pd(0) -NPs there is approximate twice the amount of Pd found in PdI_2-NPs. This result is comprehensible because in Pd(0)-NPs the particle is formed by the Pd sphere and surrounded by the PVP stabiliser. The PdI_2-NPs have iodine atoms in their structure, in addition to the stabiliser, which decreases the percentage by mass of Pd.

The characterisations performed for both synthesized nanoparticles show that the systems have many equivalences: same size, shape and stabiliser, dispersity, and stability. They differ, however, in the oxidation state of the metal atom. These allow the isolation of other parameters, enabling the evaluation of the effect of the oxidation state of palladium in the reactions.

4.2 PALLADIUM NANOPARTICLES AS CATALYST FOR ARYL ALKENYLATION

After the synthesis and characterisation of the catalysts, they were applied in the C-C coupling reaction between a diazonium salt and an olefin. Since PdI_2-NPs exhibit unprecedented properties, they were tested first.

Scheme 22. Heck-Matsuda reaction between a substituted arenediazonium salt and styrene with all its possible products.

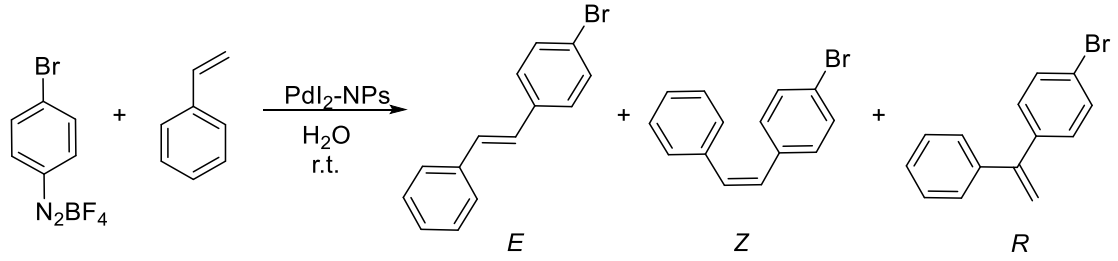

Source: the author, 2021.

The catalyst loading was the first parameter to be evaluated. The other conditions were standardised: 0.39 mmol of 4-bromobenzenodiazonium tetrafluoroborate, 0.26 mmol of styrene, 2.0 mL of H_2O, at room temperature and in the absence of a base. The amount of PdI_2-NPs was varied from 8 - 0.5 mol% of Pd. Under all conditions, the formation of the only product *(E)*-4-bromo-stilbene was observed (Figures A1 and A1 in the Appendix). The amount of catalyst tested and its respective yield after chromatographic column on silica gel is shown in Table 3. The results showed that 1 mol% of palladium or larger quantities provide the same amount of product, however 0.5 mol% results in a much lower yield. Consequently, 1 mol% was considered the ideal amount of catalyst.

Table 3. Variation of the amount of PdI_2-NPs applied in the reaction between 4-bromobenzenediazonium and styrene and their respective yields for the formation of *E*-stilbene.[a]

PdI_2-NPs	**Yield (%)[b]**
8 mol%	94
4 mol%	96
2 mol%	95
1 mol%	95
0.5 mol%	47

[a] Reaction conditions: diazonium salt (0.39 mmol), styrene (0.26 mmol), H_2O (2.0 mL), 24 h of reaction; [b] isolated yields for the formation of *E*-stilbene, determined after purification by silica gel chromatography.

Source: the author, 2021.

Then, the effect of the solvent in the reaction was evaluated. In addition to water, ethanol and mixtures of ethanol and water were applied. In these conditions, only the *E*-isomer was detected as well. The isolated yield showed it is strongly influenced by the addition of ethanol, which led to lower yields as shown in Table 4.

Table 4. Effect of the solvent in the yield of *E*-stilbene in the reaction between 4-bromobenzenediazonium and styrene with 1 mol% of PdI_2-NPs.[a]

Solvent	Yield (%)[b]
H_2O	95
EtOH	1
EtOH/H_2O (2:1)	17
EtOH/H_2O (1:2)	25

[a] Reaction conditions: catalysts (1 mol% of total Pd), diazonium salt (0.39 mmol), styrene (0.26 mmol), solvent (2.0 mL), 24 h of reaction; [b] isolated yields for the formation of *E*-stilbene, determined after purification by silica gel chromatography.

Source: the author, 2021.

After finding the optimal reaction conditions with PdI_2-NPs, water as a solvent and 1 mol% of Pd, the catalytic activity was compared to palladium catalysts obtained from commercial sources and also with Pd(0)-NPs. The results obtained are compiled in the Table 5.

Table 5. Effect of different palladium catalysts in the yield of *E*-stilbene in the reaction between 4-bromobenzenediazonium and styrene with 1 mol% of Pd.[a]

Entry	Catalyst	Yield (%)[b]
1	PdI_2-NPs	95
2	$Pd(OAc)_2$	44
3	$Pd(PPh_3)_4$	8
4	PdI_2 commercial	55
5	PdI_2 commercial + PVP	58
6	Pd(0)-NPs	22

[a] Reaction conditions: catalysts (1 mol% of total Pd), diazonium salt (0.39 mmol), styrene (0.26 mmol), H_2O (2.0 mL), 24 h of reaction; [b] Isolated yields for the formation of *E*-stilbene, determined after purification by silica gel chromatography.

Source: the author, 2021.

Traditionally, the C-C coupling of a diazonium salt with an olefin and Pd catalysis is treated as a Heck-Matsuda reaction and has an established catalytic cycle. In this cycle, it is mandatory to start with Pd(0) which undergoes oxidative addition and starts the reaction. However, the results in Table 5 show that among the tested catalysts, the best yields were achieved for those in which the metal was in the 2+ oxidation state.

With these results, the question of how Pd (II) would act in the catalysis of this coupling reaction and why it results in even better yields than Pd(0) arose. The literature shows that in cases where Pd(II) complexes and salts are used, the metal can initially be reduced in a Wacker-type reaction causing the oxidation of the olefin.[50] In this case, PdI_2-NPs would act as a reservoir of Pd(II) ions that would be converted homoeopathically to Pd(0) atoms while styrene would be oxidised by atmospheric oxygen.

To evaluate this hypothesis, an experimental test was carried out in which a large amount of PdI_2-NPs was added to the reaction medium, so that a possible olefin oxidation product, acetophenone, could be detected. Styrene and 50 mol% of PdI_2-NPs were mixed and maintained for 24 h under the optimised conditions, aqueous medium, room temperature and absence of base, according to Scheme 23. Another procedure was performed similarly, but with the addition of the diazonium salt for the sake of comparison.

Scheme 23. Wacker-type reaction between styrene and atmospheric oxygen yielding acetophenone and Pd(0).

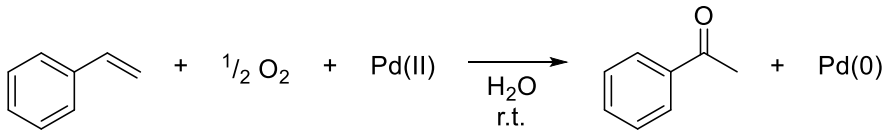

Source: the author, 2021.

After 24 hours, the reaction media of both experiments was analysed by ^{1}H, ^{13}C NMR and ESI-MS. In none of the cases, there was even a trace of acetophenone. The hypothesis that the Wacker reaction converts Pd(II) to Pd(0) and then starts the cycle of a Heck-Matsuda reaction was, therefore, ruled out.

From these results, it was assumed that a mechanism via Pd(0) would be unlikely to be operating. Hence, another hypothesis was addressed. The reaction could be taking place through a radical mechanism, similar to Meerwein's arylation, for instance.[51]

A frequently adopted procedure for collecting evidences of a radical reaction is the addition of a radical trap to the reaction medium. This forms an adduct with the radical intermediate and prevents the reaction from proceeding.[102] For this purpose, the reaction was carried out under standard conditions with the addition of the radical trap TEMPO, according to Scheme 24.

Scheme 24. Scheme for the reaction between DS-Br and styrene catalysed by PdI_2-NPs in the presence of the radical inhibitor TEMPO and possible products.

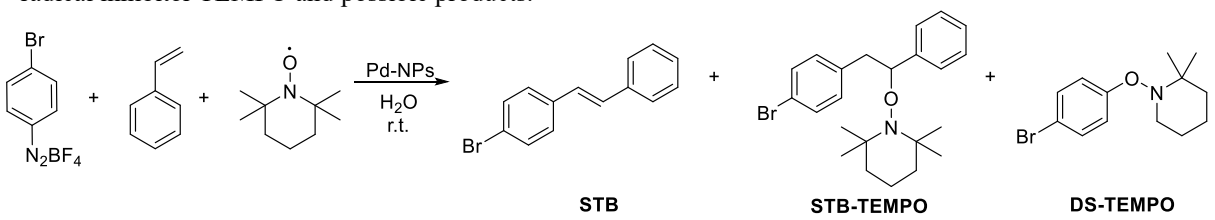

Source: the author, 2021.

Right after the 24 hours of reaction, ^{13}C NMR and ESI-MS analyses were performed to identify the products. It was observed that the formation of the STB product was completely inhibited by the addition of TEMPO in the reaction medium. And only the DS-TEMPO adduct (m / z = 312.095 $[M + H]^+$) was detected in large quantities, Figures A3 and A4 in the appendix

In view of the results, a mechanism for the arylation of styrene with 4-bromobenzenodiazonium tetrafluoroborate in water is proposed in Scheme 25, under PdI_2-NPs catalysis.

The Meerwein arylation mechanism occurs with the generation of an aryl radical under reductive conditions.[11] It was assumed, in this case, that the iodide from the PdI_2-NPs acts as the reducing agent in the initial stage. This proposition is based on previous reports which indicate that an electron from the iodide is assigned to the diazonium ion resulting in the formation of the radical **4**.[56] The next step, following path **a**, consists of an attack of the formed radical to the double bond of styrene and, path **b**, attacking the complex formed between palladium and styrene. Since adduct **9** is not formed, it is more likely that in the presence of Pd (II) coming from nanoparticles, the reaction proceeds via path **b**, only. Thus, intermediate **7** must be formed and, subsequently, undergoes a β-elimination step that leads to the formation

of product **3** and reduction of the metal to Pd(0). Palladium, however, under aerobic conditions can be regenerated in the form of Pd(II).

Scheme 25. Proposed mechanism for the reaction of styrene with the bromo-arenediazonium salt in the presence of PdI_2-NPs

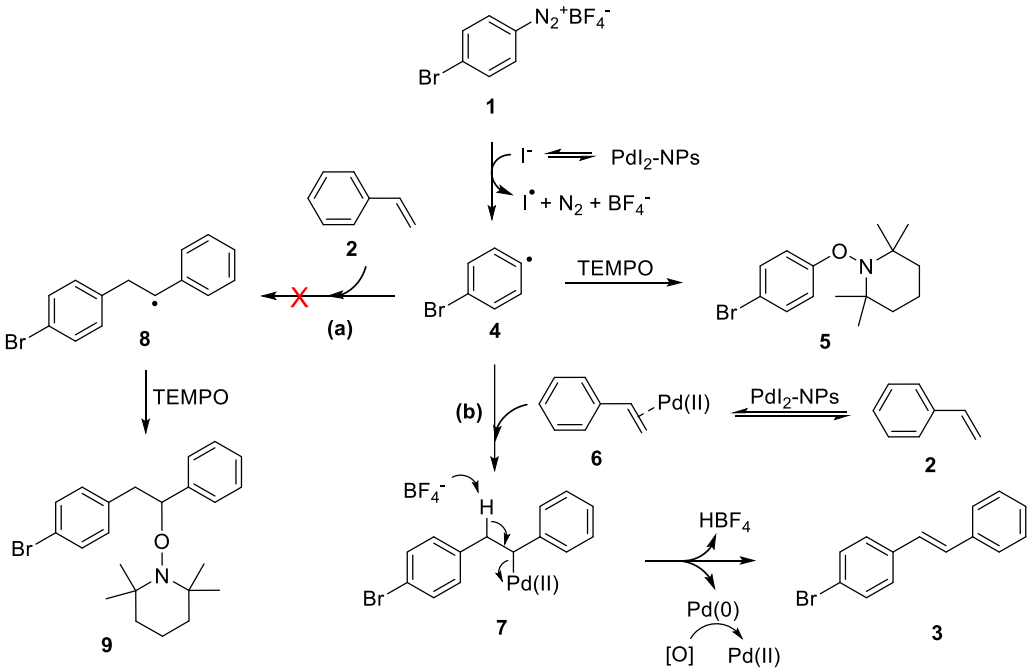

Source: the author, 2021.

Based on the proposed catalytic cycle as well as the results contained in Table 5, it can be stated that in the studied reaction conditions, the formation of *trans*-stilbene (C-C coupling product) is favoured by the radical mechanism with Pd(II) catalysis. The low yields observed when Pd(0) catalysts were applied, where the Heck-Matsuda catalytic cycle should predominate, can be attributed to the fact that the reaction is carried out in the absence of base. The base is responsible for the regeneration of the Pd(0) catalyst in the last stage of the catalytic cycle to initiate another turnover.

4.3 UNCAGING MEDIATED BY PALLADIUM NANOPARTICLES

The first substrate investigated in the uncaging reaction mediated by Pd-NPs was the 7-propargyloxycarbonylhydroxy-4-methylcoumarin (characterisation in the appendix, Figure A5). In order to monitor the kinetics of the coumarin deprotection reaction (Scheme 21) using the UV-vis technique, the electronic spectrum of the *O*-coumarin was initially assessed to acquire a calibration curve. The obtained graphics are found in the Figure 7. The spectrum shows two λ_{max} = 322 nm and 364 nm, with a molar absorptivity coefficient equal to 11720 L mol^{-1} cm^{-1} and 6240 L mol^{-1}, respectively.

Figure 7. UV-vis spectra for different concentrations of O-Coumarin in a), and the resulting calibration curve showing the linearity in 364 nm and 322 nm in b).

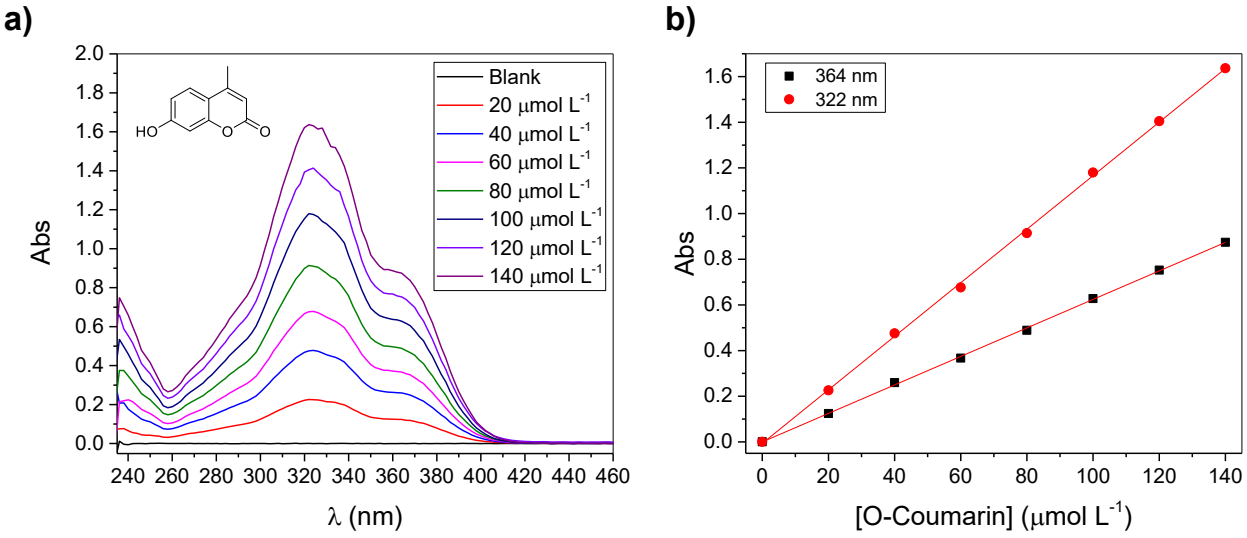

Source: the author, 2021.

After the insertion of the propargyl formate protective group in the *O*-coumarin, the electronic absorption spectrum of the product *O*-Proc-coumarin was also obtained and shown in Figure 8. The spectrum exhibited two λ_{max} = 275 nm and 310 nm, molar absorptivity coefficient equal to 10390 L mol^{-1} cm^{-1} and 9530 L mol^{-1} cm^{-1}, respectively. A hypsochromic displacement resulting from the loss of conjugation with hydroxyl oxygen was observed.

Figure 8. UV-vis spectra for different concentrations of O-Proc-Coumarin in a), and the resulting calibration curve showing the linearity in 310 nm and 275 nm in b).

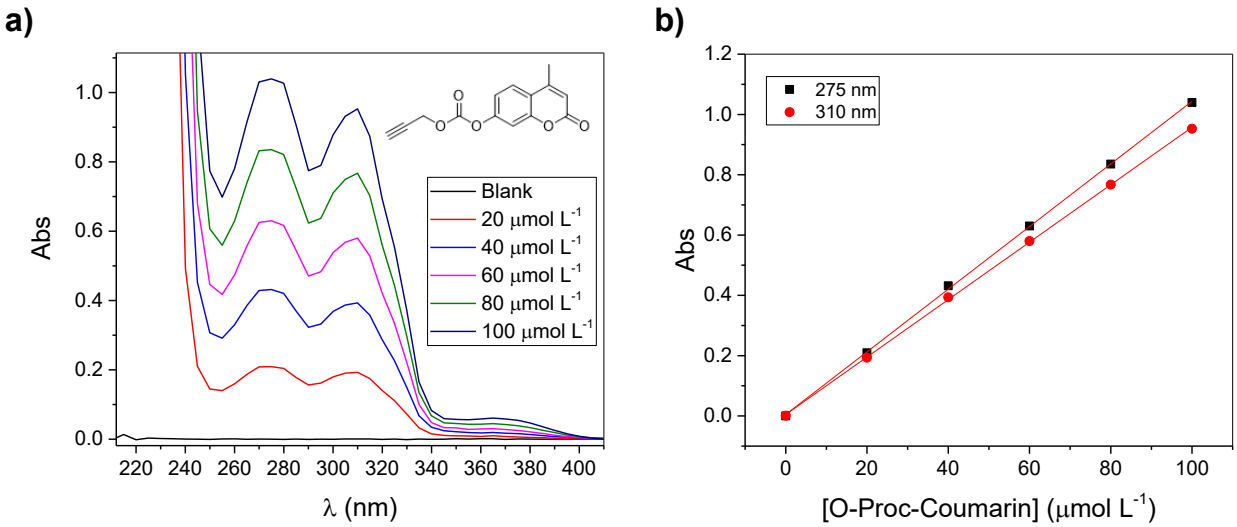

Source: the author, 2021.

The spectra of *O*-Proc-coumarin and O-coumarin were overlapped and are shown in Figure 9. It is clear there is a region, around 364 nm, where the product band is not interfered by the absorption of substrate. Thus, it is possible to monitor the kinetics of the deprotection reaction through the UV-vis absorption spectrum of the product being formed.

Figure 9. Overlapping UV-vis spectra of *O*-Proc-Coumarin and its respective unprotected coumarin.

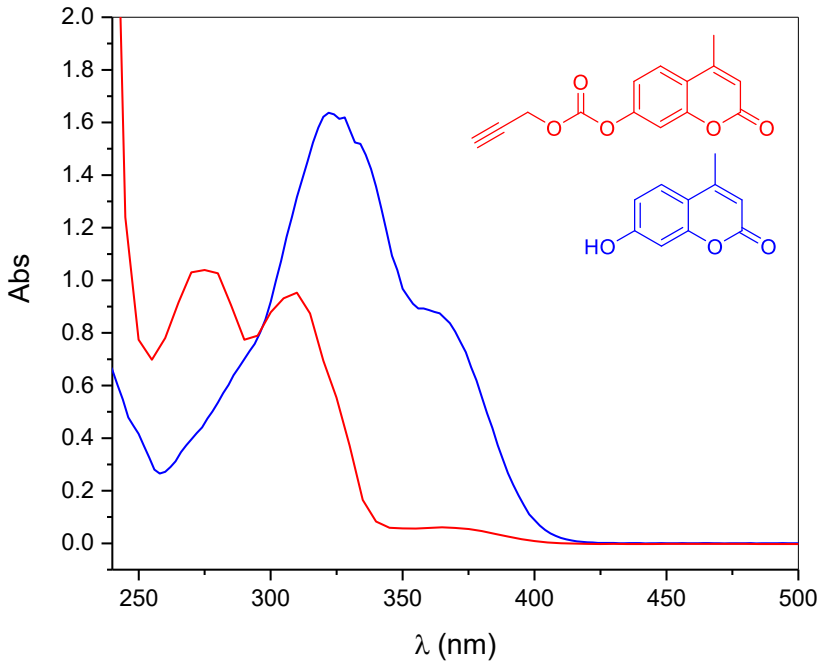

Source: the author, 2021.

After confirming the absence of interferences in the absorption spectrum of the cleavage product, it was possible to start the kinetic studies of the propargylcarbonate-coumarin deprotection reaction. The initial test was performed in the form of spectral kinetics where it was possible to observe an isosbestic point at 315 nm, with the disappearance of *O*-Proc at 275 nm and the appearance of *O*-coumarin at 364 nm, identified by the arrows in Figure 10 a. The reaction conditions in this assay were: 100 µmol L-1 of *O*-Proc-coumarin, 25 mol% of palladium catalyst, PBS buffer (5% DMSO), pH 7.4 and temperature of 37 ºC.

Figure 10. (a) *O*-Proc-coumarin uncaging followed by UV-vis spectral kinetics, (b) *O*-coumarin appearance kinetics at 364 nm. Reaction conditions: 100 µmol L^{-1} *O*-proc-coumarin, 25 µmol L^{-1} PdI_2-NPs, PBS buffer (5% DMSO), 37°C.

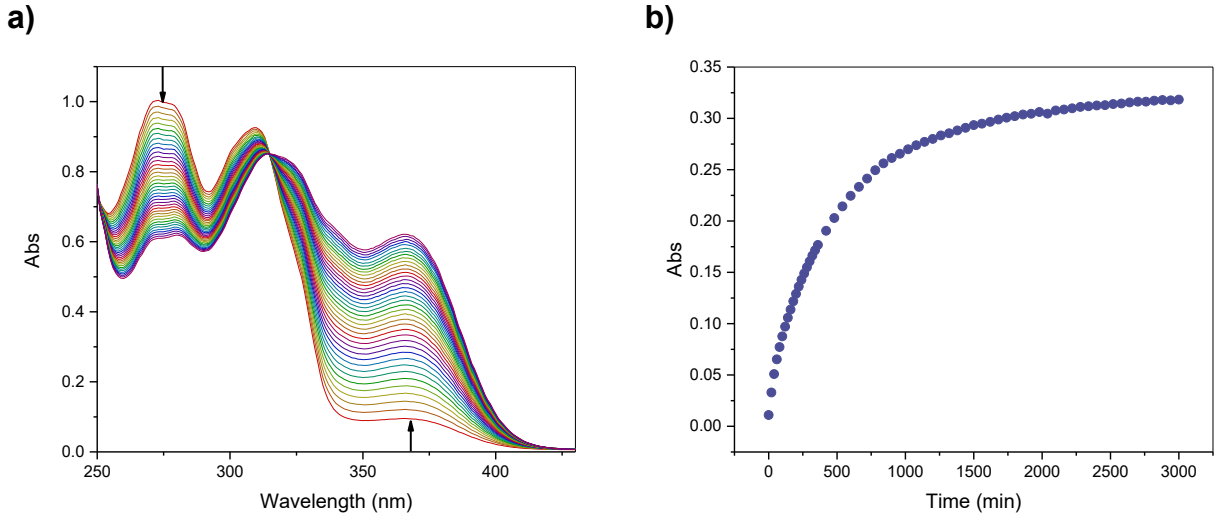

Source: the author, 2021.

In the initial test, both nanoparticulate catalysts, PdI_2-NPs and Pd(0)-NPs, and the commercial salt Na_2PdCl_4 were evaluated. For the reaction with Pd(0)-NPs, a profile corresponding to a first-order kinetics was observed, which could be linearised to obtain the rate constant k_1, as shown in Figure 11 a. In the reactions with Pd(II), both for Na_2PdCl_4 and for PdI_2-NPs, a more complex kinetic profile was observed, composed of two first-order parallel reactions meaning that the product is being formed by two reactions of different rate. In this case, the linearization of the kinetic profile allowed the curve to be fitted according to the rate law shown in Eq. 1, from which the k_1 and k_2 rate constants were obtained, as shown in Figure 11 b and c.[91]

$$\frac{[O-coumarin]_{inf}}{[O-coumarin]_t} = Fe^{-k_1 t} + Se^{-k_2 t} \qquad Eq.1$$

Figure 11. Linearisation of the kinetic profiles corresponding to the reaction mediated by a) Pd(0)-NPs, b) PdI_2-NPs and c) Na_2PdCl_4.

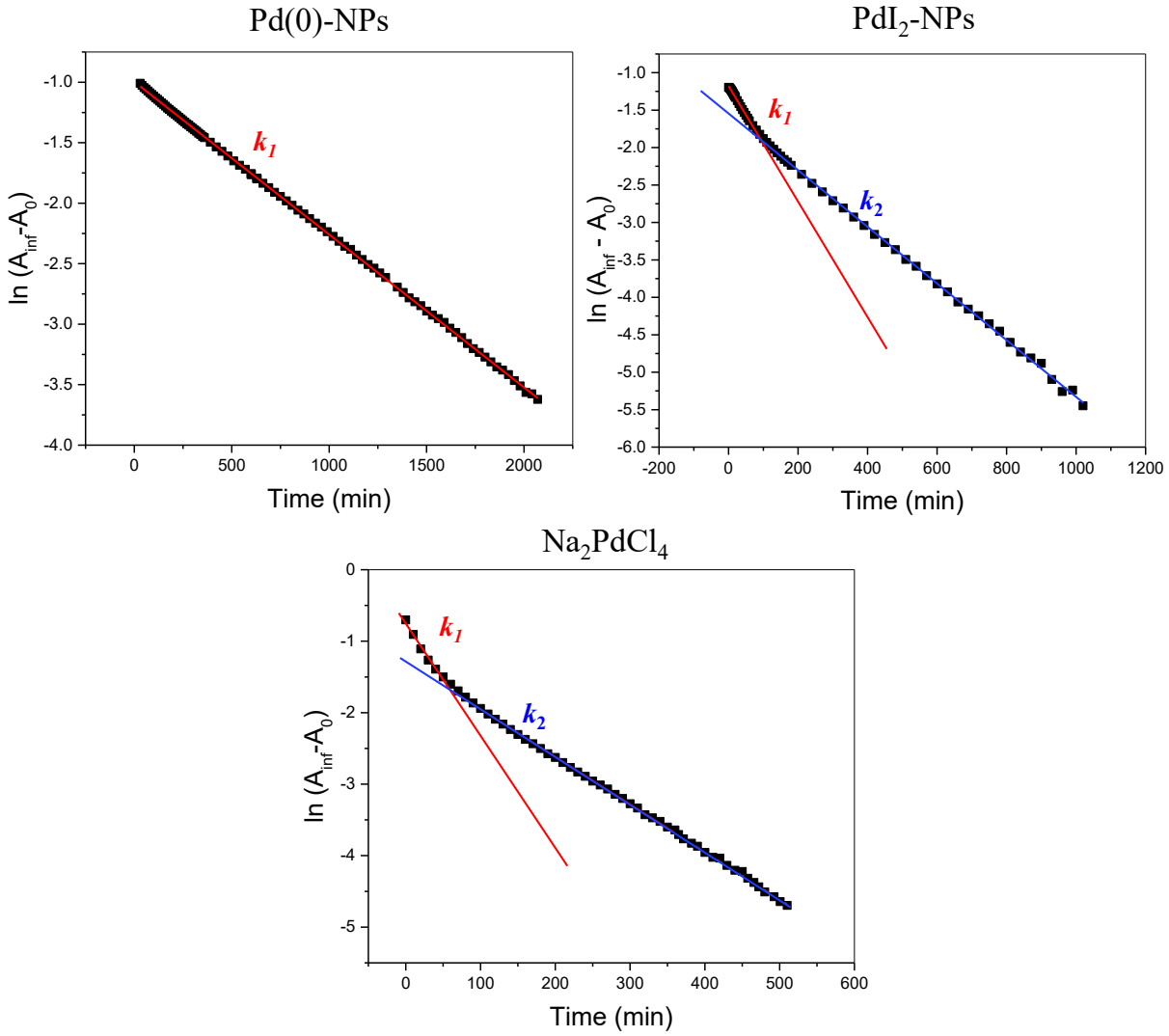

Source: the author, 2021.

Thus, the rate constants for the three evaluated catalysts were determined. The results, shown in Figure 12, show a greater activity for the systems composed of Pd (II), being even faster the reaction with Na_2PdCl_4.

Figure 12. Rate constants k_1 and k_2 for the deprotection of *O*-Proc-coumarin mediated by Na_2PdCl_4, PdI_2-NPs and Pd(0)-NPs. Experimental conditions: 100 µmol L^{-1} of *O*-Proc-coumarin, 25 mol% of Pd, PBS buffer (5% DMSO), 37°C.

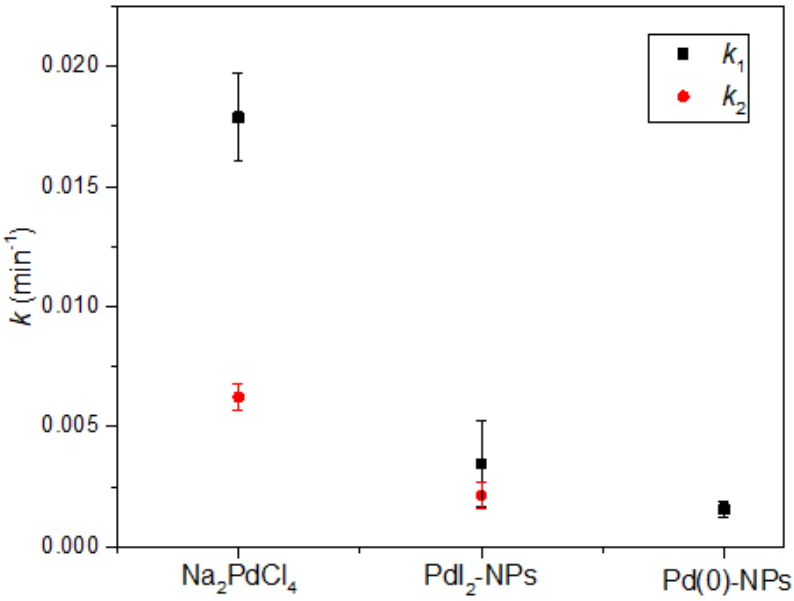

Source: the author, 2021.

For the systems discussed thus far, it was observed that *O*-Proc-coumarin undergoes deprotection under conditions favoured by the presence of palladium +2. When palladium zerovalent is used, the outcome, for both conversion and rate, are remarkably close to those obtained in the absence of the metal.

However, it was observed that the reaction was taking place even in the absence of palladium, which is shown in Figure 13. This graph is correspondent to the formation of *O*-coumarin in the medium comprised of the substrate *O*-coumarin and PBS buffer, exclusively.

Figure 13. *O*-coumarin appearance over time at 364 nm. Reaction conditions: 100 µmol L^{-1} O-proc-coumarin, PBS buffer (5% DMSO), 37°C.

Source: the author, 2021.

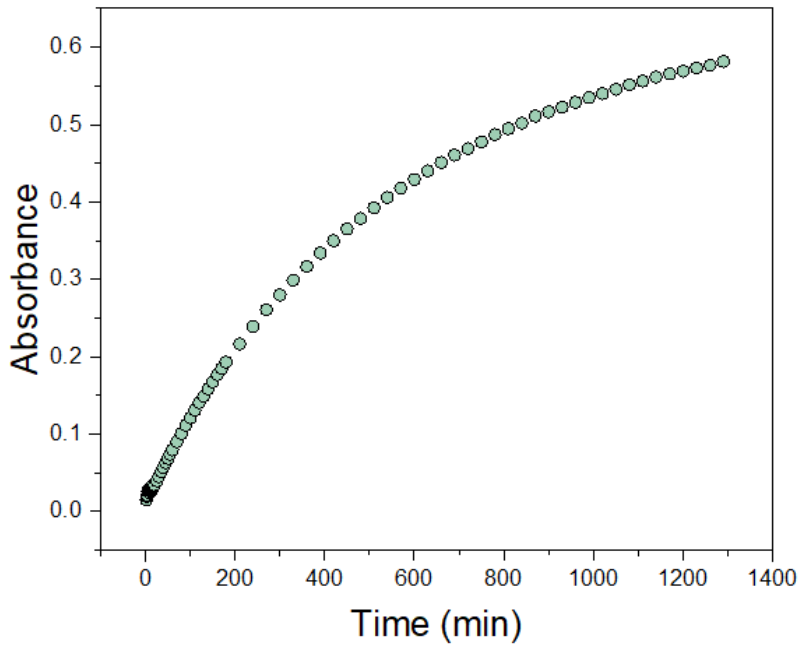

On this basis, it became evident that the high reactivity of *O*-Proc-coumarin against conditions that emulate the physiologic medium is not ideal and, therefore, it does not consist of a proper model for the study of bioorthogonal reactions. Thus, a less reactive substrate was chosen, the *N*-Proc-coumarin.

The *N*-Proc-coumarin was prepared according to Scheme 16 (characterisation in the appendix, Figure A6). The protecting group supressed the fluorescence of the free coumarin and therefore the uncaging of the *N*-Proc-coumarin (Scheme 21) could be monitored by means of fluorimetry, as evidenced by the overlapping spectra showed below, Figure 14. Fluorimetry became a more suited technique for this set of experiments instead of UV-vis spectroscopy because it enables the analysis of lower concentrations of *N*-coumarin which is less soluble than *O*-coumarin in aqueous medium.

Figure 14. Overlapping fluorescence spectra of *N*-Proc-Coumarin and its respective unprotected coumarin.

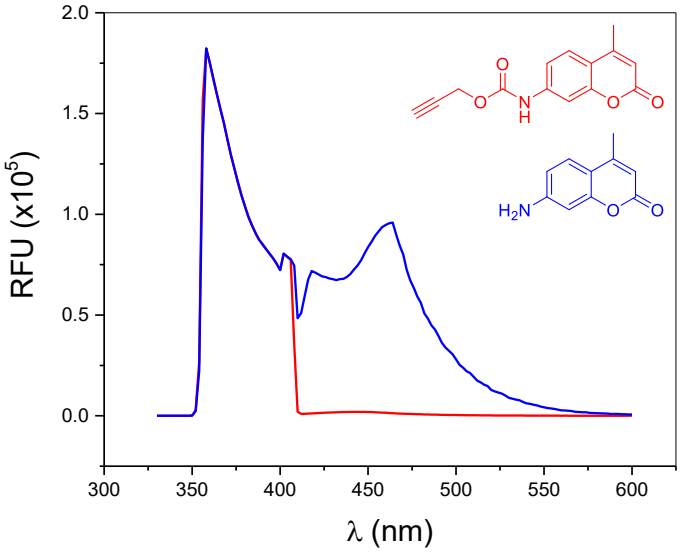

Source: the author, 2021.

Also, even though it is not its maximum wavelength, the compound showed a linear behaviour of fluorescence intensity in relation to concentration at λ = 500 nm and a calibration curve could be obtained, Figure 15.

Figure 15. Fluorescence spectra for different concentrations of *N*-Coumarin in a), and the resulting calibration curve showing the linearity in 500 nm in b), λ_{ex} = 380 nm.

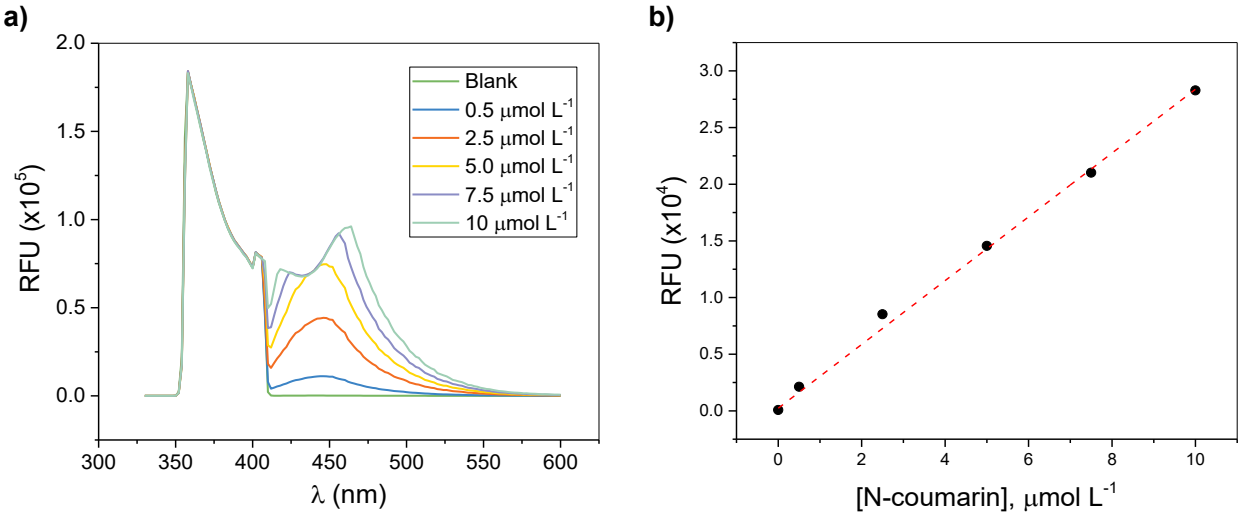

Source: the author, 2021.

In the preliminary tests, the uncaging reaction of *N*-Proc-coumarin with the Pd-NPs in both valence states were performed in PBS (5% DMSO), at 37 °C and the appearance of the deprotected coumarin was followed by the fluorescence spectra obtained in λ_{ex} = 380 nm and shown in Figure 16 a. Figure 16 b shows the conversion as function of time for PdI_2-NPs along with Pd(0)-NPs with the data acquired as spectral kinetics in λ_{em} = 500 nm.

Figure 16. (a) N-Proc-coumarin uncaging followed by fluorescence spectral kinetics, (b) *N*-coumarin appearance kinetics at 500 nm, λ_{ex} = 380 nm. Reaction conditions: 10 µmol L^{-1} *N*-proc-coumarin, 2.5 µmol L^{-1} Pd-NPs, PBS buffer (5% DMSO), 37°C.

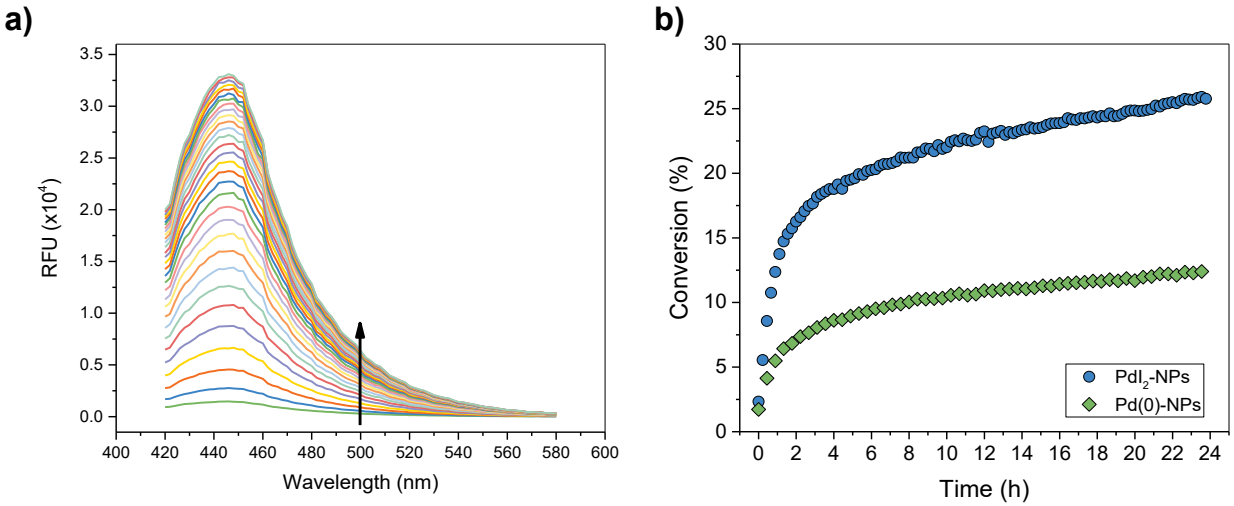

Source: the author, 2021.

Once the parameters were set to obtain kinetic data, the effect of the palladium concentration, of both nanoparticulated systems, in the reaction yield was determined, as exhibited in Figure 17. The concentration of the metal was varied in the range of 2 – 50 µmol L^{-1} corresponding to 0.2-500 mol% of Pd in relation to the substrate once *N*-Proc-coumarin concentration was fixed in 10 µmol L^{-1}.

Figure 17. Influence of the palladium concentration in the yield of the *N*-Proc-Coumarin uncaging mediated by PdI_2-NPs (a) and Pd(0)-NPs (b). Reaction conditions: 10 µmol L^{-1} *N*-proc-coumarin, PBS buffer (5% DMSO), 37°C. λ_{em} =500 nm, λ_{ex} = 380 nm, followed for 24 h.

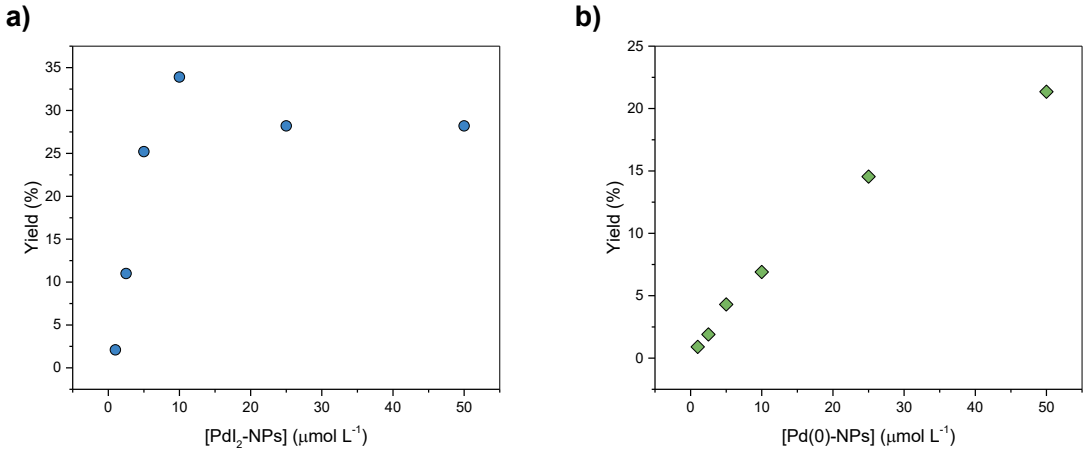

Source: the author, 2021.

Figure 17 a displays a growing relation of the yield with the amount of NPs, however, around the region of 10 µmol L^{-1} of PdI_2-NPs a plateau was reached. This result has two possible interpretations: 1) above the equimolar conditions, an excess of palladium will not affect the yield of the reaction or 2) once we are working with nanoparticles, surface effects are likely contributing to the product formation (and later it will be shown that they do). In this second case, the total superficial atoms should be accounted. For a palladium nanoparticle of approximate diameter of 2.2 nm, there are approximately 50% of atoms in the surface. In this case, the Pd concentration should be reduced by half and therefore, the plateau is reached with palladium performing two turnovers, which was already demonstrated in the literature for Pd(II)-mediated depropargylation.[91]

In the case of Pd(0)-NPs, shown in Figure 17 b, a saturation profile was not achieved in the studied concentration range, but the behaviour of the data indicates that in higher concentrations of Pd(0)-NPs it is likely to plateau. This along with the fact that full conversion was never accomplished indicate that not all atoms of palladium are active, or transformations might be occurring and affecting the nanoparticles.

Then, a reaction progress kinetic analysis (RPKA) was conducted to gather information regarding the catalyst stability throughout the course of the reaction.[103] RPKA is a graphical method to obtain the rate law of chemical reactions and, according to this method, when the reaction is carried out with different concentrations of the substrate and the same

[excess] (in this case the second reactant being Pd-NPs), it is expected that the curves of the rate of the reaction versus the substrate concentration overlay if the catalysts remain unaltered during the process. The rate of the reactions of *N*-proc-coumarin, in two different initial concentrations and constant [excess] was obtained for PdI_2-NPs and Pd(0)-NPs as follows: [*N*-proc-coumarin] = 10.0 mmol L^{-1}, [Pd] = 7.5 mmol L^{-1} and [*N*-proc-coumarin] = 7.5 mmol L^{-1}, [Pd] = 5.0 mmol L^{-1} in which the [excess] was kept 2.5 mmol L^{-1}. The resulting graphical rate equations are shown below in Figure 19.

Figure 18. Rate of the reaction of *N*-proc-coumarin, in two different initial concentrations and constant [excess], a) PdI_2-NPs and b) Pd(0)-NPs. [*N*-proc-coumarin] = 10.0 mmol L^{-1}, [Pd] = 7.5 mmol L^{-1} in black and [*N*-proc-coumarin] = 7.5 mmol L^{-1}, [Pd] = 5.0 mmol L^{-1} in red. Both with [excess] = 2.5 mmol L^{-1}.

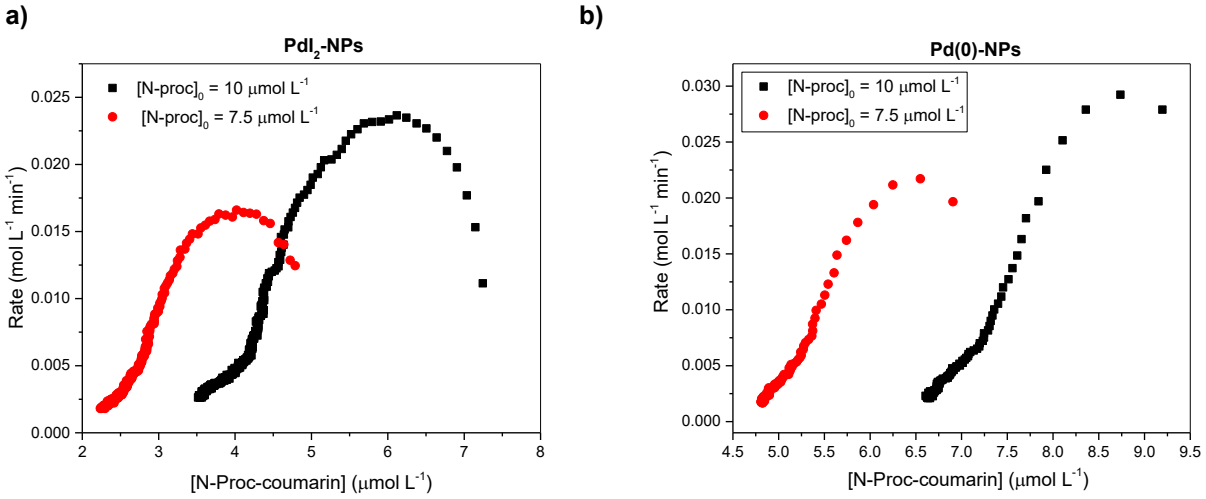

Source: the author, 2021.

The lack of overlay in the data is clear and implies that the palladium precursor was changing over time. Inhibition by product could also be considered, but accounting for the nanoparticle's complex equilibrium in solution, their dynamic activity of leaching and surface restructuring is more likely to be taking place.

Once there was evidence the catalysts were going through changes during the reaction, the next step focused on understanding the sort of process the nanoparticles were going through. The most likely alterations were regarding their oxidation state and/or their structure, that might be affected due to leaching.

The analysis of the metal valence in reaction medium is a rather complicated information to probe directly. Therefore, an indirect procedure was required to perform this task.

Considering the different pathways that these reactions might take, and the fact that mercury poisons palladium surfaces, it is clear that if the reaction occurs in a heterogeneous fashion, the same would be inhibited in the presence of mercury. If the reaction occurs through Pd(0) leached atoms, the product formation might be inhibited by the addition of carbon disulphide (CS_2), because it binds to zerovalent palladium atoms and not to Pd(II). Finally, if the reaction is dependent on the leaching of Pd(II) ions, it might be inhibited by the addition of EDTA, which strongly complexes with Pd(II) but not with Pd(0), as shown in the Figure 19.[97]

Figure 19. Illustration of the most plausible pathways for reactions mediated by palladium nanoparticles and the means of identifications by poisoning experiments. a) Surface catalysis can be probed with Hg(0) poisoning, b) leaching of Pd(0) with CS_2 and c) leaching of Pd^{+2} with EDTA.

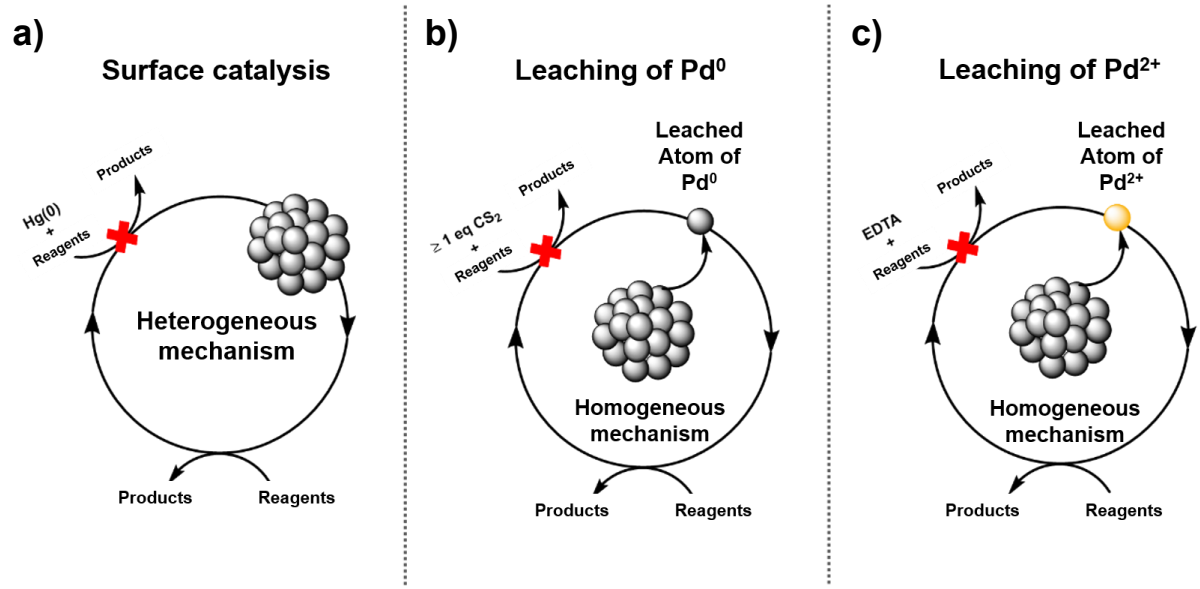

Source: the author, 2021.

The first test was conducted with the addition of a Hg(0) drop in the beginning of the reaction with the PdI_2-NPs and Pd(0)-NPs, followed by the addition of N-Proc-coumarin. Mercury inhibition was also investigated with the addition in the middle of the reaction, after 30 minutes. Figure 20 shows the effect of Hg in the conversion over time for both nanoparticles.

Figure 20. Mercury poisoning test, with addition of Hg(0) at the beginning and after 30 min of reaction compared to the standard condition, without Hg for a) PdI_2-NPs and b) Pd(0)-NPs. Reaction conditions: 100 µmol L^{-1} *O*-proc-coumarin, 25 µmol L^{-1} Pd-NPs, PBS buffer (5% DMSO), 37°C.

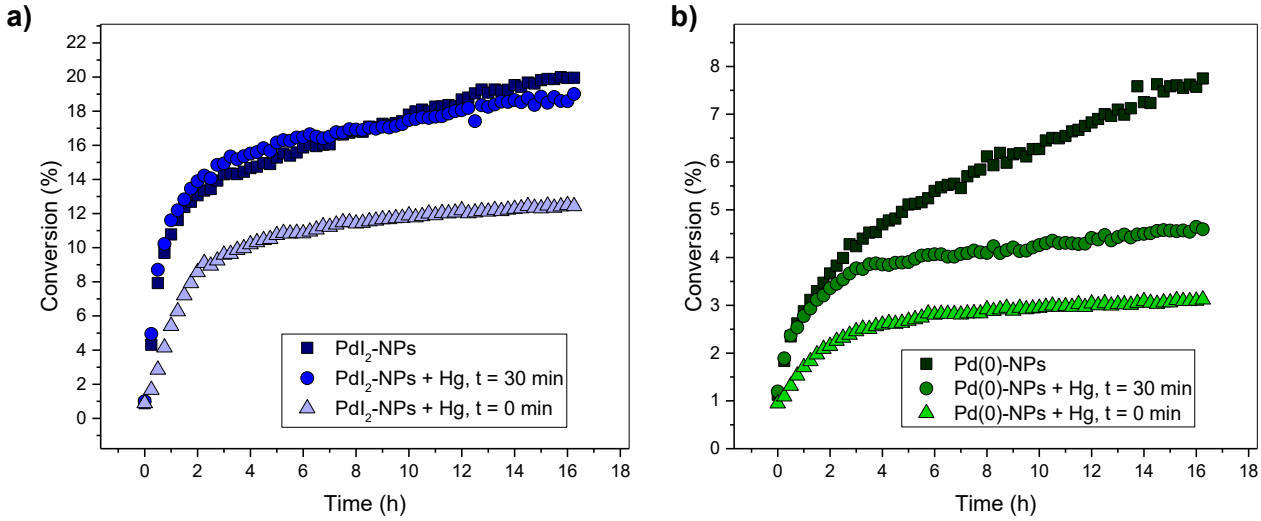

Source: the author, 2021.

The mercury poisoning had an interesting effect to the PdI_2-NPs: when initially added, it resulted in some inhibition of the product formation. However, when it was added after 30 minutes, no effect was observed. Most likely is that after the reaction begins, the active species in solution do not strongly interacts with the mercury.

The addition of Hg(0) in the beginning of the reaction with Pd(0)-NPs led to a great inhibition in the product formation. It is probably due to the amalgamation of the metallic surface that became inactive and unable to leach atoms to the solution. When Hg(0) was added after 30 minute, the inhibition was not that pronounced because it is likely that this time was enough for some lixiviation from the surface to take place and these lixiviated species are not affect by the poisoning.

Even though the mercury poisoning test has been used for many years, recently was brough to attention some inconsistencies in its interpretation.[104,105] Therefore, a cautious measure is to conduct this experiment in association with others bearing related purpose. In this way, to validate the findings through Hg(0) poisoning, inhibition by CS_2 was evaluated. Different amounts of CS_2, ranging from 0.0 - 1.0 equivalent, were added to the reaction medium in the beginning of the reaction. And, for the sake of comparison, the reaction without CS_2 was also carried out. Figure 21 shows the influence of CS_2 in the final conversion to N-coumarin when mediated by PdI_2-NPs and Pd(0)-NPs, respectively.

Figure 21. Poisoning by CS_2, shown as conversion versus amount of CS_2 added to the reaction medium for a) PdI_2-NPs and b) Pd(0)-NPs. Reaction conditions: 100 µmol L^{-1} *O*-proc-coumarin, 25 µmol L^{-1} Pd-NPs, PBS buffer (5% DMSO), 37°C, carried out for 24 h.

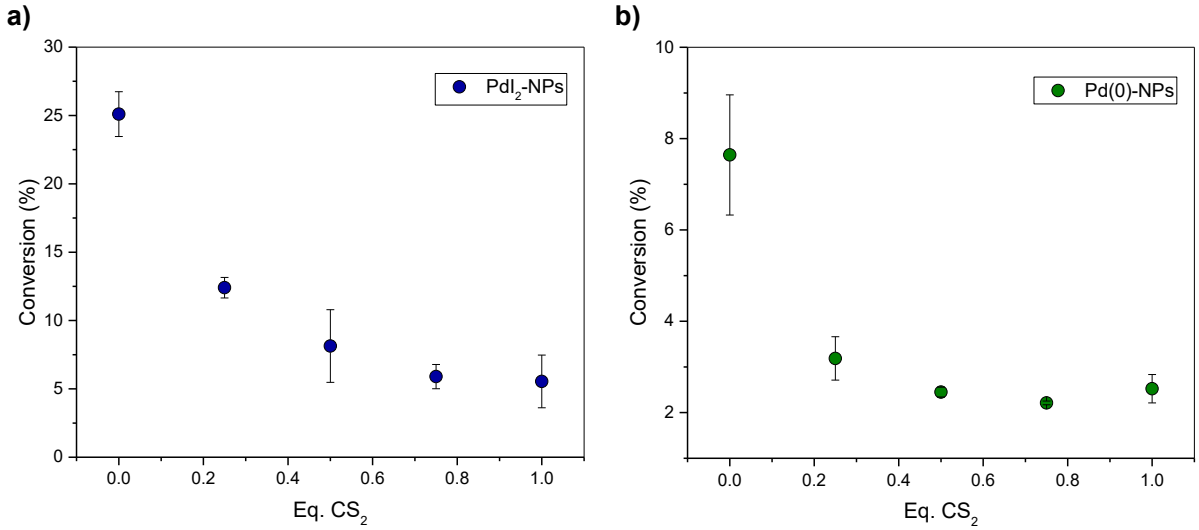

Source: the author, 2021.

The principle behind this test is that if the inhibition of product formation occurs only with equivalent amount of CS_2, then the reaction is probably occurring by a homogenous pathway. However, the data showed that any of amount of CS_2 affected the conversion and therefore, nanoparticle's surface must be involved in the reaction. The surface contribution hinted by this experiment corroborates the results obtained with mercury inhibition. At last, Pd(II) contribution to the product formation was also probed. By adding EDTA in the beginning of the reaction, it would inactive Pd(II) species due to complex formation and, therefore, the product it yields would be inhibited.

Figure 22. Poisoning by EDTA in a) PdI_2-NPs and b) Pd(0)-NPs. Reaction conditions: 100 µmol L^{-1} *O*-procoumarin, 25 µmol L^{-1} Pd-NPs, PBS buffer (5% DMSO), 37°C.

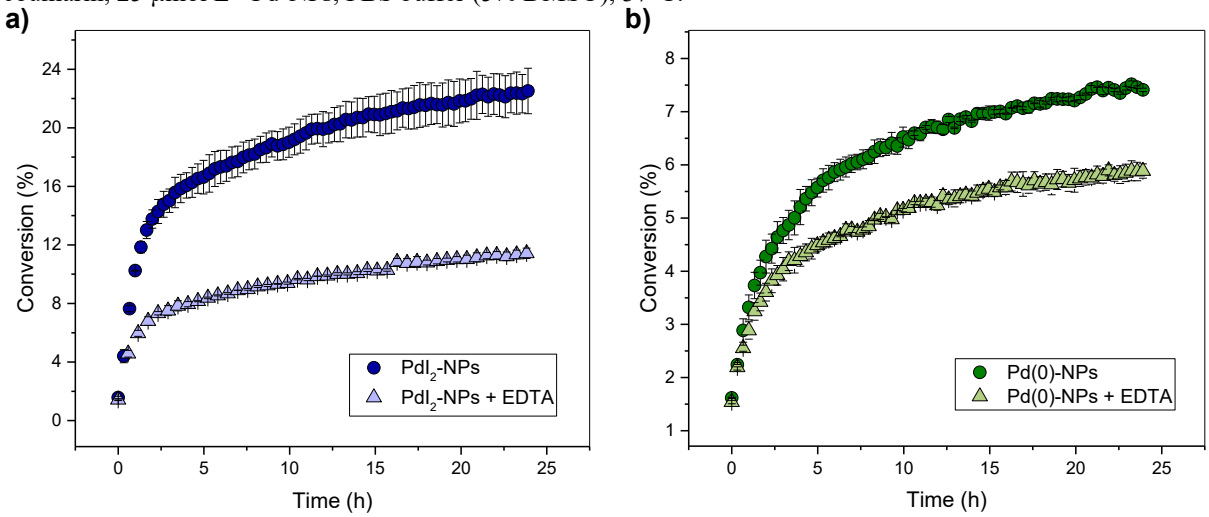

Source: the author, 2021.

It was observed that the conversion in the kinetic mediated by PdI_2-NPs, was greatly inhibited by the addition of EDTA, (Figure 22 a) while the reaction with Pd(0)-NPs (Figure 22 b) the decrease in conversion is much less pronounced. Interestingly, when Pd(II)-NPs were treated the EDTA solution, the conversion dropped to approximately 8%, which corresponds to the full conversion observed for Pd(0)-NPs under the same conditions.

The results obtained show that, in all the tests that were executed, there was some percentage of inhibition in the uncaging mediated by palladium nanoparticles. This indicates that palladium must be active in more than one form in the reaction and that the different species are likely to be interconverting in the reaction medium, supporting the cocktail of catalysts premise. Still, it was also observed that the reactions mediated by palladium in its divalent form were always faster and led to higher conversions.

4.4 UNCAGING IN CELLS

In order to evaluate the uncaging in living cells, the breast cancer cell line SKBR3 was chosen as model due to relevant results reported previously.[106] The initial step was to determine the toxicity of the nanoparticles alone. Cells were incubated, for 72 h, with different concentrations of nanoparticle to determine the cell viability by CellTiter-Blue assay. In this assay, viability is directly proportional to the ability of living cells to convert the redox dye non-fluorescent resazurin into fluorescent resorfurin. Due to losing metabolic capacity, nonviable cells are unable to perform this conversion. The resulting fluorescence intensity is normalised to one obtained for the cells cultured only with 5% DMSO, which were assumed to be 100% viable. Figure 23 shows the effect of the palladium concentration in the cell viability for both nanoparticulated systems.

Figure 23. Cell viability studies with a) PdI_2-NPs and b) Pd(0)-NPs in SKBR3 cells. Cell viability was determined by CellTiter-Blue® assay.

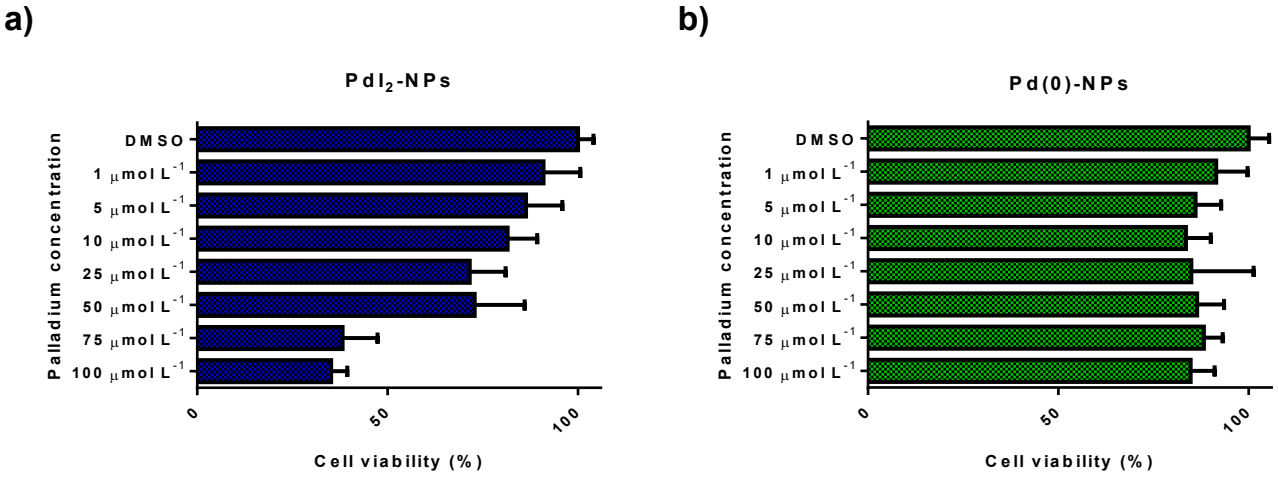

Source: the author, 2021.

The graphs above show that PdI_2-NPs are more toxic than Pd(0)-NPs, even though there is a wide concentration range in which the cell viability is barely affected. It is important to note that in these assays, the particles were incubated with the cells for 72 hours without change of media, resulting in an enhanced toxicity when compared to the real conditions of application. The study was conducted in such manner to make sure that, when applying the nanoparticles in the uncaging, the toxicity would be caused by the prodrug release exclusively.

As control, the toxicity of the stabilising agent PVP was also investigated. The cells were incubated with aqueous solutions of the polymer in different concentrations for 72 h. The exceptionally low toxicity of the polymer is shown on Figure 24.

Figure 24. Cell viability studies with different concentrations of PVP in SKBR3 cells. Cell viability was determined by CellTiter-Blue® assay.

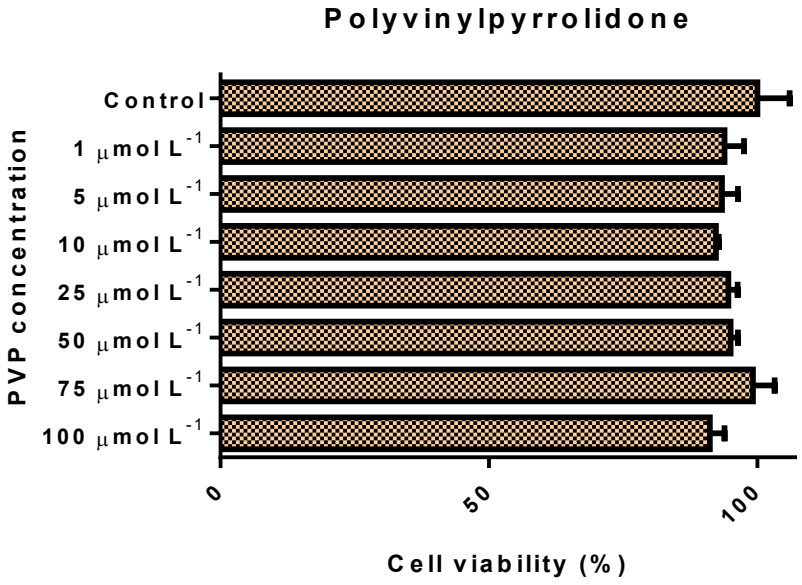

Source: the author, 2021.

Considering the viability data obtained for the nanoparticles, it could be said the toxicity was consequence of either the nanoparticulated structure or its components: palladium and stabilising agent. The stabilising agent toxicity data showed that the polymer does not exhibit toxicity in the conditions of the assays, and since Pd(0)-NPs was virtually non-toxic as well, it is likely that the higher toxicity exhibited by PdI_2-NPs is due to the Pd(II). This result is in strong agreement with various reports in the literature that state that Pd(II) is considerably more toxic than Pd(0).[107]

Pursuing the idea of uncaging the N-coumarin to use it as fluorescent marker inside living cells, the fluorophore in its free form, with N-Proc and N-Alloc protecting groups were tested for cell viability in SKBR3. The dose response curve is shown in Figure 25.

Figure 25. Coumarin and protected (*N*-Alloc and *N*-Proc) coumarins cytotoxicity in SKBR3 breast cancer cells. Cell viability was determined by CellTiter-Blue® assay.

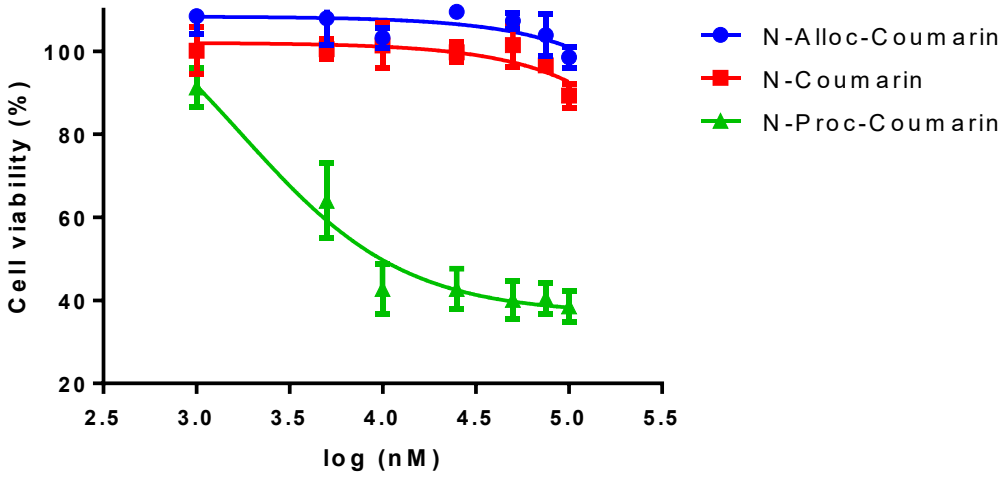

Source: the author, 2021.

This result was unexpected since it showed that *N*-Proc-Coumarin is much more toxic than *N*-Alloc-Coumarin and even than the coumarin itself. The origin of said toxicity has been difficult to rationalise but the data alone is reason enough to state that this substrate is not suitable for bioorthogonal purposes.

To overcome the toxicity issues encountered with the propargylated carbamate coumarin, different substrates to be bioorthogonally uncaged were prepared. Proc- and Alloc-Doxorubicin are frequently used in bioorthogonal uncaging, in such way, it has become sort of model prodrug for *in vitro* and *in vivo* studies.[70,72,108,109] Proc- and Alloc-Dox were synthesized (characterisation in the appendix, Figures A7 and A8, respectively) and the toxicity of the prodrugs along with the respective drug was assessed in SKBR3 cell line as shown by the dose response curves below in Figure 26.

Figure 26. Prodrug and drug cytotoxicity of Doxorubicin in SKBR3 cells. Cell viability was determined by CellTiter-Blue® assay.

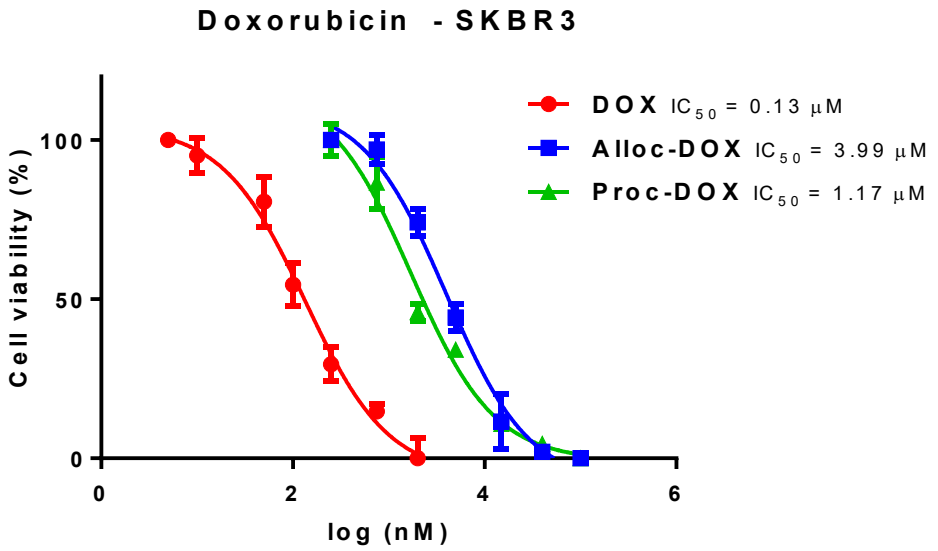

Source: the author, 2021.

Allyl and propargyl carbamates showed great efficiency as biorthogonal protecting groups for doxorubicin. The IC_{50}, in relation to the drug, exhibited a 9-fold and 30-fold increase for propargyl and allyl, respectively. This means that there is a broad window in which the prodrug is safe for use while the drug preserves its toxicity upon release. Making use of these information, preliminary tests of uncaging were conducted.

In the first uncaging assay in living cells, the experiment was not set up to target intra or extracellular uncaging exclusively. It was performed in such fashion that both could be taking place at the same time: the prodrug and the nanoparticles were added simultaneously, without change of medium. Doxorubicin was tested with both protecting groups and both nanoparticles and their effect in cell viability along with the corresponding controls are shown in Figure 27.

Figure 27. Cell viability of SKBR3 cells after treatment with a) Proc-DOX or b) Alloc-DOX and subsequent uncaging by PdI_2-NPs and Pd(0)-NPs targeting intra and extracellular milieus. [Proc-DOX] = [Alloc-DOX] = [DOX] = 0.75 μmol L^{-1}; [PdI_2-NPs] = [Pd(0)-NPs] = 10 μmol L.

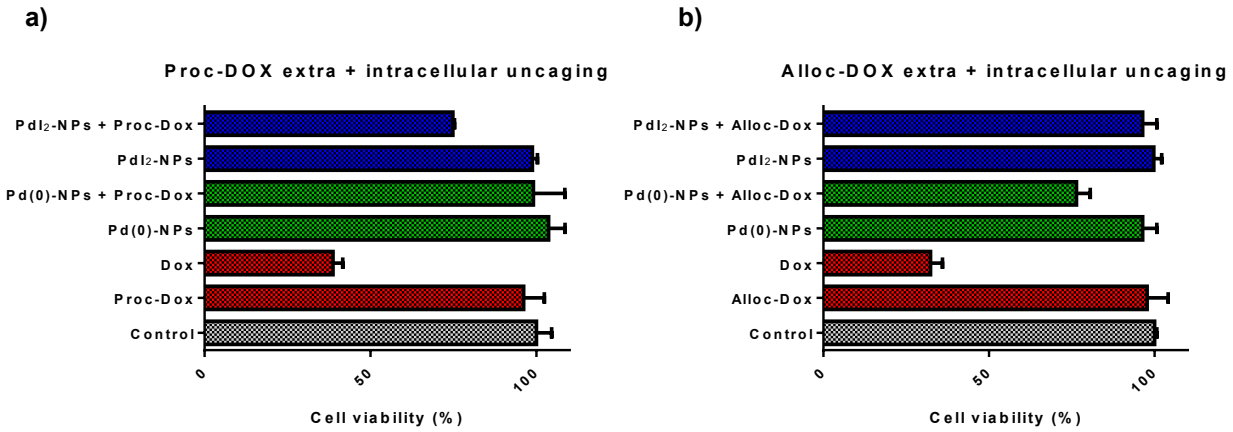

Source: the author, 2021.

When allowing both extra and intracellular uncaging to take place, PdI_2-NPs barely showed activity towards Alloc cleavage whilst they were able to trigger the Proc-DOX uncaging. On the other hand, Pd(0)-NPs were able to perform Alloc-DOX uncaging but had poor activity towards Proc-DOX. These results are, to some extent, in agreement with those observed in the reaction flasks and in kinetic experiments, even though the efficiency is modest.

However, one might argue that the biggest advantage of using transition metal nanoparticles instead of simple salts resides in the fact that they are capable of accumulating inside the cells.[110] And they can, therefore, perform the uncaging in a spatially controlled manner with enhanced activity. In the pursuit of these benefits, the experimental setup was adapted to target only intracellular uncaging: cells were incubated for 24 h in the presence of the Pd-NPs, followed by the change of media and then the addition of the prodrug. The outcome of this strategy is shown on Figure 28.

Figure 28. Cell viability of SKBR3 cells after preincubation with a) PdI_2-NPs and b) Pd(0)-NPs followed by the treatment with Proc-DOX and Alloc-DOX for subsequent uncaging. . [Proc-DOX] = [Alloc-DOX] = [DOX] = 0.75 μmol L^{-1}; [PdI_2-NPs] = [Pd(0)-NPs] = 10 μmol L.

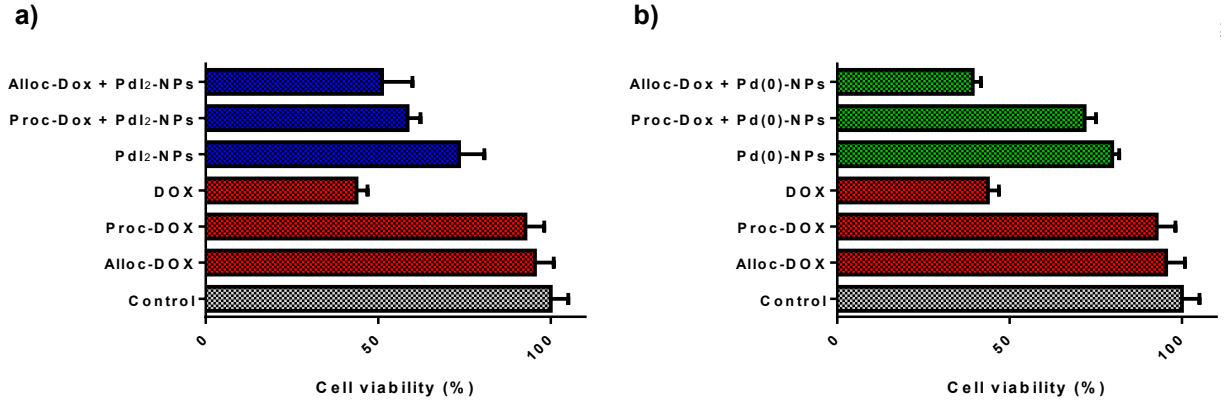

Source: the author, 2021.

The graphs above showed an increase in the efficiency of the uncaging, however the Pd(II)/Proc and Pd(0)/Alloc preference was not noticeable, thus selectivity was lost. Regardless of the protecting group and the trigger oxidation state, the reduction in the cell viability is virtually the same.

Taking into account that the intracellular environment is much more reductive than the extracellular one,[111] it is likely that during the 24 hours of incubation the particles are accumulating and being reduced intracellularly. So, by the time the prodrug is added, both nanoparticulated systems are equally formed by reduced (zerovalent) palladium. Therefore, the reaction would be triggered by equivalent palladium species which might explain such similar activity with different precursors.

As a strategy to overcome this issue and being able to distinguish the nanoparticles in the intracellular space, it was considered that if the Pd-NPs were periodically renewed in the media the metal reacting would be kept in its initial oxidation state longer. In that way, after adding the prodrug, successive doses of nanoparticles were added every 24 hours for three days, changing the media every time. The effect is shown in Figure 29.

Figure 29. Cell viability of SKBR3 cells after treatment with Proc-DOX and Alloc-DOX and three doses of a) PdI_2-NPs and b) Pd(0)-NPs for subsequent uncaging. [Proc-DOX] = [Alloc-DOX] = [DOX] = 0.75 μmol L^{-1}; [PdI_2-NPs] = [Pd(0)-NPs] = 10 μmol L.

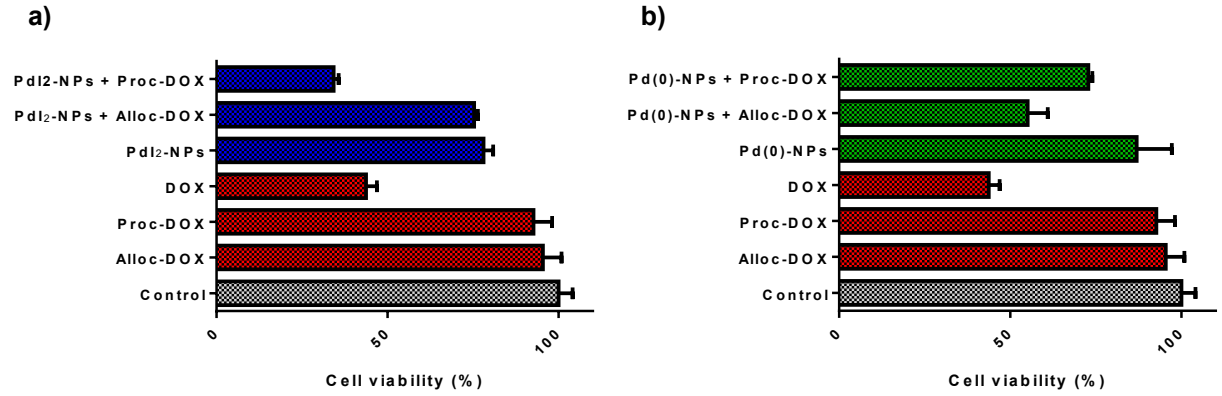

Source: the author, 2021.

With the addition of successive doses of the triggers, the Pd(II)/Proc and Pd(0)/Alloc preference is restored. This is probably because the reaction is being triggered by the metal in its initial form before it becomes fully reduced inside the cells. The efficiency of the uncaging was also significantly increased under these conditions.

To evaluate the robustness of the method, the nanoparticles and the doxorubicin derivatives were applied in a different cell line in another medium. Hence, HeLa, which is one of the most common cell linages applied in cancer research, was used in the assay conducted in the similar setup optimised for SKBR3 (Figure 30).

Figure 30. Cell viability of HeLa cells after treatment with Proc-DOX and Alloc-DOX and three doses of a) PdI_2-NPs and b) Pd(0)-NPs for subsequent uncaging. [Proc-DOX] = [Alloc-DOX] = [DOX] = 0.75 μmol L^{-1}; [PdI_2-NPs] = [Pd(0)-NPs] = 10 μmol L.

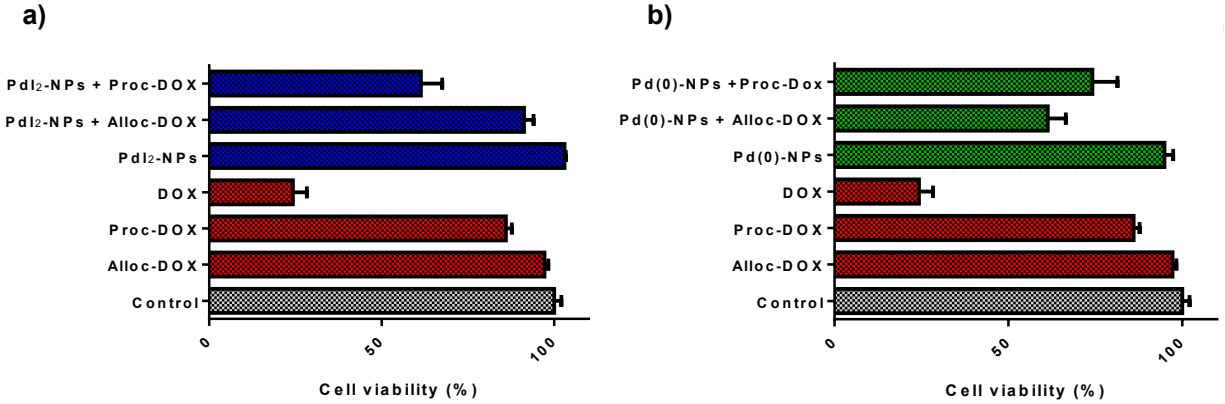

Source: the author, 2021.

Even though in HeLa the uncaging efficiency is not as pronounced, which is expected since the optimisation was conducted for SKBR3, the same behaviour was observed, as shown in Figure 30. The cell viability decreases more dramatically for Proc-DOX with Pd(II) and for Alloc-DOX with Pd(0). These results show that the method in its essence is valid for different cells and that even in such complex medium, the nanoparticles can trigger the uncaging.

As proof of concept, the rhodamine 110 (Rho) Alloc and Proc derivatives were synthesised, so their release could be investigated visually by fluorescence microscopy. Figure 31 and Figure 32 show the epifluorescence micrographs of the Proc and Alloc fluorophores, respectively, being uncaged by the nanoparticles.

Figure 31. Pd-NPs uncaging of Proc-Rhodamine 110 in SKBR3 cells followed by epifluorescence microscopy. DAPI EVOS light cube was used to image nuclei stained by Hoechst 33342 and GFP EVOS light cube was used for imaging Rhodamine.

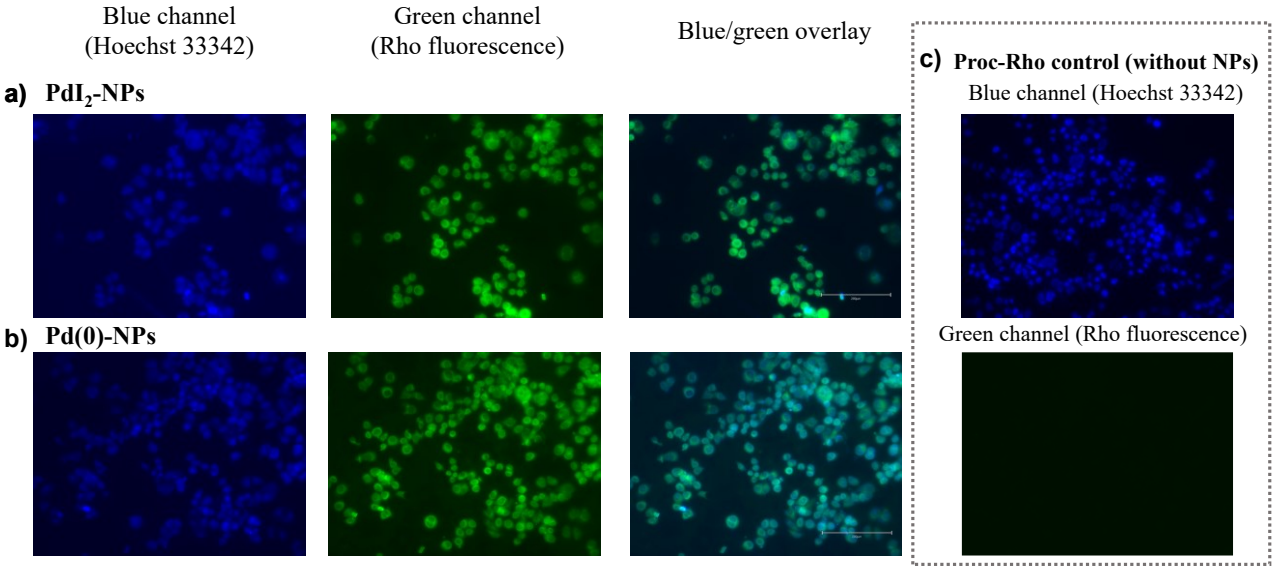

Source: the author, 2021.

Figure 31 a shows SKBR3 cells incubated with PdI_2-NPs followed by the addition of Proc-Rho. The blue channel shows the nucleus stained by Hoechst 33342 while the green channel shows the rhodamine 110, resulting from the uncaging reaction that took place intracellularly. The blue/green merged confirms that the fluorophore is concentrated in the nucleus of the cells. The same outcome is observed for Pd(0)-NPs in Figure 31 b.

As control, cells were incubated in the absence of nanoparticles and, in this case as shown in Figure 31 c, the fluoresce of the rhodamine was not recovered meaning that without Pd-NPs, no uncaging reaction occurred.

Analogously, Figure 32 shows the Epifluorescence micrographs of SKBR3 cells incubated with the nanoparticles and added posteriorly, Alloc-Rho. In Figure 32 a can be seen that PdI_2-NPs successfully released the fluorophore as well as Figure 32 b shows the same for Pd(0)-NPs.

Again, in the absence of the nanoparticles (Figure 32 c) no signal was seen in the green channel because the metal is required to uncage the rhodamine.

Figure 32. Pd-NPs uncaging of Alloc-Rhodamine 110 in SKBR3 cells followed by epifluorescence microscopy. DAPI EVOS light cube was used to image nuclei stained by Hoechst 33342 and GFP EVOS light cube was used for imaging Rhodamine.

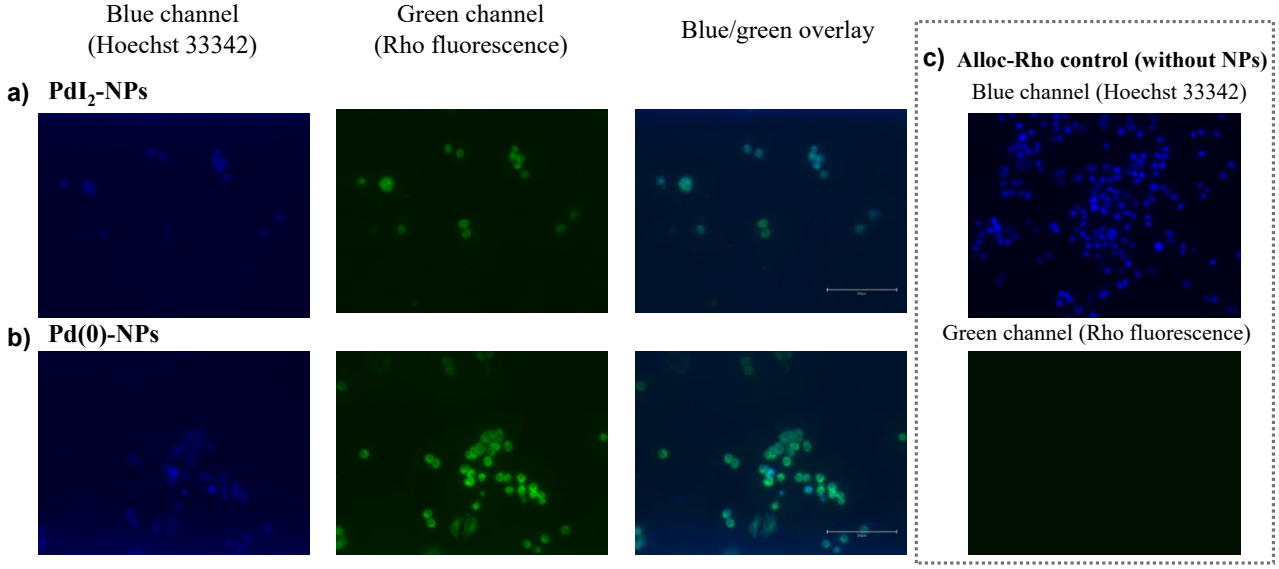

Source: the author, 2021.

Unfortunately, this experiment failed to illustrate the preference of propargylated substrate for Pd(II) and allylated for Pd(0). As previously discussed, the PdI_2-NPs are susceptible to reductive environment of the intracellular space. When they are incubated with the cells for longer periods without renewing the Pd(II) source by means of successive doses, the divalent metal is likely being reduced to Pd(0). In the case of the epifluorescence imaging assays, this was the only set up possible since the fluorophore is too toxic to be incubated with cells before the nanoparticles as well as it is not possible to incubate for longer periods for the addition of further doses of Pd-NPs.

However, the fluorescence imaging still managed to confirm the palladium nanoparticles were able to accumulate in cells, where they triggered the intracellular uncaging reaction of the fluorophore release.

5 CONCLUSION

Palladium nanoparticles were synthesized with a similar procedure, size and dispersity varying, however, in the oxidation state of the metal atom, being composed of palladium (II) or (0). These particles were characterized by relevant techniques such as TEM and SAXS to elucidate their morphological properties and XAS, XPS and FAAS concerning their composition.

The Pd-NPs were initially applied in a carbon-carbon coupling reaction of the aryl alkenylation type. In this study, palladium catalysts were reacted with arenediazonium salt and styrene in an aqueous medium, at room temperature and in the absence of base and inert atmosphere. The formation of the product was observed, according to a traditional Heck-Matsuda reaction. However, efforts in the investigation of the reaction mechanism in the presence of palladium (II) nanoparticles revealed a different pathway. By adding a radical trap to the reaction medium, it was observed the formation of a radical intermediate, which implies in a single electron transfer mechanism enabled by the PdI_2-NPs.

Subsequently, the nanoparticles were applied in the C-O bond cleavage reaction of protected substrates in the form of propargyl carbamates. Kinetic and poisoning studies of Pd-NPs showed that this reaction is favoured by divalent palladium. However, as they consist of nanoparticulated metal clusters, dynamic processes such as leaching, and surface restructuring might be occurring throughout the reaction and different species of palladium may contribute to the formation of the product.

The nanoparticles were also applied to cancer cells of two distinct lineages, breast, and cervical cancer, where their biocompatibility was confirmed, and the local activation of antineoplastic prodrugs was shown to be possible. The rationalisation of the results when transferring the reaction from the flask to the cell medium showed that the knowledge acquired under simple conditions can be extremely helpful to find the best way to administer the prodrug to cells. By understanding the behaviour of the reactions, specifically in this case, the higher activity in the release of propargyloxycarbonyl-protected substrates with Pd(II) and allyloxycarbonyl-protected ones with Pd(0), and how the biological milieu would affect these species, it became possible to achieve not only a great efficiency but also maintain the selectivity of the pairs comprised of prodrug and trigger.

Thus, this work constitutes a broad study of the preparation, understanding and application of palladium nanocatalysts in important organic reactions, both for forming and

breaking bonds. Therefore, the contributions regarding the mode of action of particles in bench conditions as well as in cellular environment constitute an important step in the elucidation of the bio-orthogonal cleavage mechanism that provides more data for the rationalization of catalytic systems that may be used in more complex biological environments and even in vivo.

REFERENCES

(1) Auffan, M.; Rose, J.; Bottero, J.-Y.; Lowry, G. V.; Jolivet, J.-P.; Wiesner, M. R. Towards a Definition of Inorganic Nanoparticles from an Environmental, Health and Safety Perspective. *Nature Nanotechnology* **2009**, *4* (10), 634–641. https://doi.org/10.1038/nnano.2009.242.

(2) Campisi, S.; Schiavoni, M.; Chan-Thaw, C. E.; Villa, A. Untangling the Role of the Capping Agent in Nanocatalysis: Recent Advances and Perspectives. *Catalysts* **2016**, *6* (12), 185. https://doi.org/10.3390/catal6120185.

(3) Roucoux, A.; Schulz, J.; Patin, H. Reduced Transition Metal Colloids: A Novel Family of Reusable Catalysts? *Chem. Rev.* **2002**, *102* (10), 3757–3778. https://doi.org/10.1021/cr010350j.

(4) Jonas, S.; Munish, C. Coating Matters: Review on Colloidal Stability of Nanoparticles with Biocompatible Coatings in Biological Media, Living Cells and Organisms. *Current Medicinal Chemistry* **2018**, *25* (35), 4553–4586.

(5) Balanta, A.; Godard, C.; Claver, C. Pd Nanoparticles for C–C Coupling Reactions. *Chem. Soc. Rev.* **2011**, *40* (10), 4973. https://doi.org/10.1039/c1cs15195a.

(6) Ananikov, V. P.; Beletskaya, I. P. Toward the Ideal Catalyst: From Atomic Centers to a "Cocktail" of Catalysts. **2012**, 10.

(7) Eremin, D. B.; Ananikov, V. P. Understanding Active Species in Catalytic Transformations: From Molecular Catalysis to Nanoparticles, Leaching, "Cocktails" of Catalysts and Dynamic Systems. *Coordination Chemistry Reviews* **2017**, *346*, 2–19. https://doi.org/10.1016/j.ccr.2016.12.021.

(8) Huang, L.; Ang, T. P.; Wang, Z.; Tan, J.; Chen, J.; Wong, P. K. On the Roles of Solid-Bound Ligand Scavengers in the Removal of Palladium Residues and in the Distinction between Homogeneous and Heterogeneous Catalysis. *Inorg. Chem.* **2011**, *50* (6), 2094–2111. https://doi.org/10.1021/ic100824e.

(9) Bunk, S. Better Microscopes Will Be Instrumental in Nanotechnology Development. *Nature* **2001**, *410* (6824), 127–129. https://doi.org/10.1038/35065204.

(10) Biffis, A.; Centomo, P.; Del Zotto, A.; Zecca, M. Pd Metal Catalysts for Cross-Couplings and Related Reactions in the 21st Century: A Critical Review. *Chem. Rev.* **2018**, *118* (4), 2249–2295. https://doi.org/10.1021/acs.chemrev.7b00443.

(11) Recent Advances in Radical C–H Activation/Radical Cross-Coupling | Chemical Reviews https://pubs.acs.org/doi/10.1021/acs.chemrev.6b00620 (accessed 2020 -07 -29).

(12) Taylor, J. G.; Moro, A. V.; Correia, C. R. D. Evolution and Synthetic Applications of the Heck–Matsuda Reaction: The Return of Arenediazonium Salts to Prominence. *European Journal of Organic Chemistry* **2011**, *2011* (8), 1403–1428. https://doi.org/10.1002/ejoc.201001620.

(13) Yang, M.; Li, J.; Chen, P. R. Transition Metal-Mediated Bioorthogonal Protein Chemistry in Living Cells. *Chem. Soc. Rev.* **2014**, *43* (18), 6511–6526. https://doi.org/10.1039/C4CS00117F.

(14) Völker, T.; Meggers, E. Transition-Metal-Mediated Uncaging in Living Human Cells—an Emerging Alternative to Photolabile Protecting Groups. *Current Opinion in Chemical Biology* **2015**, *25*, 48–54. https://doi.org/10.1016/j.cbpa.2014.12.021.

(15) Hsu, H.-T.; Trantow, B. M.; Waymouth, R. M.; Wender, P. A. Bioorthogonal Catalysis: A General Method To Evaluate Metal-Catalyzed Reactions in Real Time in Living Systems Using a Cellular Luciferase Reporter System. *Bioconjugate Chem.* **2016**, *27* (2), 376–382. https://doi.org/10.1021/acs.bioconjchem.5b00469.

(16) Latocheski, E.; Forno, G. M. D.; M. Ferreira, T.; L. Oliveira, B.; L. Bernardes, G. J.; B. Domingos, J. Mechanistic Insights into Transition Metal-Mediated Bioorthogonal Uncaging Reactions. *Chemical Society Reviews* **2020**, *49* (21), 7710–7729. https://doi.org/10.1039/D0CS00630K.
(17) Li, J.; Chen, P. R. Development and Application of Bond Cleavage Reactions in Bioorthogonal Chemistry. *Nature Chemical Biology* **2016**, *12* (3), 129–137. https://doi.org/10.1038/nchembio.2024.
(18) Weiss, J. T.; Dawson, J. C.; Macleod, K. G.; Rybski, W.; Fraser, C.; Torres-Sánchez, C.; Patton, E. E.; Bradley, M.; Carragher, N. O.; Unciti-Broceta, A. Extracellular Palladium-Catalysed Dealkylation of 5-Fluoro-1-Propargyl-Uracil as a Bioorthogonally Activated Prodrug Approach. *Nat Commun* **2014**, *5* (1), 1–9. https://doi.org/10.1038/ncomms4277.
(19) Weiss, J. T.; Dawson, J. C.; Fraser, C.; Rybski, W.; Torres-Sánchez, C.; Bradley, M.; Patton, E. E.; Carragher, N. O.; Unciti-Broceta, A. Development and Bioorthogonal Activation of Palladium-Labile Prodrugs of Gemcitabine. *J. Med. Chem.* **2014**, *57* (12), 5395–5404. https://doi.org/10.1021/jm500531z.
(20) Li, B.; Liu, P.; Wu, H.; Xie, X.; Chen, Z.; Zeng, F.; Wu, S. A Bioorthogonal Nanosystem for Imaging and in Vivo Tumor Inhibition. *Biomaterials* **2017**, *138*, 57–68. https://doi.org/10.1016/j.biomaterials.2017.05.036.
(21) Strambeanu, N.; Demetrovici, L.; Dragos, D.; Lungu, M. Nanoparticles: Definition, Classification and General Physical Properties. In *Nanoparticles' Promises and Risks: Characterization, Manipulation, and Potential Hazards to Humanity and the Environment*; Lungu, M., Neculae, A., Bunoiu, M., Biris, C., Eds.; Springer International Publishing: Cham, 2015; pp 3–8. https://doi.org/10.1007/978-3-319-11728-7_1.
(22) Mody, V. V.; Siwale, R.; Singh, A.; Mody, H. R. Introduction to Metallic Nanoparticles. *Journal of Pharmacy And Bioallied Sciences* **2010**, *2* (4), 282. https://doi.org/10.4103/0975-7406.72127.
(23) Boldon, L.; Laliberte, F.; Liu, L. Review of the Fundamental Theories behind Small Angle X-Ray Scattering, Molecular Dynamics Simulations, and Relevant Integrated Application. *Nano Reviews* **2015**, *6* (1), 25661. https://doi.org/10.3402/nano.v6.25661.
(24) Reverberi, A. P.; Kuznetsov, N. T.; Meshalkin, V. P.; Salerno, M.; Fabiano, B. Systematical Analysis of Chemical Methods in Metal Nanoparticles Synthesis. *Theor Found Chem Eng* **2016**, *50* (1), 59–66. https://doi.org/10.1134/S0040579516010127.
(25) Phan, H. T.; Haes, A. J. What Does Nanoparticle Stability Mean? *J. Phys. Chem. C* **2019**, *123* (27), 16495–16507. https://doi.org/10.1021/acs.jpcc.9b00913.
(26) Vries, J. G. de. When Does Catalysis with Transition Metal Complexes Turn into Catalysis by Nanoparticles? In *Selective Nanocatalysts and Nanoscience*; John Wiley & Sons, Ltd; pp 73–103. https://doi.org/10.1002/9783527635689.ch3.
(27) Mandali, P. K.; Chand, D. K. Palladium Nanoparticles Catalyzed Suzuki Cross-Coupling Reactions in Ambient Conditions. *Catalysis Communications* **2013**, *31*, 16–20. https://doi.org/10.1016/j.catcom.2012.10.020.
(28) Bai, Y.; Feng, X.; Xing, H.; Xu, Y.; Kim, B. K.; Baig, N.; Zhou, T.; Gewirth, A. A.; Lu, Y.; Oldfield, E.; Zimmerman, S. C. A Highly Efficient Single-Chain Metal–Organic Nanoparticle Catalyst for Alkyne–Azide "Click" Reactions in Water and in Cells. *J. Am. Chem. Soc.* **2016**, *138* (35), 11077–11080. https://doi.org/10.1021/jacs.6b04477.
(29) da Silva, F. P.; Fiorio, J. L.; Rossi, L. M. Tuning the Catalytic Activity and Selectivity of Pd Nanoparticles Using Ligand-Modified Supports and Surfaces. *ACS Omega* **2017**, *2* (9), 6014–6022. https://doi.org/10.1021/acsomega.7b00836.
(30) Tavakkoli, M.; Kallio, T.; Reynaud, O.; Nasibulin, A. G.; Johans, C.; Sainio, J.; Jiang, H.; Kauppinen, E. I.; Laasonen, K. Single-Shell Carbon-Encapsulated Iron Nanoparticles:

Synthesis and High Electrocatalytic Activity for Hydrogen Evolution Reaction. *Angewandte Chemie International Edition* **2015**, *54* (15), 4535–4538. https://doi.org/10.1002/anie.201411450.

(31) Le Bars, J.; Specht, U.; Bradley, J. S.; Blackmond, D. G. A Catalytic Probe of the Surface of Colloidal Palladium Particles Using Heck Coupling Reactions. *Langmuir* **1999**, *15* (22), 7621–7625. https://doi.org/10.1021/la990144v.

(32) Vries, J. G. de. A Unifying Mechanism for All High-Temperature Heck Reactions. The Role of Palladium Colloids and Anionic Species. *Dalton Trans.* **2006**, No. 3, 421–429. https://doi.org/10.1039/B506276B.

(33) Su, D. Advanced Electron Microscopy Characterization of Nanomaterials for Catalysis. *Green Energy & Environment* **2017**, *2* (2), 70–83. https://doi.org/10.1016/j.gee.2017.02.001.

(34) Shido, T.; Prins, R. Application of Synchrotron Radiation to in Situ Characterization of Catalysts. *Current Opinion in Solid State and Materials Science* **1998**, *3* (4), 330–335. https://doi.org/10.1016/S1359-0286(98)80041-7.

(35) Frenkel, A. I.; Rodriguez, J. A.; Chen, J. G. Synchrotron Techniques for In Situ Catalytic Studies: Capabilities, Challenges, and Opportunities. *ACS Catal.* **2012**, *2* (11), 2269–2280. https://doi.org/10.1021/cs3004006.

(36) Wu, X.-F.; Anbarasan, P.; Neumann, H.; Beller, M. From Noble Metal to Nobel Prize: Palladium-Catalyzed Coupling Reactions as Key Methods in Organic Synthesis. *Angewandte Chemie International Edition* **2010**, *49* (48), 9047–9050. https://doi.org/10.1002/anie.201006374.

(37) Kashin, A. S.; Ananikov, V. P. Catalytic C–C and C–Heteroatom Bond Formation Reactions: In Situ Generated or Preformed Catalysts? Complicated Mechanistic Picture Behind Well-Known Experimental Procedures. *J. Org. Chem.* **2013**, *78* (22), 11117–11125. https://doi.org/10.1021/jo402038p.

(38) Chinchilla, R.; Nájera, C. Recent Advances in Sonogashira Reactions. *Chem. Soc. Rev.* **2011**, *40* (10), 5084–5121. https://doi.org/10.1039/C1CS15071E.

(39) Han, F.-S. Transition-Metal-Catalyzed Suzuki–Miyaura Cross-Coupling Reactions: A Remarkable Advance from Palladium to Nickel Catalysts. *Chem. Soc. Rev.* **2013**, *42* (12), 5270–5298. https://doi.org/10.1039/C3CS35521G.

(40) Cordovilla, C.; Bartolomé, C.; Martínez-Ilarduya, J. M.; Espinet, P. The Stille Reaction, 38 Years Later. *ACS Catal.* **2015**, *5* (5), 3040–3053. https://doi.org/10.1021/acscatal.5b00448.

(41) Phapale, V. B.; Cárdenas, D. J. Nickel-Catalysed Negishi Cross-Coupling Reactions: Scope and Mechanisms. *Chem. Soc. Rev.* **2009**, *38* (6), 1598–1607. https://doi.org/10.1039/B805648J.

(42) Beletskaya, I. P.; Cheprakov, A. V. The Heck Reaction as a Sharpening Stone of Palladium Catalysis. *Chem. Rev.* **2000**, *100* (8), 3009–3066. https://doi.org/10.1021/cr9903048.

(43) Shaughnessy, K. H. Development of Palladium Precatalysts That Efficiently Generate LPd(0) Active Species. *Israel Journal of Chemistry* **2020**, *60* (3–4), 180–194. https://doi.org/10.1002/ijch.201900067.

(44) Kikukawa, K.; Matsuda, T. Reaction of Diazonium Salts with Transition Metals. i. Arylation of Olefins with Arenediazonium Salts Catalyzed by Zero Valent Palladium. *Chem. Lett.* **1977**, *6* (2), 159–162. https://doi.org/10.1246/cl.1977.159.

(45) Kikukawa, K.; Nagira, K.; Terao, N.; Wada, F.; Matsuda, T. Reaction of Diazonium Salts with Transition Metals. II. Palladiumcatalyzed Arylation of Ethylene with

Arenediazonium Salts. *BCSJ* **1979**, *52* (9), 2609–2610. https://doi.org/10.1246/bcsj.52.2609.

(46) Kikukawa, K.; Nagira, K.; Wada, F.; Matsuda, T. Reaction of Diazonium Salts with Transition Metals—III11Part II: K. Kikukawa, N. Terao, K. Nagira, F. Wada, T. Matsuda, Bull. Chem. Soc. Japan 52, 2609, (1979).: Palladium(0)-Catalyzed Arylation of Unsaturated Compounds with Arenediazoium Salts. *Tetrahedron* **1981**, *37* (1), 31–36. https://doi.org/10.1016/S0040-4020(01)97711-7.

(47) Sabino, A. A.; Machado, A. H. L.; Correia, C. R. D.; Eberlin, M. N. Probing the Mechanism of the Heck Reaction with Arene Diazonium Salts by Electrospray Mass and Tandem Mass Spectrometry. *Angewandte Chemie International Edition* **2004**, *43* (19), 2514–2518. https://doi.org/10.1002/anie.200353076.

(48) Siqueira, F. A.; Taylor, J. G.; Correia, C. R. D. The First Intramolecular Heck–Matsuda Reaction and Its Application in the Syntheses of Benzofurans and Indoles. *Tetrahedron Letters* **2010**, *51* (16), 2102–2105. https://doi.org/10.1016/j.tetlet.2010.02.011.

(49) Amatore, C.; Jutand, A. Anionic Pd(0) and Pd(II) Intermediates in Palladium-Catalyzed Heck and Cross-Coupling Reactions. *Acc. Chem. Res.* **2000**, *33* (5), 314–321. https://doi.org/10.1021/ar980063a.

(50) Machado, A. H. L.; Milagre, H. M. S.; Eberlin, L. S.; Sabino, A. A.; Correia, C. R. D.; Eberlin, M. N. "Dba-Free" Palladium Intermediates of the Heck–Matsuda Reaction. *Org. Biomol. Chem.* **2013**, *11* (20), 3277–3281. https://doi.org/10.1039/C3OB40142A.

(51) Kindt, S.; Heinrich, M. R. Recent Advances in Meerwein Arylation Chemistry. *Synthesis* **2016**, *48* (11), 1597–1606. https://doi.org/10.1055/s-0035-1561586.

(52) Kurti, L.; Czako, B. *Strategic Applications of Named Reactions in Organic Synthesis*; Elsevier, 2005.

(53) Meerwein, H.; Büchner, E.; Emster, K. van. Über Die Einwirkung Aromatischer Diazoverbindungen Auf α,β-Ungesättigte Carbonylverbindungen. *Journal für Praktische Chemie* **1939**, *152* (7–10), 237–266. https://doi.org/10.1002/prac.19391520705.

(54) Rondestvedt, C. S. Arylation of Unsaturated Compounds by Diazonium Salts (The Meerwein Arylation Reaction). In *Organic Reactions*; American Cancer Society, 2011; pp 189–260. https://doi.org/10.1002/0471264180.or011.03.

(55) Kochi, J. K. The Meerwein Reaction. Catalysis by Cuprous Chloride. *J. Am. Chem. Soc.* **1955**, *77* (19), 5090–5092. https://doi.org/10.1021/ja01624a041.

(56) Galli, C. Radical Reactions of Arenediazonium Ions: An Easy Entry into the Chemistry of the Aryl Radical. *Chem. Rev.* **1988**, *88* (5), 765–792. https://doi.org/10.1021/cr00087a004.

(57) Hang, H. C.; Yu, C.; Kato, D. L.; Bertozzi, C. R. A Metabolic Labeling Approach toward Proteomic Analysis of Mucin-Type O-Linked Glycosylation. *Proceedings of the National Academy of Sciences* **2003**, *100* (25), 14846–14851. https://doi.org/10.1073/pnas.2335201100.

(58) Scinto, S. L.; Bilodeau, D. A.; Hincapie, R.; Lee, W.; Nguyen, S. S.; Xu, M.; am Ende, C. W.; Finn, M. G.; Lang, K.; Lin, Q.; Pezacki, J. P.; Prescher, J. A.; Robillard, M. S.; Fox, J. M. Bioorthogonal Chemistry. *Nature Reviews Methods Primers* **2021**, *1* (1), 1–23. https://doi.org/10.1038/s43586-021-00028-z.

(59) Walper, S. A.; Turner, K. B.; Medintz, I. L. Bioorthogonal Labeling of Cellular Proteins by Enzymatic and Related Mechanisms. In *Chemoselective and Bioorthogonal Ligation Reactions*; Algar, W. R., Dawson, P. E., Medintz, I. L., Eds.; Wiley-VCH Verlag GmbH & Co. KGaA: Weinheim, Germany, 2017; pp 165–230. https://doi.org/10.1002/9783527683451.ch7.

(60) Thirumurugan, P.; Matosiuk, D.; Jozwiak, K. Click Chemistry for Drug Development and Diverse Chemical–Biology Applications. *Chem. Rev.* **2013**, *113* (7), 4905–4979. https://doi.org/10.1021/cr200409f.
(61) Spicer, C. D.; Davis, B. G. Selective Chemical Protein Modification. *Nat Commun* **2014**, *5* (1), 4740. https://doi.org/10.1038/ncomms5740.
(62) Greene's Protective Groups in Organic Synthesis, 4th Edition | Wiley https://www.wiley.com/en-us/Greene%27s+Protective+Groups+in+Organic+Synthesis%2C+4th+Edition-p-9780470053485 (accessed 2021 -04 -22).
(63) Barany, G.; Merrifield, R. B. A New Amino Protecting Group Removable by Reduction. Chemistry of the Dithiasuccinoyl (Dts) Function. *J. Am. Chem. Soc.* **1977**, *99* (22), 7363–7365. https://doi.org/10.1021/ja00464a050.
(64) Tu, J.; Xu, M.; Franzini, R. M. Dissociative Bioorthogonal Reactions. *ChemBioChem* **2019**, *20* (13), 1615–1627. https://doi.org/10.1002/cbic.201800810.
(65) Shieh, P.; Hill, M. R.; Zhang, W.; Kristufek, S. L.; Johnson, J. A. Clip Chemistry: Diverse (Bio)(Macro)Molecular and Material Function through Breaking Covalent Bonds. *Chem. Rev.* **2021**, *121* (12), 7059–7121. https://doi.org/10.1021/acs.chemrev.0c01282.
(66) Streu, C.; Meggers, E. Ruthenium-Induced Allylcarbamate Cleavage in Living Cells. *Angew. Chem. Int. Ed.* **2006**, *45* (34), 5645–5648. https://doi.org/10.1002/anie.200601752.
(67) Yusop, R. M.; Unciti-Broceta, A.; Johansson, E. M. V.; Sánchez-Martín, R. M.; Bradley, M. Palladium-Mediated Intracellular Chemistry. *Nature Chemistry* **2011**, *3* (3), 239–243.
(68) Pérez-López, A. M.; Rubio-Ruiz, B.; Sebastián, V.; Hamilton, L.; Adam, C.; Bray, T. L.; Irusta, S.; Brennan, P. M.; Lloyd-Jones, G. C.; Sieger, D.; Santamaría, J.; Unciti-Broceta, A. Gold-Triggered Uncaging Chemistry in Living Systems. *Angewandte Chemie International Edition* **2017**, *56* (41), 12548–12552. https://doi.org/10.1002/anie.201705609.
(69) Kislukhin, A. A.; Hong, V. P.; Breitenkamp, K. E.; Finn, M. G. Relative Performance of Alkynes in Copper-Catalyzed Azide–Alkyne Cycloaddition. *Bioconjugate Chem.* **2013**, *24* (4), 684–689. https://doi.org/10.1021/bc300672b.
(70) Wang, X.; Liu, Y.; Fan, X.; Wang, J.; Ngai, W. S. C.; Zhang, H.; Li, J.; Zhang, G.; Lin, J.; Chen, P. R. Copper-Triggered Bioorthogonal Cleavage Reactions for Reversible Protein and Cell Surface Modifications. *J. Am. Chem. Soc.* **2019**, *141* (43), 17133–17141. https://doi.org/10.1021/jacs.9b05833.
(71) Hamilton, G. S. Antibody-Drug Conjugates for Cancer Therapy: The Technological and Regulatory Challenges of Developing Drug-Biologic Hybrids. *Biologicals* **2015**, *43* (5), 318–332. https://doi.org/10.1016/j.biologicals.2015.05.006.
(72) Stenton, B. J.; Oliveira, B. L.; Matos, M. J.; Sinatra, L.; Bernardes, G. J. L. A Thioether-Directed Palladium-Cleavable Linker for Targeted Bioorthogonal Drug Decaging. *Chem. Sci.* **2018**, *9* (17), 4185–4189. https://doi.org/10.1039/C8SC00256H.
(73) Oliveira, B. L.; Stenton, B. J.; Unnikrishnan, V. B.; de Almeida, C. R.; Conde, J.; Negrão, M.; Schneider, F. S. S.; Cordeiro, C.; Ferreira, M. G.; Caramori, G. F.; Domingos, J. B.; Fior, R.; Bernardes, G. J. L. Platinum-Triggered Bond-Cleavage of Pentynoyl Amide and N-Propargyl Handles for Drug-Activation. *J. Am. Chem. Soc.* **2020**, *142* (24), 10869–10880. https://doi.org/10.1021/jacs.0c01622.
(74) Li, J.; Yu, J.; Zhao, J.; Wang, J.; Zheng, S.; Lin, S.; Chen, L.; Yang, M.; Jia, S.; Zhang, X.; Chen, P. R. Palladium-Triggered Deprotection Chemistry for Protein Activation in Living Cells. *Nature Chem* **2014**, *6* (4), 352–361. https://doi.org/10.1038/nchem.1887.

(75) Wang, J.; Cheng, B.; Li, J.; Zhang, Z.; Hong, W.; Chen, X.; Chen, P. R. Chemical Remodeling of Cell-Surface Sialic Acids through a Palladium-Triggered Bioorthogonal Elimination Reaction. *Angewandte Chemie International Edition* **2015**, *54* (18), 5364–5368. https://doi.org/10.1002/anie.201409145.
(76) Dumas, A.; Couvreur, P. Palladium: A Future Key Player in the Nanomedical Field? *Chem. Sci.* **2015**, *6* (4), 2153–2157. https://doi.org/10.1039/C5SC00070J.
(77) Tsuji, J.; Takahashi, H.; Morikawa, M. Organic Syntheses by Means of Noble Metal Compounds XVII. Reaction of π-Allylpalladium Chloride with Nucleophiles. *Tetrahedron Letters* **1965**, *6* (49), 4387–4388. https://doi.org/10.1016/S0040-4039(00)71674-1.
(78) Dixneuf, P.; Cadierno, V. *Metal-Catalyzed Reactions in Water*; John Wiley & Sons, 2013.
(79) Song, F.; Garner, A. L.; Koide, K. A Highly Sensitive Fluorescent Sensor for Palladium Based on the Allylic Oxidative Insertion Mechanism. *J. Am. Chem. Soc.* **2007**, *129* (41), 12354–12355. https://doi.org/10.1021/ja073910q.
(80) Trost, B. M.; Van Vranken, D. L. Asymmetric Transition Metal-Catalyzed Allylic Alkylations. *Chem. Rev.* **1996**, *96* (1), 395–422. https://doi.org/10.1021/cr9409804.
(81) Tsuji, J. *Organic Synthesis with Palladium Compounds*; Springer Science & Business Media, 2012.
(82) Garner, A. L.; Song, F.; Koide, K. Enhancement of a Catalysis-Based Fluorometric Detection Method for Palladium through Rational Fine-Tuning of the Palladium Species. *J. Am. Chem. Soc.* **2009**, *131* (14), 5163–5171. https://doi.org/10.1021/ja808385a.
(83) Martínez-Calvo, M.; Couceiro, J. R.; Destito, P.; Rodríguez, J.; Mosquera, J.; Mascareñas, J. L. Intracellular Deprotection Reactions Mediated by Palladium Complexes Equipped with Designed Phosphine Ligands. *ACS Catal.* **2018**, *8* (7), 6055–6061. https://doi.org/10.1021/acscatal.8b01606.
(84) Pohorilets, I.; Tracey, M. P.; LeClaire, M. J.; Moore, E. M.; Lu, G.; Liu, P.; Koide, K. Kinetics and Inverse Temperature Dependence of a Tsuji–Trost Reaction in Aqueous Buffer. *ACS Catal.* **2019**, *9* (12), 11720–11733. https://doi.org/10.1021/acscatal.9b03011.
(85) Ou, Z.; He, L.; Gao, Y.; Li, P.; Li, T.; Zhang, J.; Dong, Y.; Zhou, W.; Zhang, Y. Ratiometric Fluorescent Determination of Palladium Based on the C–N Bond Cleavage of Allyl Quaternary Ammonium. *New J. Chem.* **2021**, *45* (11), 5206–5212. https://doi.org/10.1039/D0NJ06271E.
(86) Pal, M.; Parasuraman, K.; Yeleswarapu, K. R. Palladium-Catalyzed Cleavage of O/N-Propargyl Protecting Groups in Aqueous Media under a Copper-Free Condition [1]. *Org. Lett.* **2003**, *5* (3), 349–352. https://doi.org/10.1021/ol027382t.
(87) Santra, M.; Ko, S.-K.; Shin, I.; Ahn, K. H. Fluorescent Detection of Palladium Species with an O-Propargylated Fluorescein. *Chem. Commun.* **2010**, *46* (22), 3964–3966. https://doi.org/10.1039/C001922D.
(88) Rambabu, D.; Bhavani, S.; Swamy, N. K.; Basaveswara Rao, M. V.; Pal, M. Pd/C-Mediated Depropargylation of Propargyl Ethers/Amines in Water. *Tetrahedron Letters* **2013**, *54* (9), 1169–1173. https://doi.org/10.1016/j.tetlet.2012.12.093.
(89) Weiss, J. T.; Dawson, J. C.; Macleod, K. G.; Rybski, W.; Fraser, C.; Torres-Sánchez, C.; Patton, E. E.; Bradley, M.; Carragher, N. O.; Unciti-Broceta, A. Extracellular Palladium-Catalysed Dealkylation of 5-Fluoro-1-Propargyl-Uracil as a Bioorthogonally Activated Prodrug Approach. *Nat Commun* **2014**, *5* (1), 3277. https://doi.org/10.1038/ncomms4277.
(90) Amatore, C.; Carre, E.; Jutand, A.; M'Barki, M. A. Rates and Mechanism of the Formation of Zerovalent Palladium Complexes from Mixtures of Pd(OAc)2 and Tertiary Phosphines and Their Reactivity in Oxidative Additions. *Organometallics* **1995**, *14* (4), 1818–1826. https://doi.org/10.1021/om00004a039.

(91) Coelho, S. E.; Schneider, F. S. S.; de Oliveira, D. C.; Tripodi, G. L.; Eberlin, M. N.; Caramori, G. F.; de Souza, B.; Domingos, J. B. Mechanism of Palladium(II)-Mediated Uncaging Reactions of Propargylic Substrates. *ACS Catalysis* **2019**, 3792–3799. https://doi.org/10.1021/acscatal.9b00210.

(92) Jbara, M.; Eid, E.; Brik, A. Gold(I)-Mediated Decaging or Cleavage of Propargylated Peptide Bond in Aqueous Conditions for Protein Synthesis and Manipulation. *J. Am. Chem. Soc.* **2020**, *142* (18), 8203–8210. https://doi.org/10.1021/jacs.9b13216.

(93) Cho, S. W.; Reo, Y. J.; Sarkar, S.; Ahn, K. H. Electronic Effects on the Depropargylation Process in the Reaction-Based Fluorescent Detection of Palladium Species: Benzocoumarin-Based Ratiometric Sensing Systems. *Bulletin of the Korean Chemical Society* **2021**, *42* (1), 135–139. https://doi.org/10.1002/bkcs.12173.

(94) Latocheski, E.; Marques, M. V.; Albuquerque, B. L.; Schuh, T. J.; Signori, A. M.; Oliveira, D. C.; Pal, T.; Domingos, J. B. On the Formation of Palladium (II) Iodide Nanoparticles: An In Situ SAXS/XAS Study and Catalytic Evaluation on an Aryl Alkenylation Reaction in Water Medium. *ChemCatChem* **2018**, cctc.201801817. https://doi.org/10.1002/cctc.201801817.

(95) Breßler, I.; Kohlbrecher, J.; Thünemann, A. F. *SASfit* : A Tool for Small-Angle Scattering Data Analysis Using a Library of Analytical Expressions. *J Appl Crystallogr* **2015**, *48* (5), 1587–1598. https://doi.org/10.1107/S1600576715016544.

(96) Latocheski, E. Estudos da formação de nanopartículas de paládio por técnicas espectroscópicas de raios X e suas aplicações em catálise de reações orgânicas. Dissertação de Mestrado, Universidade Federal de Santa Catarina, 2017.

(97) Widegren, J. A.; Finke, R. G. A Review of the Problem of Distinguishing True Homogeneous Catalysis from Soluble or Other Metal-Particle Heterogeneous Catalysis under Reducing Conditions. *Journal of Molecular Catalysis A: Chemical* **2003**, *198* (1), 317–341. https://doi.org/10.1016/S1381-1169(02)00728-8.

(98) Hornstein, B. J.; Aiken, J. D.; Finke, R. G. Nanoclusters in Catalysis: A Comparison of CS2 Catalyst Poisoning of Polyoxoanion- and Tetrabutylammonium-Stabilized 40 ± 6 Å Rh(0) Nanoclusters to 5 Rh/Al2O3, Including an Analysis of the Literature Related to the CS2 to Metal Stoichiometry Issue. *Inorg. Chem.* **2002**, *41* (6), 1625–1638. https://doi.org/10.1021/ic010920y.

(99) Kragten, J. The Stability Constant of Pd-EDTA. *Talanta* **1978**, *25* (4), 239–240. https://doi.org/10.1016/0039-9140(78)80015-0.

(100) Kunzl, V. A Linear Dependence of Energy Levels on the Valency of Elements. *Collect. Czech. Chem. Commun.* **1932**, *4*, 213–224. https://doi.org/10.1135/cccc19320213.

(101) Buratto, S.; Latocheski, E.; de Oliveira, D.; Domingos, J. Influence of the Capping Agent PVP of the Outer Layer of Pd Nanocubes Surface on the Catalytic Hydrogenation of Unsaturated C−C Bonds. *J. Braz. Chem. Soc.* **2020**. https://doi.org/10.21577/0103-5053.20190250.

(102) Anslyn, E. V.; Dougherty, D. A. *Modern Physical Organic Chemistry*; University Science Books, 2006.

(103) Blackmond, D. G. Reaction Progress Kinetic Analysis: A Powerful Methodology for Mechanistic Studies of Complex Catalytic Reactions. *Angewandte Chemie International Edition* **2005**, *44* (28), 4302–4320. https://doi.org/10.1002/anie.200462544.

(104) Gorunova, O. N.; Novitskiy, I. M.; Grishin, Y. K.; Gloriozov, I. P.; Roznyatovsky, V. A.; Khrustalev, V. N.; Kochetkov, K. A.; Dunina, V. V. When Applying the Mercury Poisoning Test to Palladacycle-Catalyzed Reactions, One Should Not Consider the Common Misconception of Mercury(0) Selectivity. *Organometallics* **2018**, *37* (17), 2842–2858. https://doi.org/10.1021/acs.organomet.8b00363.

(105) Chernyshev, V. M.; Astakhov, A. V.; Chikunov, I. E.; Tyurin, R. V.; Eremin, D. B.; Ranny, G. S.; Khrustalev, V. N.; Ananikov, V. P. Pd and Pt Catalyst Poisoning in the Study of Reaction Mechanisms: What Does the Mercury Test Mean for Catalysis? *ACS Catal.* **2019**, *9* (4), 2984–2995. https://doi.org/10.1021/acscatal.8b03683.

(106) Konc, J. Chemical Biology Strategies for the Formation and Cleavage of Chemical Bonds. Thesis, University of Cambridge, 2021. https://doi.org/10.17863/CAM.65546.

(107) *Palladium*; Melber, C., Keller, D., Mangelsdorf, I., Eds.; Environmental health criteria; World Health Organization: Geneva, 2002.

(108) Miller, M. A.; Mikula, H.; Luthria, G.; Li, R.; Kronister, S.; Prytyskach, M.; Kohler, R. H.; Mitchison, T.; Weissleder, R. Modular Nanoparticulate Prodrug Design Enables Efficient Treatment of Solid Tumors Using Bioorthogonal Activation. *ACS Nano* **2018**, *12* (12), 12814–12826. https://doi.org/10.1021/acsnano.8b07954.

(109) Das, R.; Landis, R. F.; Tonga, G. Y.; Cao-Milán, R.; Luther, D. C.; Rotello, V. M. Control of Intra- versus Extracellular Bioorthogonal Catalysis Using Surface-Engineered Nanozymes. *ACS Nano* **2019**, *13* (1), 229–235.

(110) Behzadi, S.; Serpooshan, V.; Tao, W.; Hamaly, M. A.; Alkawareek, M. Y.; Dreaden, E. C.; Brown, D.; Alkilany, A. M.; Farokhzad, O. C.; Mahmoudi, M. Cellular Uptake of Nanoparticles: Journey inside the Cell. *Chem. Soc. Rev.* **2017**, *46* (14), 4218–4244. https://doi.org/10.1039/C6CS00636A.

(111) Zhang, P.; Sadler, P. J. Redox-Active Metal Complexes for Anticancer Therapy. *European Journal of Inorganic Chemistry* **2017**, *2017* (12), 1541–1548. https://doi.org/10.1002/ejic.201600908.

APPENDIX

Figure A1. ^{1}H NMR spectrum (400 MHz, $CDCl_3$) of (*E*)-4-bromostilbene.

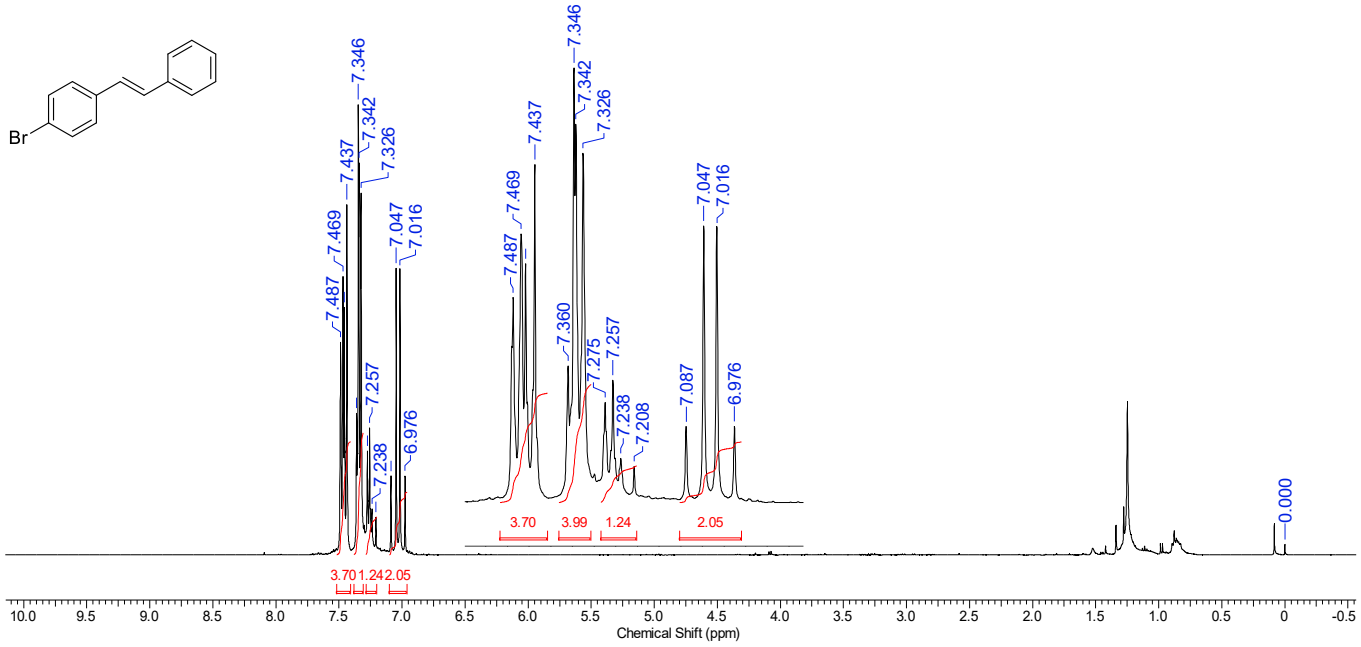

Figure A2. ^{13}C NMR spectrum (200 MHz, $CDCl_3$) of (*E*)-4-bromostilbene.

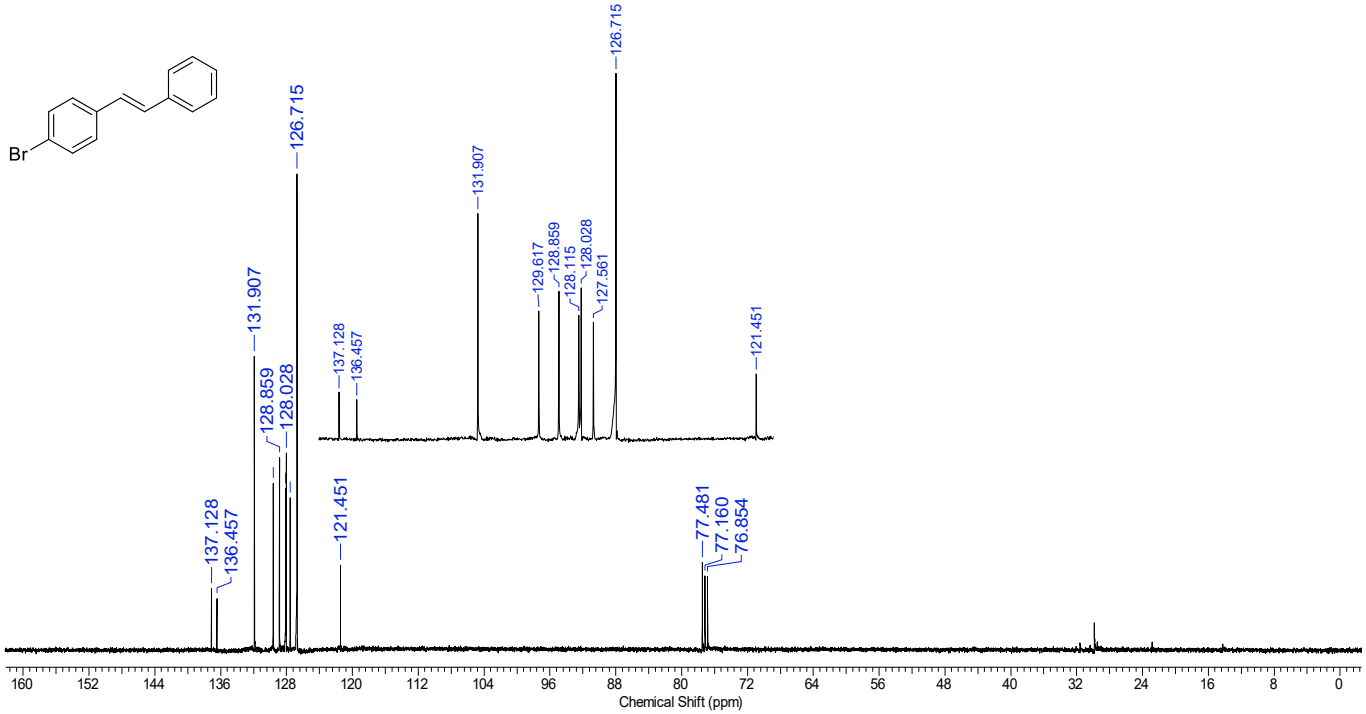

Figure A3. ESI-MS spectra of the aryl-TEMPO adduct (*m/z* = 312.095) in the reaction medium (a), experimental (b) and simulated (c).

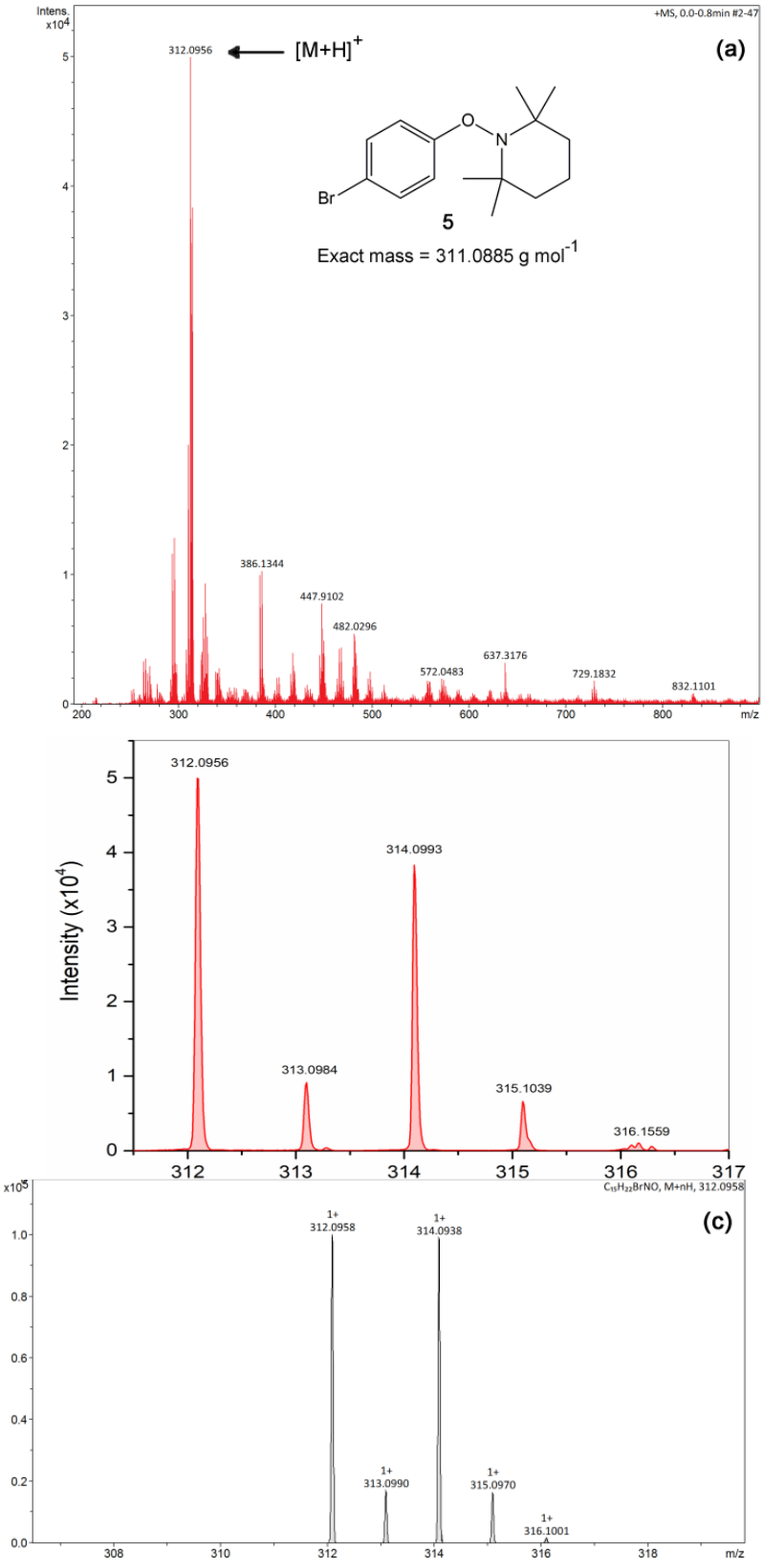

Figure A4. ^{13}C NMR spectrum (200 MHz, $CDCl_3$) of the reaction medium, as the main product, the adduct aryl-TEMPO is shown.

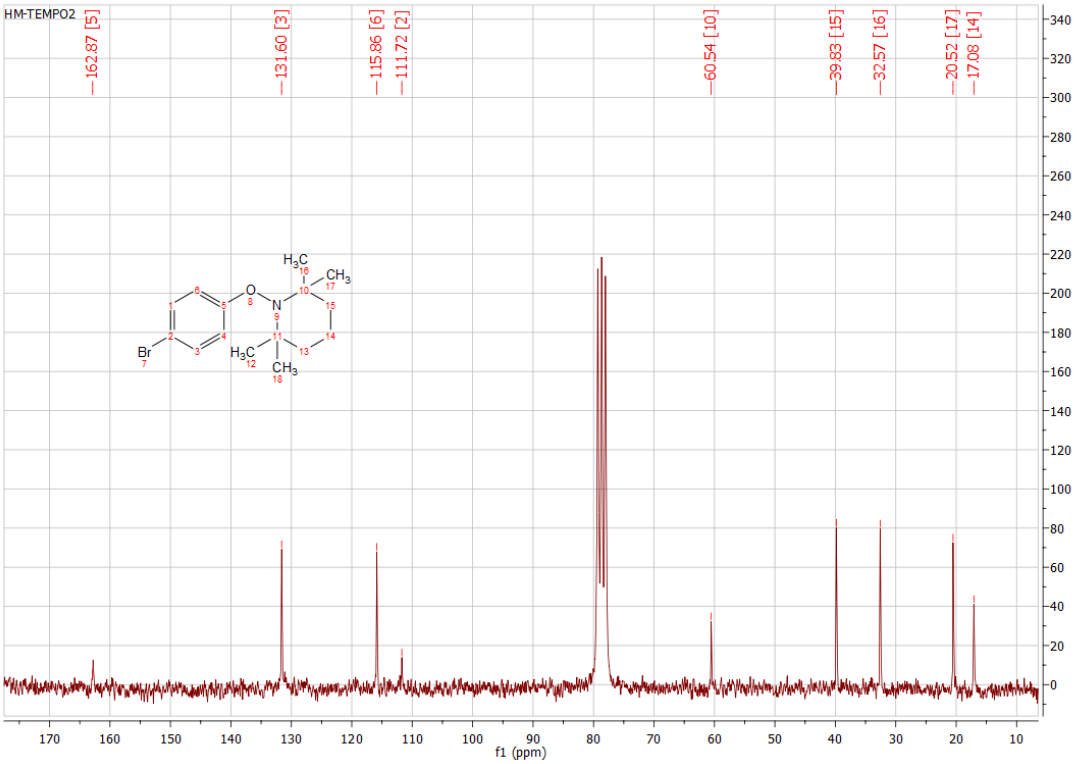

Figure A5. ^{1}H NMR spectrum (200 MHz, $CDCl_3$) of *O*-Proc-coumarin.

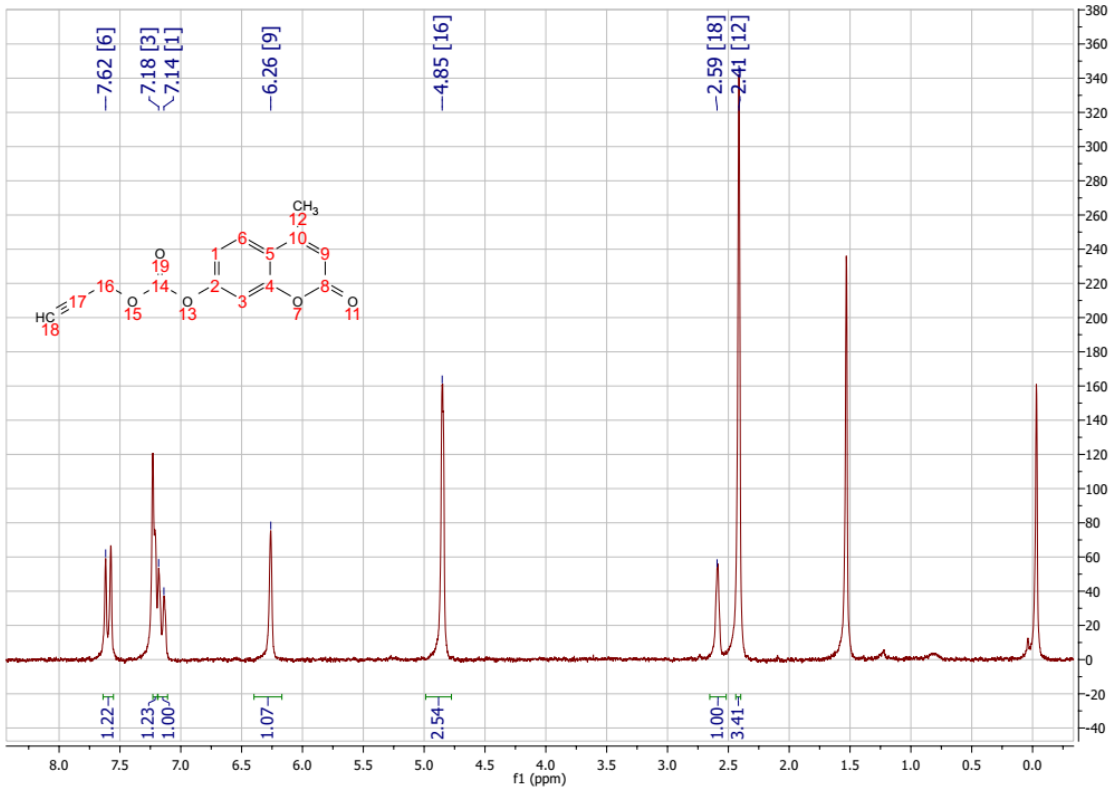

Figure A6. ^{1}H NMR spectrum (200 MHz, $CDCl_3$) of *N*-Proc-coumarin.

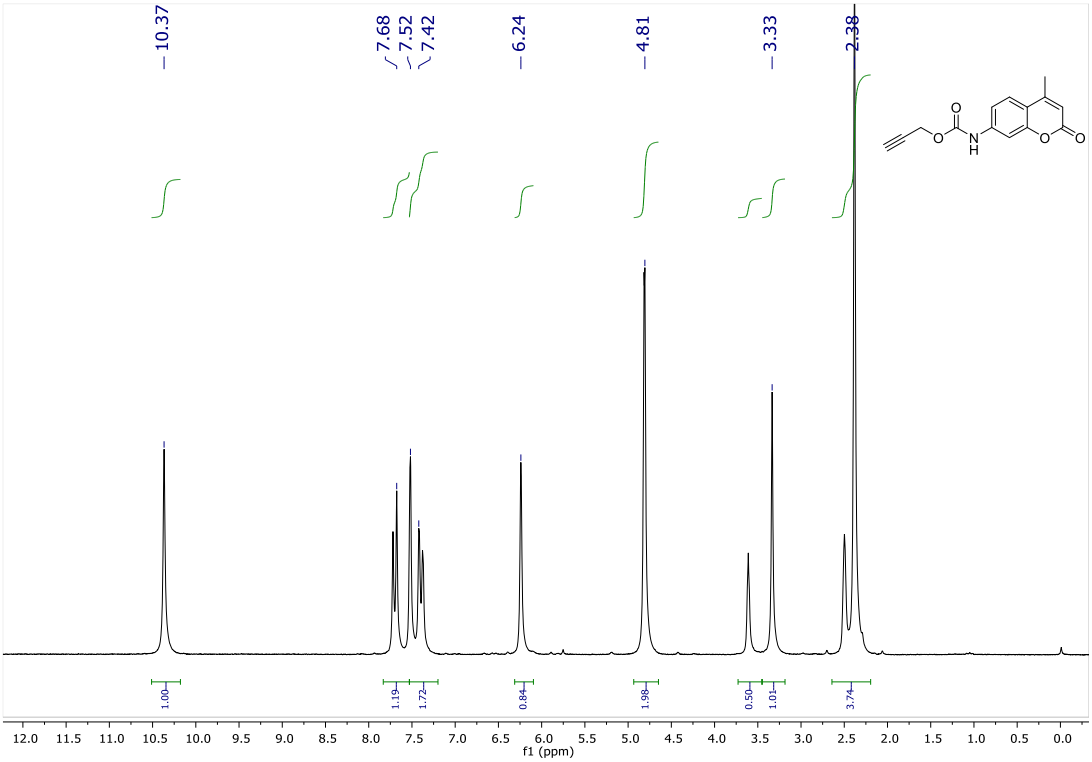

Figure A7. ^{1}H NMR spectrum (400 MHz, $CDCl_3$) of the propargyloxycarbonyl-doxorubicin (Proc-DOX).

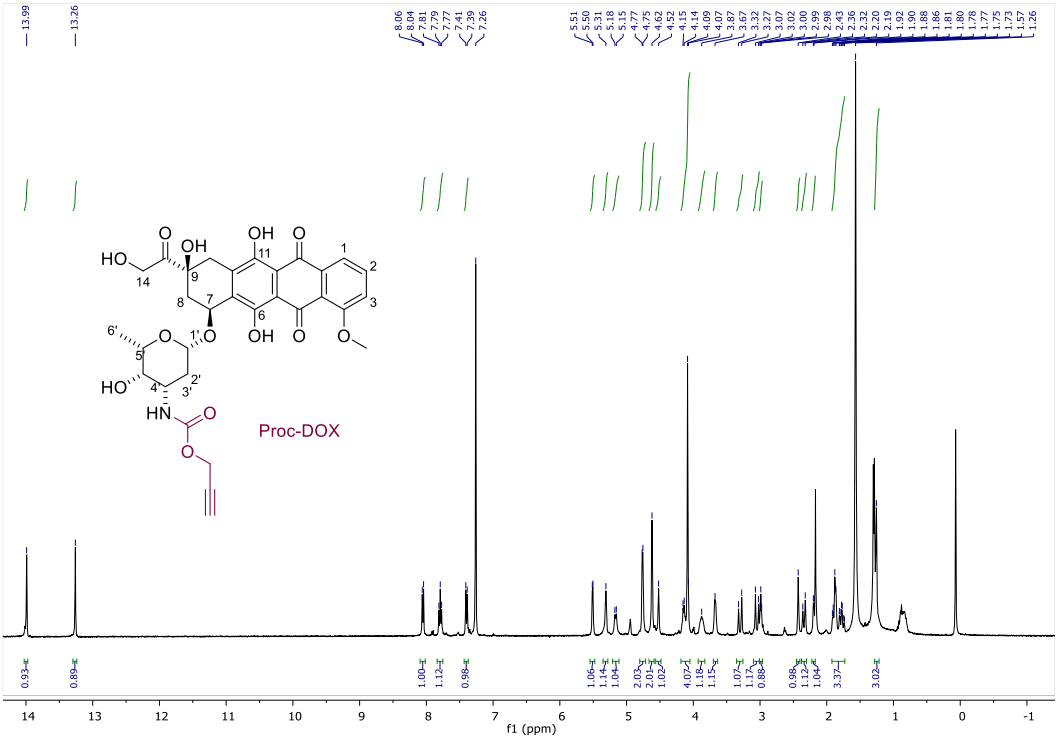

Figure A8. ^{1}H NMR spectrum (400 MHz, acetone-*d6*) of the allyloxycarbonyl-doxorubicin (Alloc-DOX).